TECHNISCHE UNIVERSITÄT MÜNCHEN

Department Chemie

Lehrstuhl für Biotechnologie

Molecular architecture, dynamics and regulation of the Hsp90 cochaperone Sti1

Alina B. Röhl

Vollständiger Abdruck der vom Department Chemie der Technischen Universität München zur Erlangung des akademischen Grades eines Dr. rer. nat. genehmigten Dissertation.

Vorsitzender:		Univ.-Prof. Dr. Lukas Hintermann
Prüfer der Dissertation:	1.	Univ.-Prof. Dr. Johannes Buchner
	2.	Univ.-Prof. Don C. Lamb, Ph.D. Ludwig-Maximilians-Universität München

Die Dissertation wurde am 05.09.2013 bei der Technischen Universität München eingereicht und durch das Department Chemie am 23.10.2013 angenommen.

Summary

Many unstable regulatory proteins such as kinases, transcription factors and steroid hormone receptors require the coordinated actions of Hsp70 and Hsp90 for their maturation. These are enabled by the adaptor protein Sti1 which physically connects Hsp70 and Hsp90 and inhibits the ATPase activity of Hsp90. For this function, Sti1 provides two modules each comprising TPR and DP domains (TPR1-DP1 and TPR2A-TPR2B-DP2). Previous studies reported TPR2A being responsible for Hsp90 binding and TPR1 for Hsp70, leaving the contribution of TPR2B ambiguous.

In this work, interaction studies and *in vivo* assays using fragments and mutants of Sti1 were employed to pinpoint the regions that contribute to the complex formation. They revealed that there are two alternative binding sites for Hsp70 *in vitro* (TPR1 and TPR2B). TPR1 exhibits a more latent role and TPR2B is crucial for the activation of different clients *in vivo*. TPR2A and TPR2B together form a joint binding site for Hsp70 and Hsp90. This most probably is enabled by the rotated arrangement of TPR2A and TPR2B which was proven to be relevant *in vivo*. Analysis of the DP domains demonstrated that client activation is very sensitive to alterations of DP2 and suggests that these domains stabilize the client interaction.

The 60 amino acid linker which connects the two TPR-DP modules was identified to play a key role in Sti1. Deletion of the linker showed that it regulates the interaction with Hsp70 and participates in client activation. Double labeled variants of Sti1 analyzed by FRET experiments revealed that the conformation of the linker is altered by Hsp90 and Hsp70. Furthermore, SAXS experiments indicated that the linker is highly flexible and that both TPR1 and DP1 are connected versatilely to the rest of the protein. Electron microscopy reconstructions recovered an Hsp90-Sti1-Hsp70 complex in which the completely bent linker induces a close proximity between TPR1 and TPR2B, and Hsp90 and Hsp70 are in intimate contact. A minority of elongated complexes was found indicating a stretched linker. To address whether the findings were transferable to the human system, Sti1 from *S. cerevisiae* and its human homolog Hop were compared. Both behaved similarly in their interaction with Hsp90 and Hsp70 and contrary to a previous publication, both inhibited the ATPase activity of both yeast and human Hsp90 suggesting a conserved mechanism. Sti1 and Hop are both phosphorylated each at mostly unique sites. Using phosphomimetic glutamate mutants, it was illustrated that this phosphorylation generally lowers client activation *in vivo* and that it is accompanied by a reduced affinity for Hsp70.

With respect to the described results, a comprehensive model explaining the client transfer from Hsp70 to Hsp90 was constructed: Sti1 allows for the handover of clients through simultaneous binding of Hsp90 and Hsp70 via TPR2A-TPR2B, while the flexibly connected TPR1(-DP1) delivers Hsp70-bound clients to the central platform via a bending of the linker.

CONTENTS

CHAPTER 1

INTRODUCTION

1.1 Protein folding

Newly synthesized proteins exit the ribosome as simple linear chains of amino acids. After that, these chains fold and adopt a unique three-dimensional structure. Generally, only this unique structure makes them capable of performing their biological function. In some cases, unfolding and misfolding leads to toxic function. Outstanding examples are many of the neurodegenerative diseases like Parkinson's or Alzheimer's disease which result from the accumulation of amyloid fibrils formed by misfolded proteins [Selkoe, 2003, Scheibel and Buchner, 2006].
The fold of a protein is mainly determined by the amino acid sequence which is encoded in the DNA [Anfinsen, 1973, Seckler and Jaenicke, 1992, Fersht and Daggett, 2002]. Also the used codons for a given amino acid can influence the structure of the protein by affecting the speed of translation [Saunders and Deane, 2010]. Hydrogen bonds between the backbone amino and carboxyl groups of neighboring amino acids define the secondary structure of a protein. Usually, these form patterns leading to regular structures like α-helices or β-sheets. The three-dimensional arrangement of these elements characterizes the tertiary structure of a protein.

The folded conformation of a protein, the native state, is the structure with minimal free energy. An important force contributing to the folding is the hydrophobic effect which leads to the burial of hydrophobic side chains in the core of the structure [Pace et al., 1996]. How proteins find the structure with the minimal free energy may be one of the most essential open questions in biology. If proteins were folded by randomly going through all the possible conformations, this would take an unrealistic amount of

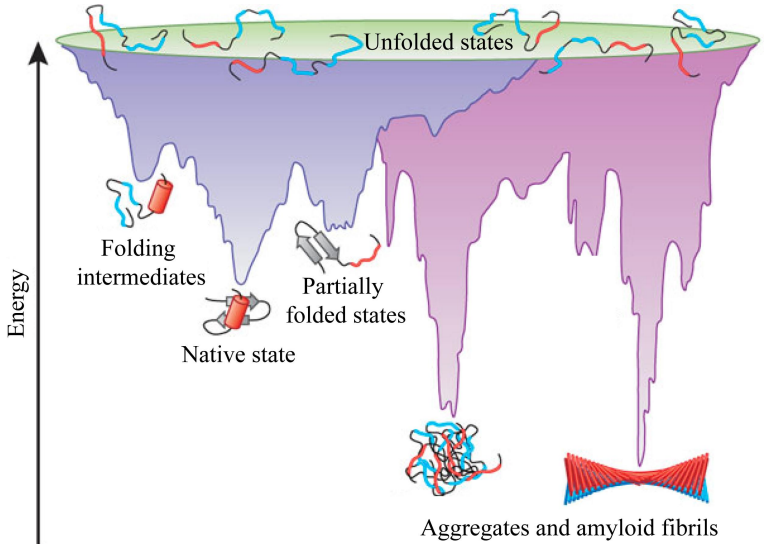

Figure 1.1: Concept of the funnel-shaped energy landscape. Unfolded high-entropy states are at the top of the funnel. During folding, they move downhill along the energy landscape to the native state at the bottom of the funnel. The energy surface contains local energy minima which represent intermediates. Proteins can be trapped in these resulting in aggregates or amyloid fibrils. Adapted from [Hartl and Hayer-Hartl, 2009].

time (Levinthals's paradox) [Levinthal, 1968]. Based on the observation that proteins fold much faster than this, the current opinion is that proteins must fold through a series of meta-stable intermediate states.
A concept for how this works is the funnel-shaped energy landscape (Figure 1.1): The unfolded states of proteins are high in entropy and are represented by the rim of the funnel. On their way downhill in the funnel towards the global free energy minimum, they pass local minima which correlate to partly folded intermediates [Ptitsyn, 1995, Ptitsyn et al., 1995]. At the exit of the funnel, they adopt the native state [Dill and Chan, 1997, Dill, 1999]. Interestingly, the folded state is usually only stabilized by an energy difference in the range of a few hydrogen bonds [Pace, 1990].

1.2 Molecular chaperones assist protein folding

Misfolding and aggregation of proteins can occur during synthesis as well as during the entire lifetime of a protein especially under stressful conditions. The crowded environment of a cell with protein concentrations of about 300 mg/ml poses a constant threat to protein integrity as it facilitates aggregation [Ellis, 2001, Tyedmers et al., 2010]. This is why cells have developed a set of differently specialized molecular chaperones which control proper folding of the proteome. These ubiquitous and highly conserved machines assist the folding and assembly of proteins and prevent their aggregation

[Hartl et al., 2011]. At the same time, they are also important for degradation and disassembly of protein complexes [Bukau et al., 2006].
While some proteins are generally in desperate need of chaperones to fold, other proteins fold spontaneously under normal conditions and only require chaperones during difficult situations. Consequently, many of the chaperones are especially highly expressed upon different stresses like high temperatures and therefore are named heat shock proteins (Hsps) [Lindquist and Craig, 1988]. The upregulation of the Hsps is a central part of the heat shock response which is induced mainly by one transcription factor, in eukaryotes this is the heat shock factor HSF [Richter et al., 2010].

Molecular chaperones can be divided into five major families which are named according to their molecular mass in kDalton: small heat shock proteins (sHsps), Hsp60, Hsp70, Hsp90 and Hsp100 (Figure 1.2). Generally, the mechanism of chaperones involves controlled binding and release of substrate proteins. Usually, the chaperones switch between states with different substrate affinity and this switch is regulated by ATP hydrolysis. These ATP-driven folding machines are called 'foldases'. In contrast, sHsps, mostly present as large oligomers, bind folding intermediates in an ATP-independent reaction ('holdases'). This prevents aggregation but release of the intermediates requires ATP-dependent chaperones which are able to refold the proteins [Haslbeck et al., 2005].
Another strategy is to encapsulate the substrate protein like Hsp60s (also referred to as chaperonins) do. The most prominent member of Hsp60s is the heat-inducible GroEL/ES complex in *E. coli*. GroEL forms a barrel composed of heptameric rings [Horwich et al., 2006, Tyagi et al., 2009]. In its cavity, proteins up to 60 kDa can be bound. GroES closes the cavity in the presence of ATP so that substrates are protected from aggregation in a crowded environment. ATP hydrolysis releases the substrate. Its eukaryotic and archaeal counterparts, called CCT/TRiC (Chaperonin containing TCP-1/TCP-1 ring complex) machinery and thermosome, follow a similar mode of action but are less well characterized [Spiess et al., 2004, Cong et al., 2011].

The most ubiquitously expressed chaperones in eukaryotes are Hsp70 and Hsp90. They are involved in the folding and activation of a wide range of key regulatory proteins such as kinases, transcription factors and steroid hormone receptors. To accomplish this, they cooperate in a multichaperone complex which can exist only in the presence of the adaptor protein Sti1/Hop [Chen and Smith, 1998]. The chaperone function of both Hsp70 and Hsp90 relies on conformational changes and an associated ATPase activity which are regulated by a set of cochaperones.
Hsp70 is also crucial for the first steps of protein folding as it associates with nascent chains emerging from the ribosome in eukaryotes. In bacteria, the so called trigger factor takes over this function. For most bacterial proteins, the interaction with trigger factor is sufficient to reach the native state [Hartl and Hayer-Hartl, 2002, Hoffmann et al., 2012]. Less well described are the Hsp100 chaperones (named Clp in *E.coli*).

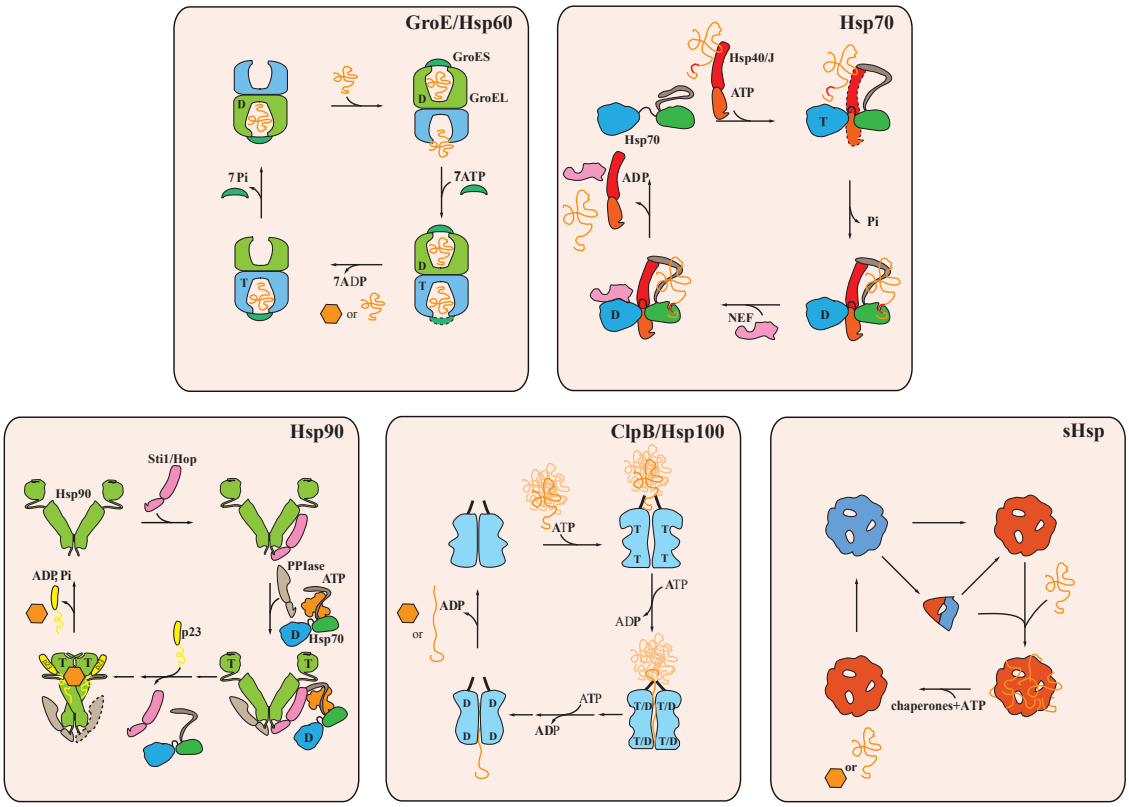

Figure 1.2: Concept of chaperone machineries. GroE/Hsp60: Two GroEL rings each enclose a central cavity where nonnative proteins are bound. Upon binding of ATP and GroES, the substrate is trapped. ATP hydrolysis results in release of the substrate. Hsp70: Hsp40/J-proteins deliver the substrate to Hsp70 and stimulate its ATPase activity. Hsp70 stabilizes the substrate in an ATP-dependent manner. NEFs induce the exchange of nucleotide. Hsp90: Substrates are delivered from Hsp70 to Hsp90 via Sti1/Hop. A complex network of cochaperones contributes to the cycling between an open and a closed conformation of Hsp90 which is coupled to ATP hydrolysis. ClpB/Hsp100: Proteins are pulled through a central channel of a hexameric structure. sHsps: sHsps form large oligomers which often exist in a active and an inactive version. They suppress aggregation by binding non-native proteins. Adapted from [Richter et al., 2010].

These ATPases are believed to pull misfolded proteins through the central pore of their hexameric ring in an unfolded state which enables proteins to refold [Barends et al., 2010, Doyle and Wickner, 2009].
Importantly, the different chaperone machineries work together cooperatively and transfer from one system to another occurs [Young et al., 2004]. In addition to molecular chaperones, folding catalysts like protein disulfide isomerases (PDIs) which reduce the specific energy barrier of slow processes also contribute to these processes [Wilkinson and Gilbert, 2004].

1.3 Hsp70 is a multi-talent chaperone

The Hsp70 family is the most conserved group of chaperones and is present in all kingdoms of life. Members of this family serve in a broad range of folding events starting from assisting folding of the nascent chain, suppressing aggregation upon stress, to refolding of aggregated proteins. They also play a role for the transport of proteins across membranes. Hsp70 accomplishes all of its functions in principle by recognizing and stabilizing exposed hydrophobic patches of the substrates in an ATP-controlled manner [Mayer and Bukau, 2005].
Most organisms express a set of different Hsp70 isoforms which have developed different substrate specificities. In *E. coli*, DnaK is the major Hsp70 in the cytosol whereas eukaryotes harbor multiple homologs in the cytosol as well as in different organelles. The cytosolic variants exhibit a broad substrate spectrum and interact with early folding intermediates right after synthesis. Actually, 15-20% of all proteins transiently interact with Hsp70 during their biogenesis [Thulasiraman et al., 1999].

In mammals, two isoforms are expressed in the cytoplasm, one is heat-inducible (Hsp70) whereas the other one is constitutively expressed (Hsc70). In *S. cerevisiae*, there are even nine Hsp70 isoforms in the cytosol (Ssa1-4, Ssb1-2, Sse1-2, Ssz). Ssa1-4 bind mostly post-translationally to a restricted set of polypeptides [Yam et al., 2005]. Only this group is essential and contains the C-terminal EEVD motif which enables the interaction with TPR (tetratricopeptide repeat) cochaperones [Chang and Lindquist, 1994]. One of the most important TPR cochaperones is Sti1/Hop which serves as an adaptor for the transfer of clients onto Hsp90. Ssb and Ssz proteins are directly associated with the ribosome and bind slowly translated and aggregation-prone nascent chains co-translationally [Nelson et al., 1992, Willmund et al., 2013].
Sse1 and Sse2 are more distantly related to the other Hsp70 homologs and belong to the Hsp110 group. Interestingly, they act as nucleotide exchange factors for other Hsp70s [Raviol et al., 2006].

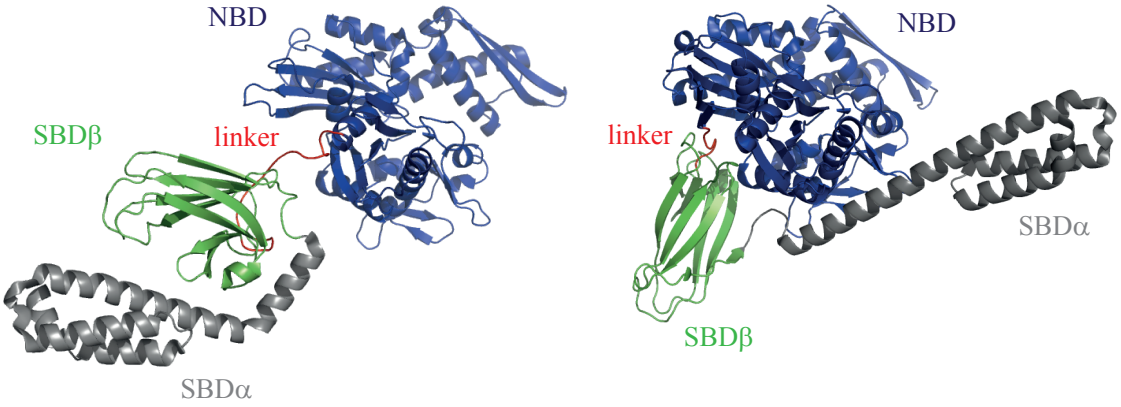

Figure 1.3: Structure and conformations of Hsp70. Crystal structure of E. coli Hsp70 DnaK in the ADP-bound state (left, PDB: 2KHO) and in the ATP-bound conformation (right, PDB: 4JNE). The NBD (blue) is connected to the SBD (green and grey) via a flexible linker (red). The SBD contains the lid (SBDα, grey) and SBDβ (green). In the ADP state, the lid blocks the peptide binding site of the SBDβ, while in the open ATP-bound state, the lid is peeled away from the SBDβ.

1.3.1 Structure and mechanism of Hsp70

The different Hsp70 homologs share the same basic structure [Mayer and Bukau, 2005]. They consist of a N-terminal nucleotide binding domain (NBD) which harbors the ATPase function and a C-terminal substrate binding domain (SBD) (Figure 1.3). The intrinsic ATPase activity of Hsp70 is very low but can be accelerated by cochaperones of the Hsp40 family [Knarr et al., 1999]. The NBD and the SBD are connected via a flexible linker. The SBD is further divided into a β-sheet sandwich consisting of eight strands which contains a cleft for substrate binding and a regulatory α-helical lid which can cover the cleft [Bukau et al., 2006]. Peptide substrates bind to the SBD in an extended conformation through a channel defined by loops of the beta sandwich [Zhu et al., 1996]. The substrate binding site is not as conserved as the other parts of Hsp70s which goes hand in hand with the rather degenerated substrate binding motif and the existence of specialized Hsp70 variants.

The folding mechanism of Hsp70 depends on cycles of binding and releasing the substrate until the folded state is reached [Mayer and Bukau, 2005]. For this function, large conformational changes are necessary which are regulated allosterically and involve extensive communication between the domains of Hsp70 (Figure 1.4). Peptide binding to the SBD induces conformational rearrangements in the NBD which stimulate ATP hydrolysis. Hydrolysis of ATP in turn results in closing of the lid which strongly enhances binding to the peptide (Figure 1.3) [Kityk et al., 2012, Zhuravleva et al., 2012]. After that, nucleotide exchange factors like BAG-1 complete the cycle.

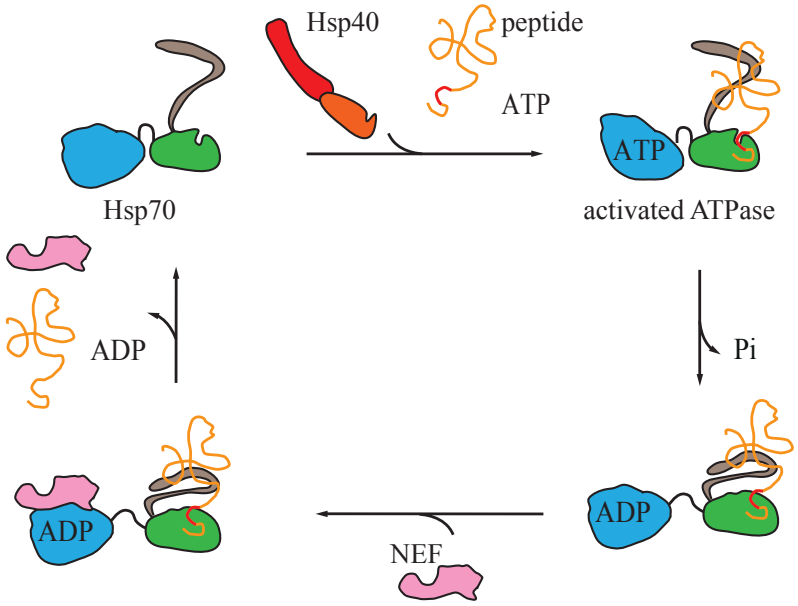

Figure 1.4: Mechanism of Hsp70. Hsp40 delivers substrates to Hsp70. Peptide binding to Hsp70-SBD (green) induces conformational rearrangements in the NBD (blue) which accelerate ATP hydrolysis. This is accompanied by closing of the lid (grey) which enhances the affinity to the peptide. Nucleotide exchange factors (NEFs) complete the cycle and the substrate is released. Adapted from [Richter et al., 2010].

1.3.2 Cooperative actions of Hsp70

Hsp70 fulfills many of its task only in conjunction with different cofactors. An important group are the Hsp40/DnaJ cochaperones. They bind unfolded polypeptides and deliver them to Hsp70. Moreover, Hsp40s stimulate the ATPase activity of Hsp70s thereby driving the cycle [Knarr et al., 1999]. They are composed of various functional domains, of which the conserved J domain is the defining region. The J domain interacts with the NBD and the linker of Hsp70s [Kampinga and Craig, 2010].
Hsp40s are expressed in many divergent isoforms and contribute to the different specificities of Hsp70 variants. Interestingly, the number of Hsp40s in the cell excels the number of Hsp70s. Of these, Ydj1 and Sis1 are the specific ones for the Ssa class which is focus of this work. Nucleotide exchange factors like BAG-1 bind to the NBD of Hsp70 and determine the lifetime of the Hsp70-substrate complex.

In addition, TPR cochaperones like Hop and Hip regulate cytosolic variants of Hsp70 and provide the link to the Hsp90 machinery for more specialized tasks. Moreover, Hsp70 cooperates with Hsp100 when it comes to solubilize aggregates and is important for the release of substrates from sHsps [Richter et al., 2010].

1.4 Hsp90 is a master regulator in eukaryotes

In the eukaryotic cytosol, Hsp90 is the most abundant chaperone comprising 1-2% of the total proteome. In contrast to the other chaperones, it does not interact promiscuously with unfolded polypeptides but exhibits a specific client profile. As these clients are involved in many important biological processes like signal transduction, telomere maintenance, steroid signaling, immune response and cancer development, Hsp90 plays a key role in the cell [Makhnevych and Houry, 2012].
Moreover, Hsp90 acts as a capacitor of evolution by buffering genetic variations because it stabilizes mutant proteins or unstable conformations [Jarosz and Lindquist, 2010, Taipale et al., 2010]. This may also be the reason why Hsp90 is intriguingly important in cancer cells. In tumor cells, Hsp90 is often overexpressed and highly active. This is directly linked to the progression and invasiveness of tumors [Siegelin, 2013]. Inhibitors which specifically target Hsp90 are therefore a promising therapeutic approach.

Hsp90 homologs are expressed in different organelles and in the cytosol, the latter one is absolutely essential for eukaryotes. Hsp90 may also be secreted from the cell where it specifically plays a role in tumor invasiveness [Wang et al., 2009]. In yeast and mammals, two isoforms exist in the cytosol: one is heat-inducible (Hsp82/Hsp90α) whereas the other one is constitutively expressed (Hsc82/Hsp90β). Another distinguishing feature of this essential version is its dependence on a large network of cochaperones which modulate Hsp90's function. Organellar homologs of Hsp90 like Trap1 in mitochondria or Grp94 in the ER as well as bacterial HtpG interestingly do not rely on cochaperones. In bacteria, Hsp90 seems not to have the same importance as in eukaryotes as it is not essential and few specific clients have been identified yet [Buchner, 2010].

1.4.1 Structure and ATPase function of Hsp90

Hsp90 is a dimer with each subunit consisting of three domains: an N-terminal ATP binding domain, a middle domain and a C-terminal dimerization domain (will be referred to as Hsp90-N, -M, -C) (Figure 1.5). A flexible linker connects Hsp90-N with Hsp90-M in eukaryotes which was deleted in the crystal structure. The C-terminus of eukaryotic cytosolic Hsp90 ends with EEVD, a motif which allows for the interaction with TPR cochaperones.
Hsp90 undergoes large conformational changes from an 'open' to a 'closed' state which are coupled to ATP hydrolysis (Figure 1.6. In the absence of nucleotides, Hsp90 adopts an open conformation [Shiau et al., 2006]. ATP binding induces closure of the lid over the bound nucleotide and causes the two N-terminal domains to dimerize leading to a twisted conformation [Ali et al., 2006]. After ATP hydrolysis, Hsp90 returns to the

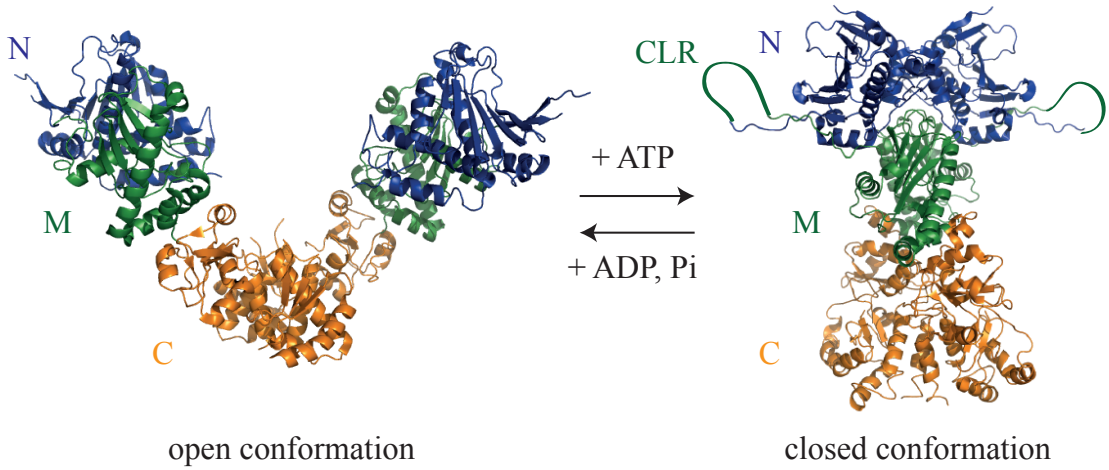

Figure 1.5: ATP-dependent conformational changes of Hsp90. Crystal structure of open Hsp90 (left, HtpG from *E. coli*, PDB: 2IOQ) and closed Hsp90 (right, Hsp90 from *S. cerevisiae*, PDB: 2CG9). The C-terminal domain (orange) is constitutively dimerized. In eukaryotes, the middle domain (green) and the N-terminal ATP-binding domain (blue) are connected via a charged linker region (CLR). Upon binding of ATP, the N domains associate. Adapted from [Röhl et al., 2013].

open state. Hsp90 turns over ATP very slowly but not the ATP hydrolysis itself but the conformational changes are the rate-limiting step of this process [Hessling et al., 2009, Richter et al., 2008]. In eukaryotic Hsp90, these conformational changes occur spontaneously and it is suggested that cochaperones stabilize specific conformations and thereby drive the cycle [Röhl et al., 2013].
Hsp90 belongs to the split ATPases, the so called Gyrase, Hsp90, Histidine Kinase, MutL (GHKL) domain ATPases, which bind ATP in a kinked conformation [Prodromou et al., 1997]. This unusual interaction is accompanied by a low binding affinity. Specific inhibitors like radicicol and geldanamycin bind much stronger to the ATP binding pocket [Sharma et al., 1998]. These substances and their derivates are therefore potent antitumor drug candidates [Alarcon et al., 2012].

1.4.2 Interaction of Hsp90 with clients

Hsp90 acts in the late stage of folding of a specialized set of client proteins. Steroid hormone receptors, oncogenic kinases like v-Src, and the tumor suppressor p53 rank among the best characterized ones. These clients belong to different families and share no common structural features. In line with this, a universal recognition site for Hsp90 has not been identified. It seems that the only characteristic that clients of Hsp90 share is their intrinsic instability [Taipale et al., 2012]. Exactly this makes studies on the interaction of Hsp90 with its clients challenging. A common client binding site

on Hsp90 may not exist as different regions of Hsp90 have been implicated [Pratt and Toft, 1997, Vaughan et al., 2006, Hagn et al., 2011, Brady et al., 2011, Genest et al., 2012]. Importantly, the mechanism by which activation of the client actually occurs is also still a mystery.
Hsp90 may be able to selectively recognize and interact with different clients because it can be adjusted precisely by cochaperones. Evidence for this are the number of client-specific cochaperones like Cdc37 for kinases, Sgt1 which is needed for the activation of nucleotide-binding leucine-rich repeat receptors or the group of peptidyl-prolyl isomerases (PPIases) which are selective for particular steroid hormone receptors [Barent et al., 1998, Zhang et al., 2010, Taipale et al., 2012]. Also, client diversity is correlated with the occurrence of cochaperones in an organism [Johnson and Brown, 2009]. Another layer of regulation is given by the posttranslational modifications. Hsp90 is highly phosphorylated and also acetylation, nitrosylation, glycosylation and methylation play a role [Mollapour and Neckers, 2012].

1.4.3 Cochaperones govern the Hsp90 cycle

A complex network of cochaperones dictates the conformational cycle of Hsp90. Cochaperones bind to Hsp90 via different surfaces, most often via TPR domains. Some of them confer additional functions such as phosphatases (Pp5/Ppt1) or peptidyl-prolyl isomerases. Others act as client recruiters like Cdc37 which specifically binds Hsp90 in complex with kinases [Vaughan et al., 2006]. Different from that is the ubiquitin ligase CHIP which directs Hsp90-bound clients to the degradation by the proteasome [Kundrat and Regan, 2010].
Cochaperones can stabilize specific conformations of Hsp90 which often impacts the rate of ATP hydrolysis. Aha1 for example promotes the formation of a closed conformation which goes hand in hand with a strong acceleration of ATPase activity [Retzlaff et al., 2010]. Intriguingly, some cochaperones have been found in asymmetric complexes with Hsp90 and another cochaperone while others are able to displace specific Hsp90-cochaperone interactions [Pratt and Toft, 2003, Siligardi et al., 2004, Li et al., 2010, Ebong et al., 2011, Hildenbrand et al., 2011, Zuehlke and Johnson, 2012, Li et al., 2013a]. Together, this has lead to a general model for the progression of the chaperone cycle which is based on a sequential binding of different cochaperones to Hsp90 (Figure 1.6): The client which is bound by Hsp70 is loaded onto Hsp90 via Sti1 which simultaneously binds to both Hsp70 and Hsp90. Only one Sti1 binds to the Hsp90 dimer and this complex readily associates with a PPIase like Cpr6. In this complex, ATP hydrolysis is inhibited. The activator Aha1 displaces Sti1 and Hsp70 from the complex and induces the closed state of Hsp90. Finally, binding of p23 displaces Aha1 leaving Hsp90 in a hydrolysis competent state. After ATP hydrolysis, the activated client and the cochaperones are released.

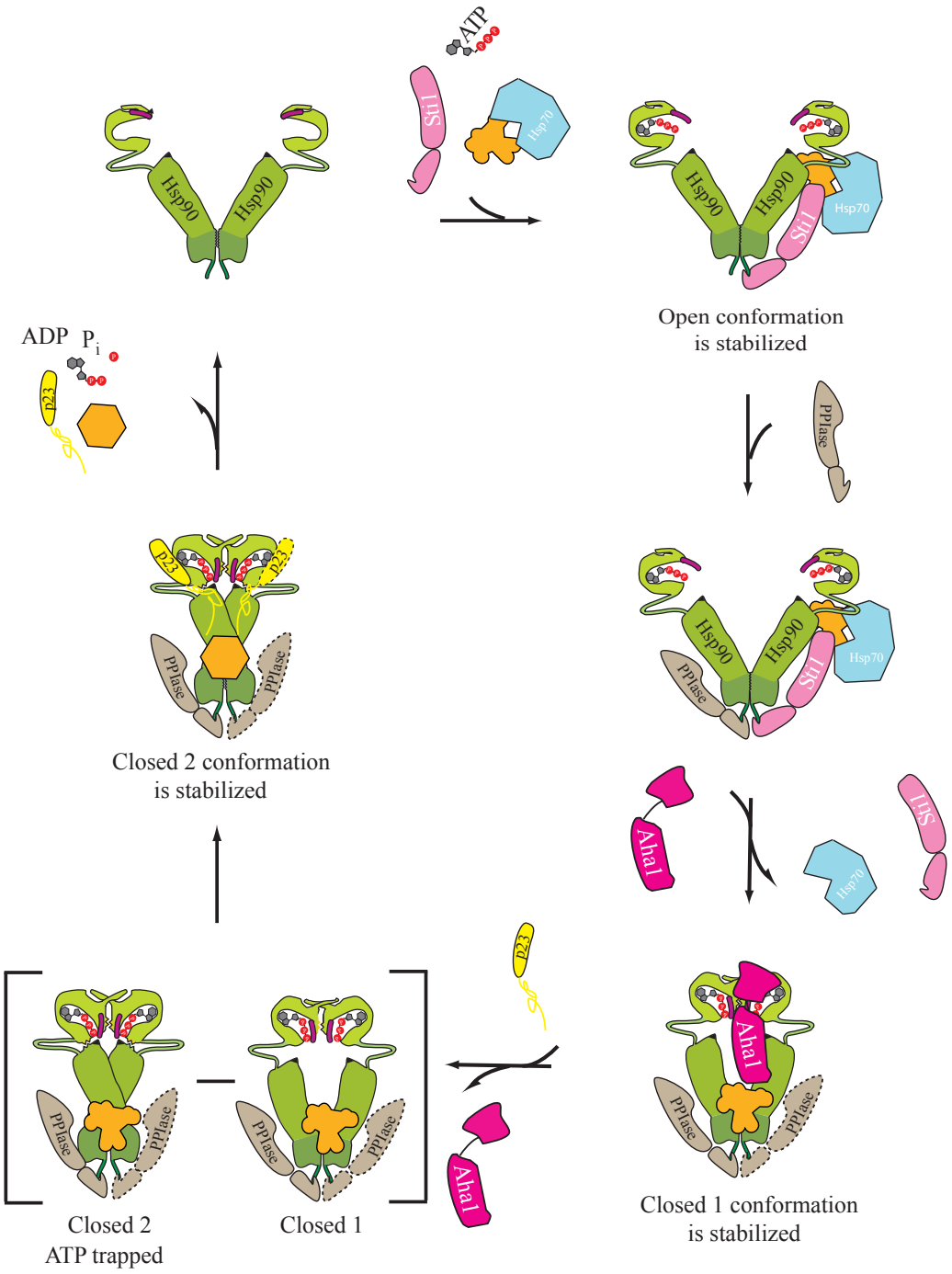

Figure 1.6: Cochaperone cycle of Hsp90. The Hsp70-bound client is loaded onto the open conformation of Hsp90 via Sti1. This ATPase-inhibited state is primed for the association of a PPIase. Aha1 displaces Sti1 and Hsp70 from the complex and accelerates the formation of an N-terminally closed state (closed 1). The completely closed state (closed 2) is induced by the binding of p23 which displaces Aha1. Finally, ATP is hydrolyzed and the client and cochaperones are released. Adapted from [Röhl et al., 2013].

Figure 1.7: Scheme of Sti1/Hop domains. Two modules comprising TPR (tetratricopeptide repeat) and DP (aspartate proline rich) domains are connected via a linker.

1.5 Sti1 connects Hsp70 and Hsp90

Sti1/Hop (Stress-inducible protein 1/ Hsp70-Hsp90-organizing protein) is a highly conserved cochaperone which acts as an adaptor between Hsp70 and Hsp90. Despite the high conservation, the homolog from *S. cerevisiae* will be referred to as Sti1 and the mammalian counterpart as Hop. Sti1/Hop is one of the few cochaperones which is substantially upregulated upon stress [Nicolet and Craig, 1989]. It is usually located in the cytoplasm, but mouse Hop was shown to be translocated to the nucleus after heat shock or specific phosphorylation [Daniel et al., 2008].
Besides simultaneously binding Hsp90 and Hsp70, Sti1 also slows down the Hsp90 ATPase activity [Prodromou et al., 1999]. This inhibition is achieved by stabilizing the open conformation of Hsp90 and involves docking of Hsp90-M with Hsp90-N [Richter et al., 2003, Hessling et al., 2009, Lee et al., 2012].

The function of Sti1/Hop is provided by its complex composition of domains. It contains two modules comprising TPR and DP (aspartate and proline rich) domains (Figure 1.7). While the TPR domains are responsible for recognizing Hsp90 and Hsp70, the DP domains contribute to substrate activation. The structures of the individual domains have been solved recently [Scheufler et al., 2000, Schmid et al., 2012]. Interestingly, although it is one of the most widely spread and conserved cochaperones comparing different organisms, some homologs like in *D. melanogaster* and *C.elegans* lack N-terminal parts of the protein [Gaiser et al., 2009, Johnson and Brown, 2009].

Among the different cochaperones, the TPR domain is a common interaction module. Examples for TPR-containing cochaperones are the large group of PPIases and the phosphatases. The TPR domain is defined by tandem repeats of a 34 amino acid consensus motif which form a cleft of 7 antiparallel α-helices capable of binding the C-terminal tails of Hsp90 and Hsp70, both ending in EEVD [Smith, 2004] (Figure 1.8). Binding of the peptide is primarily mediated by electrostatic interactions with the EEVD motif. The aspartate interacts with the 'carboxylate clamp' of the TPR domain, a highly conserved pattern among TPR domains. Additionally, hydrophobic interactions with residues upstream of the motif occur which are critical for specificity [Scheufler et al., 2000]. This results in the fact that most TPR cochaperones exhibit a pronounced specificity for Hsp90 or Hsp70. Moreover, often a second binding site contributes to this. However, from the large group of TPR containing proteins, a large

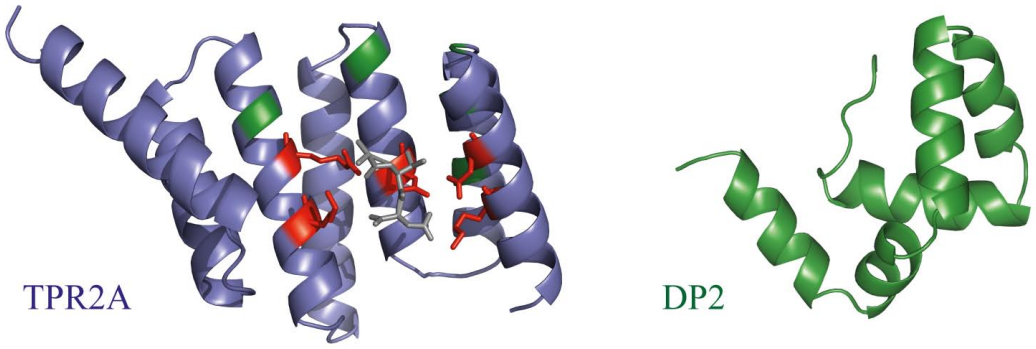

Figure 1.8: Structure of TPR and DP domains. Left: Structure of TPR2A from Sti1, the conserved carboxylate clamp is highlighted in red which interacts with the peptide (grey), Hsp90 specific interactions occur with the green residues. Right: Structure of DP2 (PDB: 2LLW) from Sti1.

fraction does not bind Hsp90 or Hsp70 but has a different function [Haslbeck et al., 2013].
In Sti1, the interaction with Hsp90 is mediated via TPR2A-TPR2B and this element is sufficient for the inhibition of the ATPase activity of Hsp90 (Figure 1.9). While Hsp90's C-terminal tail interacts with the peptide binding groove of TPR2A, Hsp90-M associates with TPR2B but leaves its peptide binding groove accessible [Schmid et al., 2012]. In addition, an interaction with Hsp90-N has been indicated [Lee et al., 2012].
For Hsp70, the situation is not as clear, as different TPR domains have been found to be involved in this interaction. Again, the EEVD motif is apparently not the only binding site of Hsp70 for Sti1 [Carrigan et al., 2004, Flom et al., 2007]. The interaction seems to be of a complex nature as the relatively low affinity of Hsp70 towards Sti1 may be enhanced by Hsp90 or Hsp40 [Hernández et al., 2002].
The precise regulation of the affinities of different TPR cochaperones for Hsp90 and Hsp70 seems to be of essential importance. An example how this can impact the fate of the bound client is the competition between CHIP and Hop in mammals which is regulated via phosphorylation of Hsp90 and Hsp70. As CHIP targets the clients for degradation, this is a mechanism to control the balance between protein folding and degradation [Kundrat and Regan, 2010].

Apart from the TPR domains, Sti1/Hop contains α-helical DP domains (Figure 1.8). This fold does not share homology with any other solved structure [Schmid et al., 2012]. Based on sequence alignments, another protein was identified which also contains a DP domain followed by a TPR domain, subsequently named Hip. It also interacts with Hsp70 but interestingly, not with the C-terminal EEVD but with the N-terminal domain of Hsp70 suggesting that such an interaction may play take place in Sti1/Hop as well [Höfeld et al., 1995, Torres et al., 2009]. Hip is considered to stabilize Hsp70-client complexes by retarding the dissociation of ADP from Hsp70 [Li et al., 2013b].

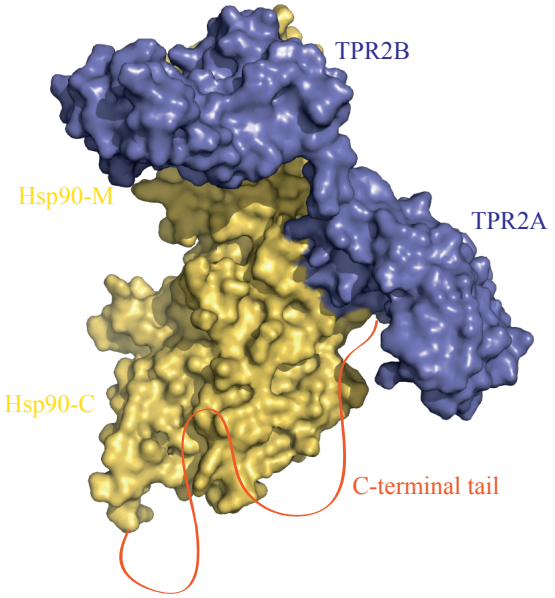

Figure 1.9: Docking model of the complex between TPR2A-TPR2B and Hsp90-MC. Hsp90-MC of one subunit of the dimer is shown (yellow) with the flexible C-terminal tail (orange) which contacts the peptide binding groove of TPR2A. Additional interactions occur between both TPR domains and Hsp90-M. The peptide binding groove of TPR2B is accessible. Adapted from [Schmid et al., 2012].

With its central position in the Hsp70-Hsp90 pathway, Sti1/Hop participates in the folding and activation of key regulatory proteins. This makes it a possible target for cancer therapy [Pimienta et al., 2011]. Understanding the complex nature of the assembly of this troika and its regulation could contribute to the development of novel drugs.

CHAPTER 2

RESULTS AND DISCUSSION

2.1 Role of the TPR domains of Sti1

Sti1 comprises three TPR domains (TPR1, TPR2A, TPR2B) which contain the interaction sites for the C-terminal EEVD tails of Hsp90 and Hsp70. Crystallographic and peptide binding studies showed that while TPR1 preferentially binds Hsp70 peptides, TPR2A is highly specific for Hsp90 peptides [Scheufler et al., 2000, Schmid et al., 2012]. The TPR2B domain seems not to have a preferred binding partner based on its peptide binding properties.
In the interaction of Sti1 with Hsp90, not only the C-terminal EEVD binds to the peptide binding groove of TPR2A but additional interactions between Hsp90-M and regions in TPR2A-TPR2B distinct from their peptide binding grooves have been mapped by NMR experiments [Schmid et al., 2012]. As these studies concentrated on isolated domains or peptides, interaction analysis including full-length proteins and in the context of both chaperones were performed in order to provide a more comprehensive picture of how Sti1 functions.

2.1.1 TPR domain requirements for complex formation in vitro

A suitable method to monitor interactions between multiple proteins in solution without any matrix or surface is analytical ultracentrifugation. With the help of Sti1 mutants and fragments, this technique was used to investigate which of the TPR domains is required for complex formation with Hsp70 and Hsp90.
For this purpose, yHsp70 (Ssa1) was labeled with carboxyfluorescein (FAM, degree of

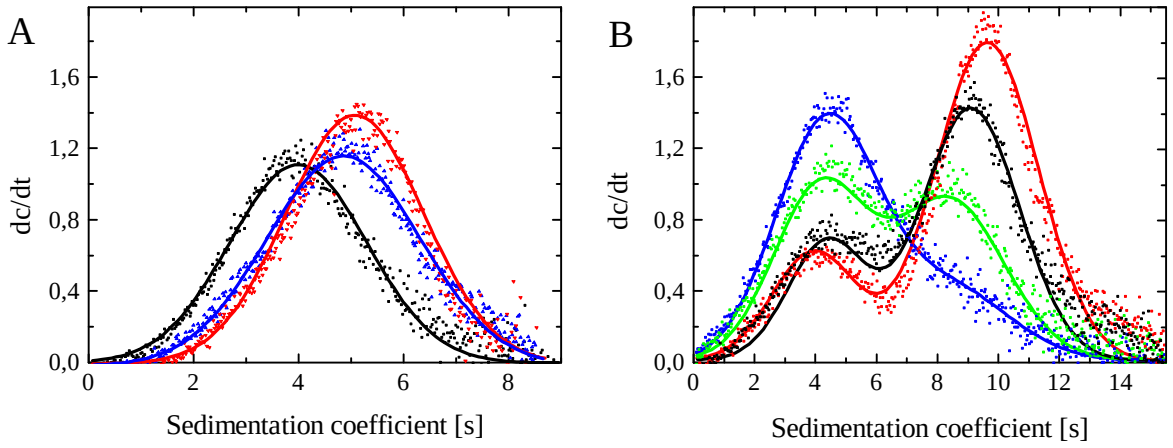

Figure 2.1: Formation of complexes between labeled yHsp70, Sti1 variants and yHsp90 investigated by analytical ultracentrifugation. A: Binary complexes formed by labeled yHsp70 (black: yHsp70 alone) with Sti1 wildtype (red) and with TPR2A-TPR2B (blue). B: Ternary complexes formed by labeled yHsp70 with yHsp90 and Sti1 wildtype (black), Sti1 N435A (red), TPR2A-TPR2B (green). TPR2A-TPR2B N435A (blue) formed no complexes with Hsp70. 0.5 µM labeled yHsp70 and 3 µM of unlabeled proteins were used. The data was fitted with (bi-) Gaussian functions.

labeling = 70 %) and the other components were added unlabeled. Fluorescence detection during the ultracentrifugation allowed only yHsp70 and complexes containing it to be detected.

Alone, Hsp70 sedimented with 4 S and after addition of Sti1 wildtype, the peak shifted to 5.5 S indicating the formation of the binary complex (Figure 2.1, A). In the additional presence of yHsp90 (Hsp82), a shift to about 9 S was observed which represents the ternary complex (Figure 2.1, B). This basic setup allowed to analyze the ability of different Sti1 variants to form ternary complexes.
The fragment comprising only the central element of the protein, TPR2A-TPR2B, was able to form binary complexes with labeled yHsp70 (5 S) and ternary complexes together with yHsp90 (8.5 S). Complexes resulted in slightly smaller sedimentation coefficients as TPR2A-TPR2B is only about half the size of full-length Sti1. This shows that the two domains already support the simultaneous binding of both chaperones.

To identify the role of TPR2B, mutations in its peptide binding groove were introduced into different Sti1 constructs. Here, conserved residues from the carboxylate clamp were replaced by alanine (N435A, R465A, R469A; Figure 2.2). These mutations in the isolated TPR2B domain caused complete loss of their ability to bind the Hsp70 peptide although the proteins were structurally intact (Stephan Lagleder, PhD Thesis). In the analytical ultracentrifugation setup using TPR2A-TPR2B containing the mutations, no complex formation with Hsp70 was detected. This proves that introduction

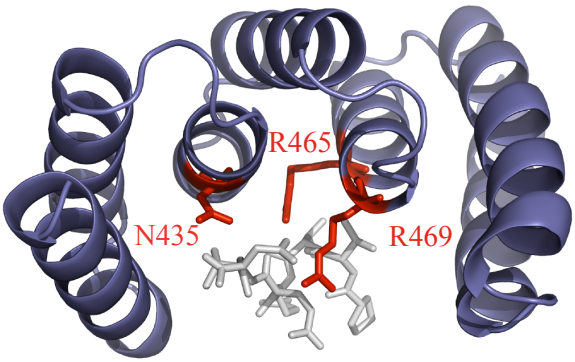

Figure 2.2: Mutations in the peptide binding groove of TPR2B. PDB: 3UPV, Hsp70 peptide is shown in grey, mutated positions in red.

of these point mutations disrupts the ability of TPR2A-TPR2B to bind Hsp70. In contrast, full-length Sti1 harboring the mutations was still able to form ternary complexes (Figure 2.1, B). This demonstrates that another region of Sti1 besides TPR2A-TPR2B is able to bind Hsp70.
The amount of ternary complex formed differed for the Sti1 variants. For TPR2A-TPR2B, less ternary complexes were monitored, whereas for Sti1 N435A, the ternary complex was more populated compared to Sti1 wildtype. This indicates altered affinities of the Sti1 variants towards Hsp70 and/or Hsp90 which will be again in addressed in following sections (see section 2.2).

In conclusion, ternary complexes between Sti1, Hsp90 and Hsp70 can be visualized by analytical ultracentrifugation. To my knowledge, this is the most direct and convincing proof of the existence of this complex. Others used indirect methods like co-immunoprecipitation or mass spectrometry to demonstrate the presence of ternary complexes [Chen and Smith, 1998, Wegele et al., 2003, Flom et al., 2007, Ebong et al., 2011].
Moreover, ternary complexes can already be formed with TPR2A-TPR2B but not after mutating TPR2B within this construct. Together with the information that TPR2A is highly specific for Hsp90 [Scheufler et al., 2000, Schmid et al., 2012], this suggests that in the two-domain-construct, TPR2A binds the C-terminal tail of Hsp90 while TPR2B contacts the C-terminal tail of Hsp70.
Strikingly, full-length Sti1 supports simultaneous binding of both chaperones even if TPR2B is disrupted. Again assuming that TPR2A is the main interaction site for Hsp90 and with TPR2B not being accessible, TPR1 must serve also as a Hsp70 binding site. TPR1 has been implemented in this function before [Scheufler et al., 2000, Odunuga et al., 2003, Carrigan et al., 2004] but it was never investigated in the presence of Hsp90.

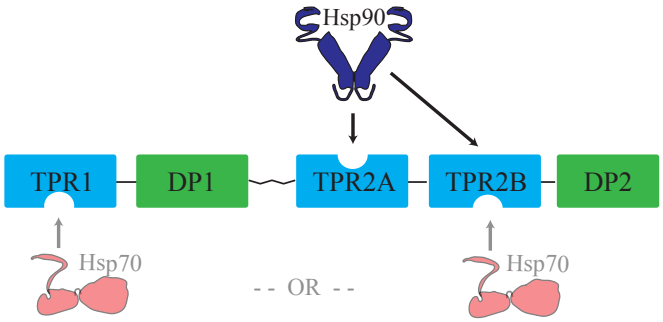

Figure 2.3: Summary of TPR domain interactions. Hsp90 binds with its C-terminal part mainly to TPR2A and at the same time, additional interactions occur between Hsp90-M and TPR2B. Hsp70 can contact two alternative binding sites in Sti1, TPR1 and TPR2B.

This is schematically summarized in Figure 2.3: While Sti1 contains one main Hsp90 binding site (peptide binding groove of TPR2A), there are two alternative Hsp70 binding sites (peptide binding grooves of TPR1 and of TPR2B) which both individually allow the formation of ternary complexes.

2.1.2 Function of TPR domains in vivo

As a client of both Hsp70 and Hsp90, the activation of the glucocorticoid receptor (GR) is dependent on a functional chaperone machinery. Using a *S. cerevisiae* strain harboring an expression plasmid for human GR and a corresponding β-Galactosidase reporter plasmid, the amount of mature GR can be measured. The observation that in Δ*sti1* yeast cells, GR activation is compromised [Chang et al., 1997] was used to address whether certain variants of Sti1 can substitute in this process. The role of different Sti1 fragments on the maturation of the GR had already been established by Dr. Andreas Schmid [Schmid et al., 2012]. In these experiments, it has become evident that the DP domains are very important for GR activation *in vivo* and that TPR1 is not necessary at least for this particular client. This indicated that only one of the two Hsp70 binding sites is necessary in this context.

To prove this, different Sti1 constructs harboring the mutations in the peptide binding groove of TPR2B were generated in p425 vectors. After transformation in Δ*sti1* yeast strains containing GR expression and GR reporter plasmids, these were tested for GR activation *in vivo* (Figure 2.4).
The loss of TPR1 (ΔTPR1) did not change GR activation compared to wildtype but after introduction of the mutations in TPR2B failed to support GR activation and showed only background levels. Also with full-length Sti1 containing the mutations, GR activity was completely abolished.

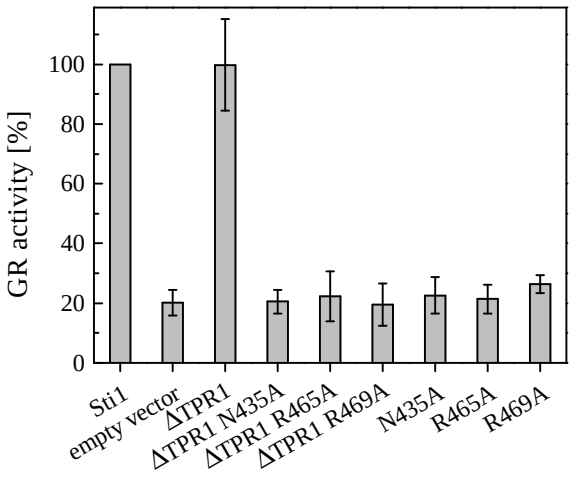

Figure 2.4: Effects of TPR2B defective mutants on GR activation in *S. cerevisiae*. Mutations in the peptide binding groove of TPR2B in the context of full-length Sti1 as well as in TPR1 deleted Sti1 disrupt ability to support GR activation. Means of at least three independent experiments are shown with their standard deviation.

Together, this shows that TPR2B is the crucial Hsp70 binding site for GR activation *in vivo* and that TPR1 cannot compensate for the loss of TPR2B peptide binding in this process.
This raised the question whether Sti1 uses the two different Hsp70 binding TPR domains depending on the specific client which is to be transferred. Different clients could require different orientations or distances between Hsp70 and Hsp90 during their transfer which might be conveyed by Hsp70 binding to either TPR1 or TPR2B. Moreover, it was unclear if the maturation of clients is generally linked to the same domains of Sti1. Therefore, the activity of another client, V-Src, was tested for its dependence on different Sti1 domains. V-Src belongs to a different class of clients, the kinases, and is considered strikingly different to GR. Once V-Src is properly activated, it is toxic and leads to death of wildtype yeast. In contrast, Δ*sti1* yeast strains survive as less V-Src is activated [Chang et al., 1997]. This allowed to measure the level of V-Src activation of Δ*sti1* strains substituted with Sti1 fragments by a growth assay.

Plasmids expressing the different Sti1 fragments were transformed into Δ*sti1* cells harboring a galactose-inducible V-Src expression plasmid and growth was assessed on galactose medium as well as on glucose medium as a control (Figure 2.5). After introduction of a plasmid expressing Sti1 in Δ*sti1* strains, the cells behaved like wildtype yeast and were not able to grow on galactose anymore.
Strikingly, most of the fragments restored viability under V-Src expressing conditions showing that they were not able to support V-Src activation. Already deletion of DP2 lead to loss of V-Src activity. TPR1, in contrast, was dispensable for V-Src activation as cells expressing ΔTPR1 were not able to grow on galactose.

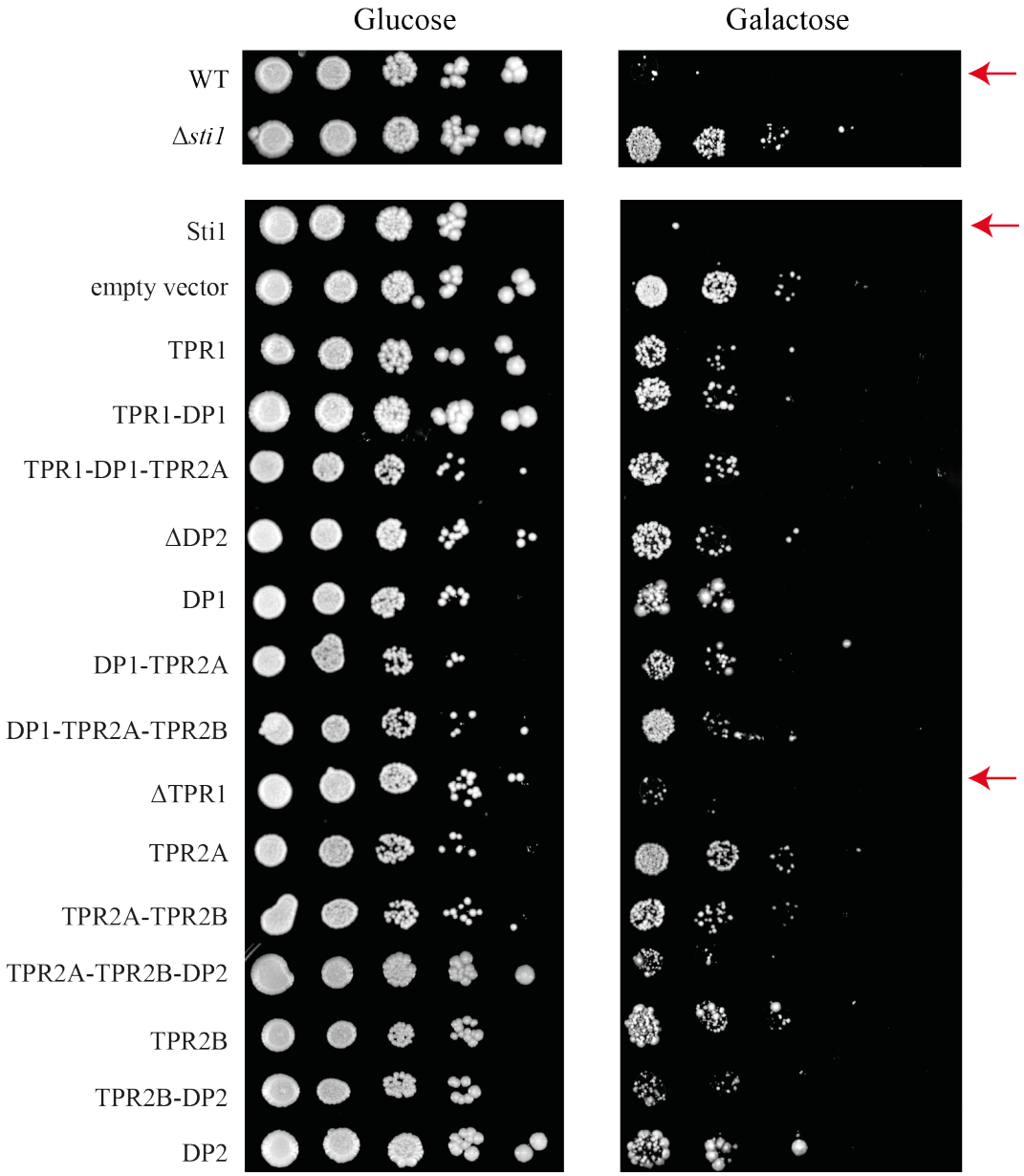

Figure 2.5: V-Src activation in *S. cerevisiae* in dependence on Sti1 fragments. Dilution series of wildtype and Δ*sti1* yeast strains expressing V-Src under a galactose promotor grown on glucose (left) and galactose (right). In Δ*sti1* yeast, plasmids for expression of Sti1 fragments were introduced. The red arrows indicate strains for which growth on galactose was inhibited the most which translates into highest levels of V-Src activation.

In conclusion, V-Src activation is dependent on the same domains of Sti1 as GR activation: TPR1 is dispensable which leaves only TPR2B as the Hsp70 binding site. The DP domains, especially DP2, are important for client activation. This suggests that the mechanism by which Sti1 transfers clients from Hsp70 to Hsp90 is basically the same for different clients. The finding that TPR2B is the important Hsp70 binding site *in vivo* but *in vitro* Hsp70 can interact with TPR1 or with TPR2B leads to the idea that TPR1 presents an 'inactive' Hsp70 binding site which does not contribute to client activation but might play a role for storage or delivery of Hsp70. This furthermore suggests that Hsp70 can switch between TPR1 and TPR2B.

2.2 Interaction of Sti1 with Hsp70

The presence of two alternative Hsp70 binding sites in Sti1 (TPR1 and TPR2B) raised the presumption that these two TPR domains are differentially activated under certain conditions. One idea was that the presence of Hsp90 could influence the accessibility of one of the two domains. In order to analyze this, the interaction of different Sti1 variants was probed in the absence and in the presence of Hsp90. To address the role of the two TPR domains individually, full-length Sti1 with a mutation in the peptide binding groove of either TPR1 or TPR2B and different fragments of Sti1 were generated. The TPR2B defective mutations have already been described in section 2.1.1. Analogous to this, a part of the highly conserved carboxylate clamp of the peptide binding groove of TPR1 was replaced by alanine in order to specifically disrupt interaction of TPR1 with Hsp70 (N39A).

2.2.1 Contributions to Hsp70 interaction

In the first approach, yHsp70 (Ssa1) was coupled to an SPR chip and different variants of Sti1 were used as analytes. As different chips were used, Sti1 wildtype was measured as a reference in each experiment. The apparent dissociation constants were calculated from the titration curves and normalized to wildtype levels (Figure 2.6).

The dissociation constant of Sti1 for Hsp70 was unaffected by the introduction of the TPR1 disrupting mutation (N39A). Likewise, fragments of Sti1 comprising intact TPR2A-TPR2B (TPR1-DP1-TPR2A-TPR2B, TPR2A-TPR2B, TPR2A-TPR2B-DP2) exhibited similar affinities towards Hsp70. The affinities of TPR2A-TPR2B and TPR2A-TPR2B-DP2 were slightly higher compared to wildtype Sti1 but this effect might be negligible considering the error of the measurement. If considered, it indicates that in the full-length protein, other domains weaken binding of Hsp70.

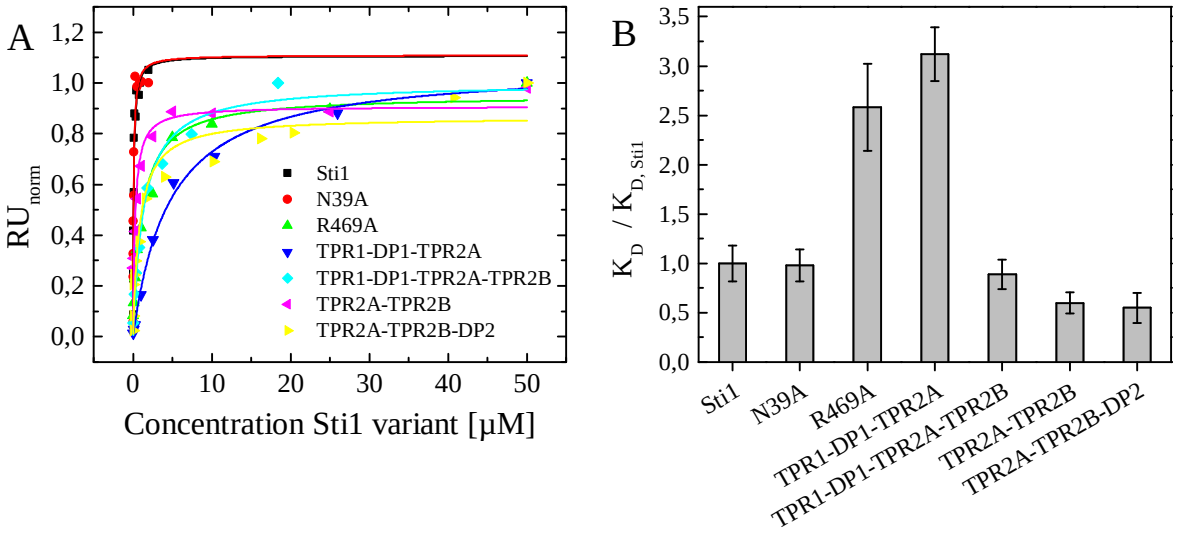

Figure 2.6: Affinities of Sti1 variants for yHsp70 measured by SPR. A: yHsp70 was coupled to a CM5 chip and the Sti1 variants were titrated onto the chip. The response units were normalized and fitted as described in section 4.5.7. B: Derived dissociation constants from different chips normalized to wildtype Sti1 are shown with the fitting error.

In contrast, mutation of the peptide binding groove of TPR2B (R469A) or complete loss of TPR2B (TPR1-DP1-TPR2A) reduced the affinity towards Hsp70 more than two fold compared to Sti1 wildtype. With the isolated TPR1, TPR2A or TPR2B domain, no reliable dissociation constant could be determined as they bound only weakly to Hsp70.

In conclusion, this shows that TPR1 does not efficiently contribute to the interaction with Hsp70 under the conditions tested. Instead, intact TPR2A-TPR2B is necessary for the interaction and the peptide binding groove of TPR2B is crucial in these respects. Therefore, it is assumed that within TPR2A-TPR2B, the C-terminal EEVD of Hsp70 solely or at least mainly binds to TPR2B, not to TPR2A. This is furthermore justified by the peptide specificity of the domains [Schmid et al., 2012] and previous experiments which showed that the two domain construct with compromised TPR2B does not form complexes with Hsp70 (see section 2.1.1).
However, the fact that isolated TPR2A or TPR2B were not sufficient as binding sites strongly suggests that additional interactions take place and that TPR2A-TPR2B represents a joint binding site for Hsp70. Moreover, even though lower affinities have been determined, binding to Hsp70 was still observable after loss of functional TPR2B (R469A and TPR1-DP1-TPR2A). The remaining affinity is considered to result either from interactions with regions of Hsp70 distinct from the C-terminal EEVD or from TPR1.

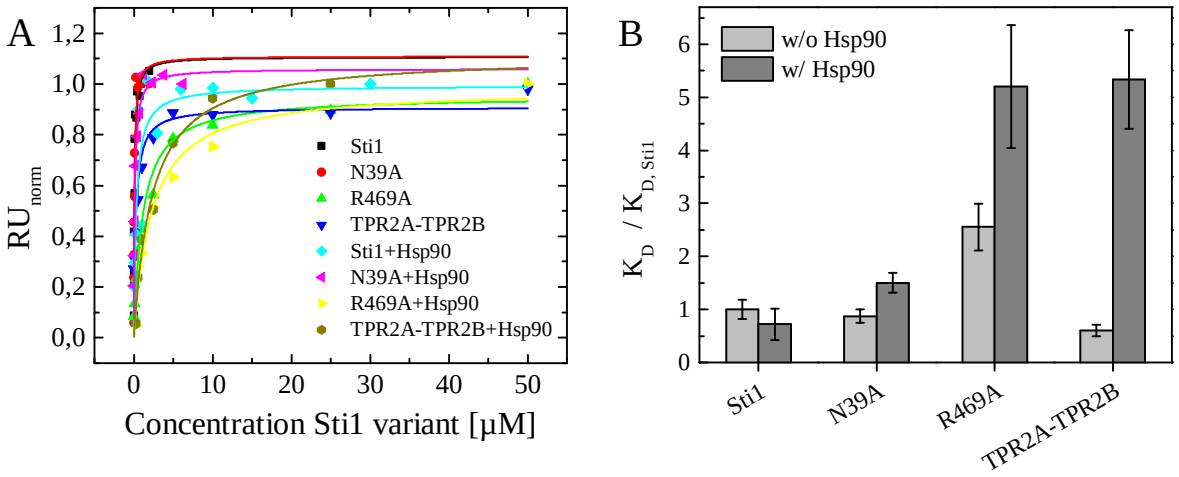

Figure 2.7: Affinities of Sti1 variants for yHsp70 in presence of yHsp90 measured by SPR. A: yHsp70 was coupled to a CM5 chip and the Sti1 variants were titrated onto the chip, in the second part of the analysis together equimolar concentrations of yHsp90. The response units were normalized and fitted as described in section 4.5.7. B: Derived dissociation constants from different chips normalized to wildtype Sti1 with the fitting error are shown.

TPR1 not participating in the interaction with Hsp70 contradicts various studies [Scheufler et al., 2000, Odunuga et al., 2003, Carrigan et al., 2004, Flom et al., 2006, Flom et al., 2007], including this work (see section 2.1.1), which detected interaction of Hsp70 with TPR1. This might be explained by TPR1 only playing a role for Hsp70 binding under certain conditions.

2.2.2 Contributions to Hsp70 interaction in the presence of Hsp90

In the second part of this project, the influence of Hsp90 on the interaction with Hsp70 was investigated. To this end, Sti1 variants plus equimolar concentrations of yHsp90 (Hsp82) were added to the Hsp70 bound chip (Figure 2.7). A direct interaction of Hsp90 with Hsp70 was excluded as no binding signal was observed in the absence of Sti1 and this was also confirmed in separate analytical ultracentrifugation experiments.

The affinity of Sti1 wildtype for Hsp70 increased slightly when Hsp90 was added although the accuracy of the measurement does not allow to draw a definite conclusion. In the case of the other variants which contain only one intact Hsp70 binding site (Sti1 N39A, Sti1 R469A, TPR2A-TPR2B), the presence of Hsp90 generally weakened binding to Hsp70. This was most pronounced for TPR2A-TPR2B (about ten fold) while for the TPR1 defective mutant, only a slight effect was observed.
The apparent affinities determined must be interpreted carefully: When Hsp90 is bound by Sti1 and this complex is applied onto the Hsp70-bound chip, the signal measured

does not only change according to the affinity but also with the increasing mass of the analyte. Nevertheless, as always the same mass is added it seems legitimate to compare the values with each other qualitatively.
The increased affinity of Sti1 wildtype for Hsp70 upon addition of Hsp90 (0.42 µM versus 0.29 µM) is in principle in line with the literature although the effect measured in this work is not as pronounced. A study evaluating co-immunoprecipitation experiments reports five fold increased affinities of Hop for Hsp70 in the presence of Hsp90 (1.3 µM versus 0.25 µM) but in this case higher concentrations of Hsp90 were used [Hernández et al., 2002]. A different study based on mass spectrometry could even hardly detect interaction of Hsp70 in the absence of Hsp90 [Ebong et al., 2011].

The Sti1 variants which harbor only one functional TPR domain were all affected in the opposite direction upon the addition of Hsp90 indicating that Hsp90 influences the interaction with Hsp70 differentially. TPR2A-TPR2B was most severely affected. Considering that TPR2A-TPR2B represents a joint binding site for both Hsp70 and Hsp90, this allows the conclusion that Hsp90 partly displaces Hsp70 from this binding site. This has implications for the overall picture of client transfer mediated by Sti1: On the one hand, Hsp90 and Hsp70 have to be brought in contact for the transfer of the client but on the other hand, Hsp70 has to leave the complex at some time during client activation. The common interaction platform TPR2A-TPR2B seems to moderate both functions. This could imply that the enhanced binding of full-length Sti1 to Hsp70 in the presence of Hsp90 is due to an activation of the Hsp70 binding ability of TPR1 which basically seemed dead in the absence of Hsp90. This would be in line with the weakened affinity towards Sti1 N39A in presence of Hsp90 as here no intact TPR1 is available. Indeed, N39A was not as strongly affected by the presence of Hsp90 but other factors might contribute in this longer construct. However, the addition of Hsp90 to TPR2B defective full-length Sti1 (R469A) also decreased the affinity towards Hsp70 strongly even though here, it is assumed that Hsp70 is bound by TPR1.

Taken together, the results of these experiments show that the interaction of Hsp70 is of complex nature and that Hsp90 has major implications on it. While in the absence of Hsp90, TPR2B is the most important binding site, in the presence of Hsp90, the other domains gain relevance.

2.2.3 Ternary complex formation with TPR1 defective mutants

To monitor how the Hsp70 binding TPR domains contribute to the dynamic formation of ternary complexes, analytical ultracentrifugation runs were performed. As TPR1 was of special interest, Sti1 constructs were investigated in which TPR1 is either deleted (TPR2A-TPR2B) or its peptide binding groove is disrupted (N39A).

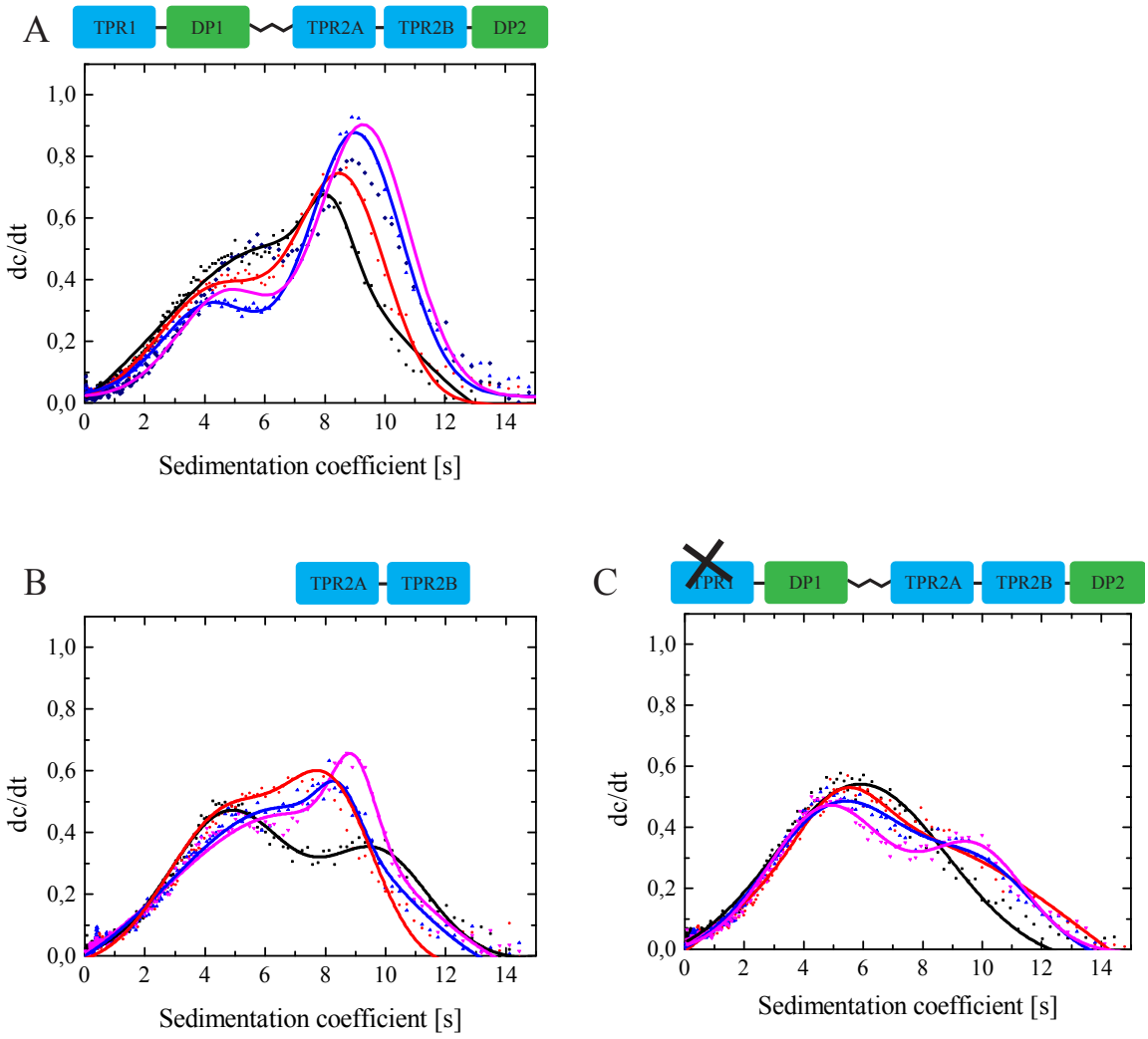

Figure 2.8: Formation of ternary complexes between labeled yHsp70, yHsp90 and increasing concentrations of Sti1 wildtype (A) and TPR1 defective mutants (B and C) investigated by analytical ultracentrifugation. 0.5 µM labeled yHsp70 with 3 µM yHsp90 under addition of 0.5 µM (black), 1 µM (red), 2 µM (blue) and 4 µM (magenta) Sti1 variant. The data was fitted with (bi-) Gaussian functions. A: Sti1 wildtype. B: TPR2A-TPR2B. C: Sti1 N39A (defective TPR1 peptide binding groove).

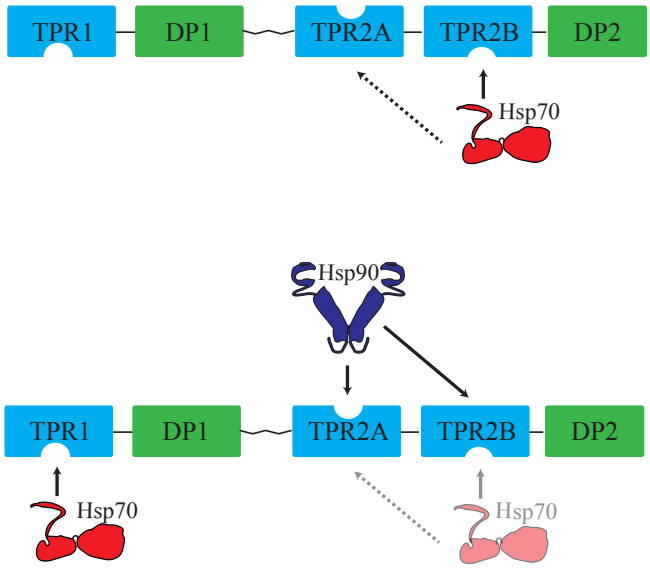

Figure 2.9: Role of the TPR domains on the interaction with Hsp70. Top: In absence of Hsp90, TPR2B is the main interaction site for the C-terminal tail of Hsp70. Additional interactions distinct from the peptide binding groove occur with TPR2A. Bottom: In presence of Hsp90, Sti1 also interacts via TPR1 with Hsp70 and TPR2B loses relevance.

Sti1 variants were titrated into constant concentrations of FAM-labeled yHsp70 (Ssa1) and yHsp90 (Hsp82) (Figure 2.8). In this experiment, three different species can be monitored: Hsp70 alone (4 s), binary complexes with Sti1 (5.5 s) and ternary complexes with Sti1 and Hsp90 (9 s).
With increasing amounts of wildtype Sti1, more ternary complexes are formed. At the same time, the amount of free Hsp70 and of the binary complex decreases. The latter two cannot be totally separated as the signals overlay. For TPR2A-TPR2B, ternary complex formation was weaker and this was even more pronounced in the TPR1-defective full-length mutant. Instead, the binary complex was preferred.

In summary, whenever TPR1 was deleted or disrupted, the formation of the ternary complex was compromised even though TPR1 did neither play a role for Hsp70 (section 2.2.1) nor Hsp90 [Schmid et al., 2012] binding alone. This is the opposite of what was observed for Sti1 N435A (defective TPR2B, see section 2.1.1): here, a stronger population of the ternary complex was observed even though the mutation reduced binding to Hsp70 alone.

This shows that TRP1 plays a intriguing role for the formation of ternary complexes. Together with the SPR analysis, it suggests that TPR1 gains importance for Hsp70 binding in the presence of Hsp90 (Figure 2.9).

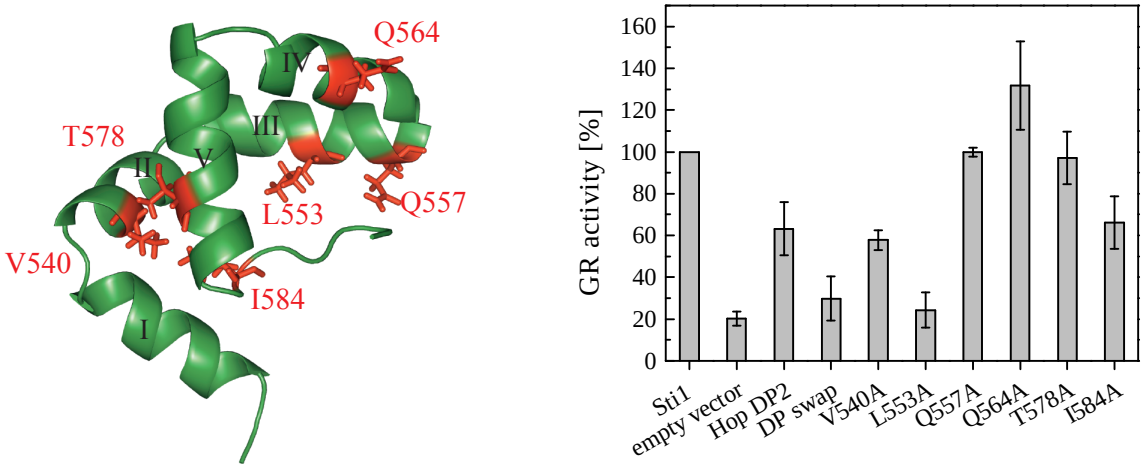

Figure 2.10: Effects of variations of the DP2 domain on GR activation in *S. cerevisiae*. Left: Point mutations in DP2 (PDB: 2LLW). Right: GR activation levels in the presence of Sti1 variants mutated in DP2, a replacement of DP2 by DP1 (DP swap) or by DP2 from human Hop (Hop DP2). Means of at least three independent experiments are shown with their standard deviation.

2.3 Important regions of DP2 in Sti1

The DP domains of Sti1, especially DP2, are important for substrate activation *in vivo* as shown in 2.1.2 and by others [Flom et al., 2007, Schmid et al., 2012]. However, the precise role is not resolved yet. As no interaction of the isolated DP domains has been detected with Hsp70 or Hsp90, it is speculated that the DP domains may stabilize the client even if Sti1 is not a chaperone on its own [Bose et al., 1996, Freeman et al., 1996]. To pinpoint the essential regions of DP2, different mutations and replacements of this domain were generated and tested for GR activation (Figure 2.10).

The complete replacement of DP2 with similar domains generally reduced client activation. The substitution with the DP2 domain of human Hop (Hop DP2) reduced GR activity almost by 50 %. It was even completely abolished by the replacement with DP1 (DP swap).
Furthermore, a number of point mutations was introduced in the different helices of DP2 (V540A, L553A, Q557A, Q564A, T578A, I584A) and these impacted GR activation levels differently. While T578A and Q557A did not influence GR activation, I584A and V540A moderately reduced GR activation. Mutations in helix III and IV of DP2 had the most pronounced effect: with L553A, the GR activation dropped to background levels whereas Q564A even enhanced client activity.

In conclusion, the function of DP2 is very sensitive to mutation. Even Hop DP2 cannot replace it although the two domains share large sequence identity and the homology model of Hop DP2 overlays almost perfectly with Sti1 DP2 (Figure 2.11). This indicates

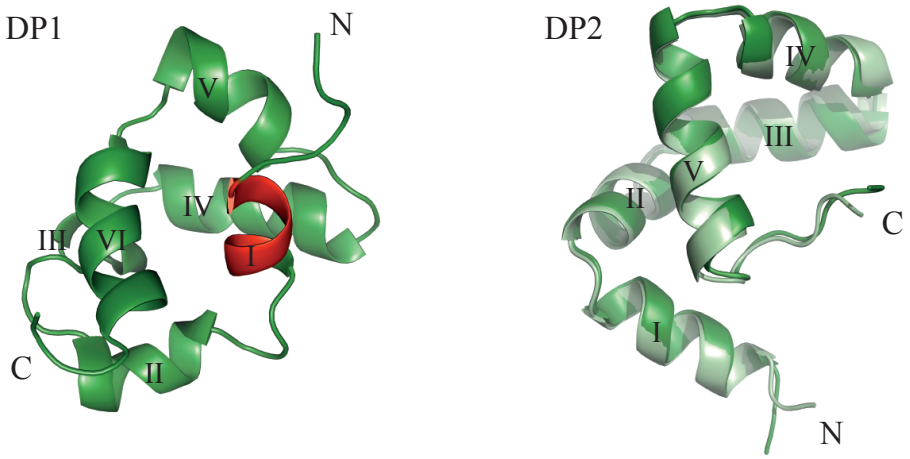

Figure 2.11: Structural comparison of the DP domains. The DP domains (PDB: 2LLV and 2LLW) are α-helical structures. Helix III and IV of DP2 (IV and V in DP1) form a wedge-shaped surface. Left: In Sti1 DP1, this surface is occupied by an additional small helix (red). Right: Overlay of Sti1 DP2 (dark green) and homology model of human DP2 generated by SWISS-MODEL (light green) show high resemblence.

that some species-specific differences exist. Considering that Hop can fully complement for Sti1 in this assay, this furthermore suggests that the different domains are precisely adjusted to one another in the two homologs.
Also DP1 cannot replace DP2 even though the the two DP domains are structurally highly similar (Figure 2.11). The major difference between the two structures is that in DP1 an additional small helix occupies the wedge-shaped surface which is formed by helix IV and V in DP1 (III and IV in DP2). This surface may represent a ligand binding site which is blocked in DP1. Of the point mutations, the ones in helix III and IV of DP2 had the strongest effects. The two residues are moreover conserved between Sti1 and Hop pointing towards their significance. Together, this emphasizes a special role for the wedge-shaped surface formed by helix III and IV which could serve as a binding site for the client.

2.4 Flexible linker of Sti1

The two TPR-DP modules of Sti1 (TPR1-DP1 and TPR2A-TPR2B-DP2) are connected by a flexible linker region [Schmid et al., 2012]. This linker is present in all of the analyzed Sti1 homologs but the region is only weakly conserved amongst them (Figure 2.12). In different yeast, the linker length is conserved to around 60 amino acid but its sequence is highly diverse. In contrast, the mammalian homologs exhibit a much shorter linker of about 30 amino acid with considerable sequence conservation

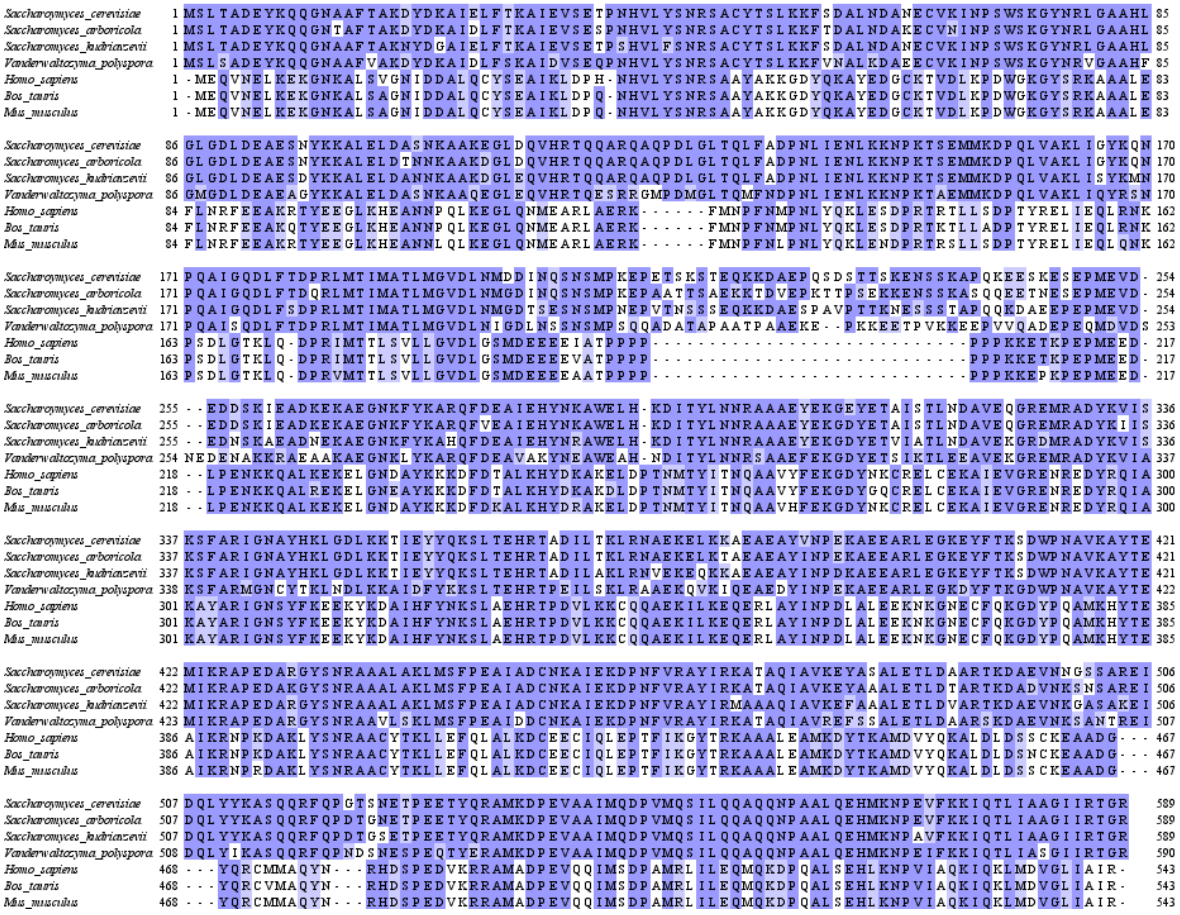

Figure 2.12: Sequence alignment of Sti1 homologs. Sequences of four Sti1 homologs closely related to *S. cerevisiae* and of three mammalian homologs were aligned with T-Coffee. The darkness of the blue color indicates the percentage of identity. The linker which comprises residues 198-258 in Sti1 from *S. cerevisiae* is the least conserved region.

which contains quite remarkable stretches like seven prolines in a row. Prolines are often 'breakers' of secondary structures and are highly enriched in non-helical linkers as they lead to isolation from the attached domains [George and Heringa, 2002].

The presence of a long flexible linker separating the two Hsp70 binding TPR domains has contributed to the idea that Hsp70 may switch between TPR1 and TPR2B under certain conditions and that the linker may mediate this process. To investigate the role of the linker of Sti1, it was replaced by a Ser-Ala-Gly-Ala linker. This four amino acid stretch was chosen in order to maintain proper domain separation. This construct was transformed into a yeast strain suitable for monitoring GR activation *in vivo*. Deletion of the linker resulted in reduced levels of GR activation, surprisingly, even lower levels than observed upon complete loss of TPR1-DP1 including the linker (Figure 2.13).

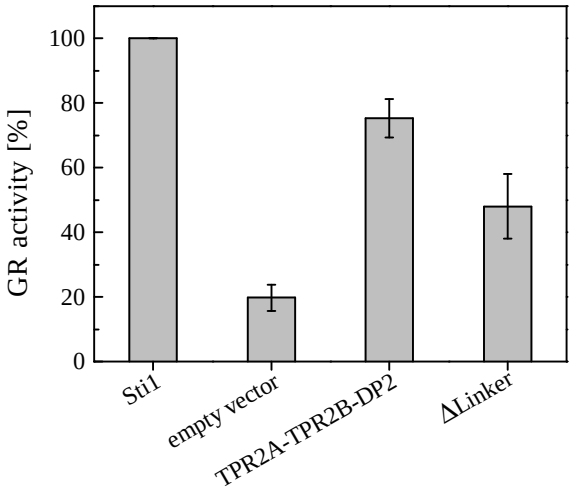

Figure 2.13: Effects of the linker deletion on GR activation in *S. cerevisiae*. For comparison, GR activation mediated by TPR2A-TPR2B-DP2, lacking the first module and the linker, is also shown. Means of at least three independent experiments are shown with their standard deviation.

2.4.1 Functional analysis of the linker-deleted Sti1

The linker deletion used in the section before in the *in vivo* experiments was also analyzed *in vitro*. The first part of these experiments, CD spectroscopy, ATPase assays and surface plasmon resonance spectroscopy (SPR), were performed by Monika Herrmann under my supervision in her Master's Thesis. Stability and secondary structure of the linker deletion were comparable to wildtype Sti1 demonstrating the intactness of the single domains. The interaction with yHsp90 (Hsp82) was probed via SPR analysis and ATPase assays (Figure 2.14). The linker-deleted Sti1 behaved like wildtype Sti1 in these assays indicating that the linker does not play a role for Hsp90 binding and ATPase inhibition.

On the contrary, deletion of the linker enhanced the affinity for yHsp70 (Ssa1) around three fold as shown by SPR analysis (Figure 2.14, B).
Two comments have to be made towards the reliability of the apparent affinities measured by SPR. First, these cannot be directly compared with affinities derived from matrix-independent methods like isothermal titration calorimetry as binding of the analyte to the surface may decrease accessibility of its binding sites. Secondly, even different chips with the same protein coupled may differ drastically. This is why in this work only affinities derived from experiments using the same coupled chip were compared or a reference was used to which values could be normalized.

To verify the altered affinity of Sti1 towards Hsp70 upon linker deletion, analytical ultracentrifugation runs were performed. Sti1 and Sti1 linker deletion were titrated to a constant concentration of FAM-labeled yHsp70 (Figure 2.15). With increasing concen-

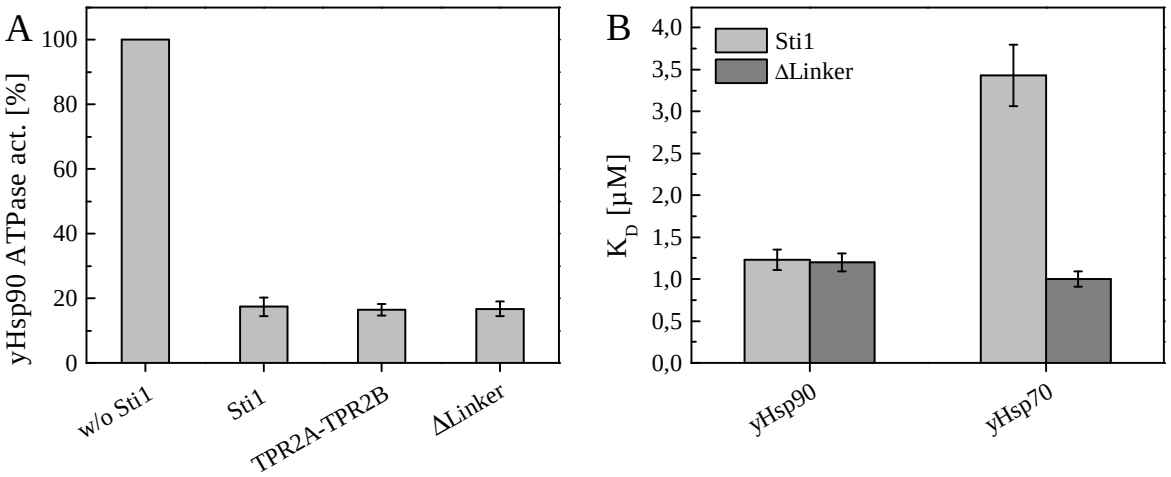

Figure 2.14: Effects of the linker deletion on interaction with yHsp90 and yHsp70. A: Influence of Sti1, Sti1 TPR2A-TPR2B and Sti1 linker deletion on the ATPase activity of yHsp90. Means of values at equimolar concentrations of yHsp90 and Sti1 variant and their standard deviations are shown, determined in three independent experiments. B: Affinities of Sti1 and linker-deleted Sti1 towards yHsp90 and yHsp70 measured by SPR using a yHsp90/yHsp70-coupled chip. Error bars indicate fitting error. For the primary data, see the Master's Thesis of Monika Herrmann.

trations of the Sti1 variant, the peak shifted from 4 s to 6 s indicating the formation of the binary complex. With the linker-deleted variant, complex formation was observed at lower concentrations of the Sti1 variant compared to wildtype Sti1 confirming an increased affinity. To visualize this more effectively, s values derived from the fits of the measurements were plotted against the concentration of Sti1 variant (Figure 2.15, C).

Furthermore, the same titration experiments were performed in the presence of constant concentrations of yHsp90 (Hsp82) (Figure 2.16). For both Sti1 variants, increased formation of ternary complexes (9.5 s) was visible for increasing concentrations of the Sti1 variant upon a certain threshold concentration. At the same time, the amount of binary complexes between yHsp70 and Sti1 (5.5 s) decreased. With concentrations above this threshold, the binary complexes replaced ternary complexes again. This highlights that certain ratios of the three components determine the population of the different complexes *in vitro*.
Importantly, the threshold concentration for the linker deletion was lower than for wildtype Sti1. Moreover, the ternary complex was never as populated and the binary Hsp70-Sti1 complex was always more abundant than with wildtype Sti1. This shows that deletion of the linker shifts the equilibrium of complex formation towards a higher population of the binary complex and lower amounts of ternary complexes going along with an increased affinity for Hsp70.

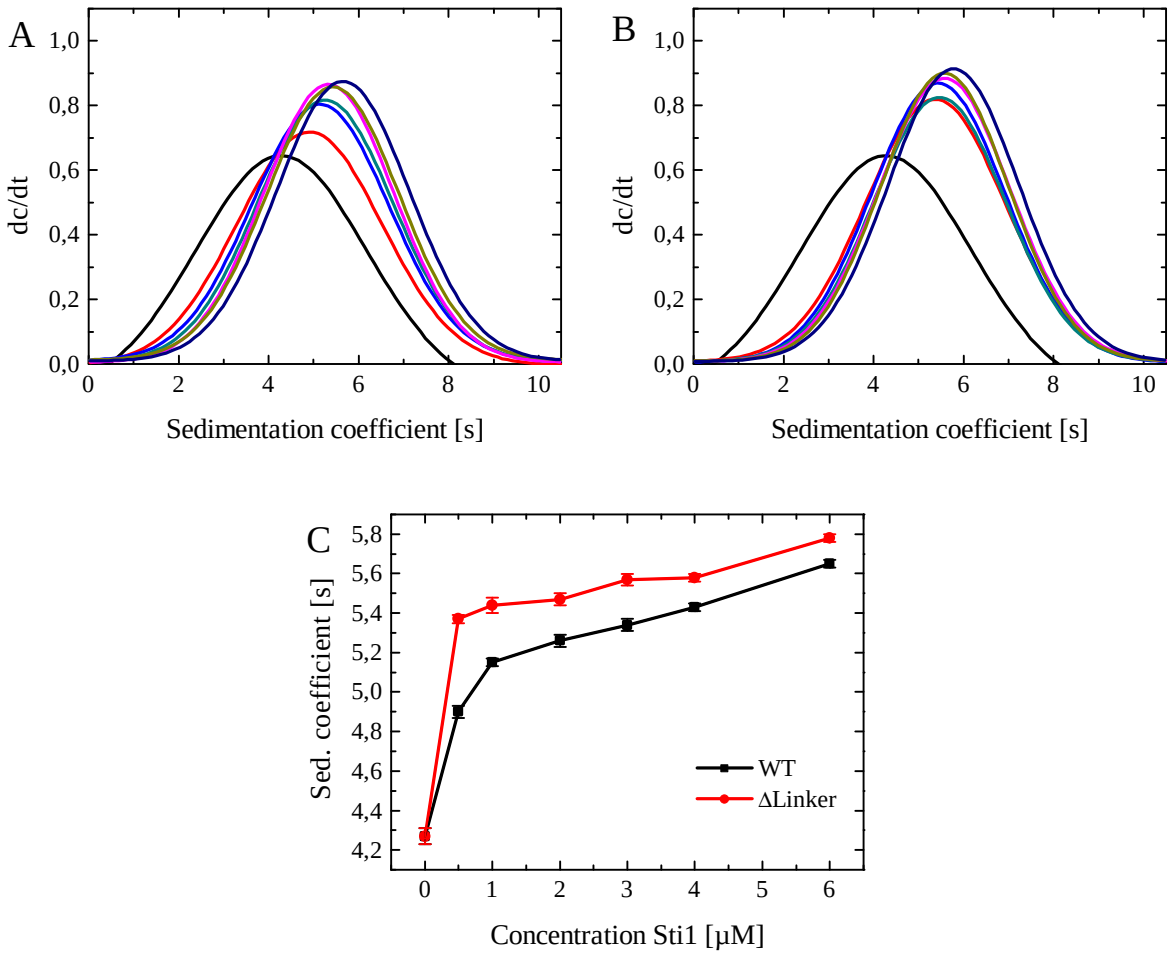

Figure 2.15: Formation of binary complexes between labeled yHsp70 and increasing concentrations of Sti1 wildtype (A) and linker-deleted Sti1 (B) monitored by analytical ultracentrifugation. A and B: 0.5 µM labeled yHsp70 (black: yHsp70 alone) under addition of 0.5 µM (red), 1 µM (blue), 2 µM (dark cyan), 3 µM (magenta), 4 µM (dark yellow), 6 µM (navy) Sti1 wildtype variant. For clarity, only (bi-) Gaussian fits are shown, standard errors were below 1%. C: Derived s values with their standard error plotted against the concentration of Sti1 variant. The continuous line serves only as a guide for the eye.

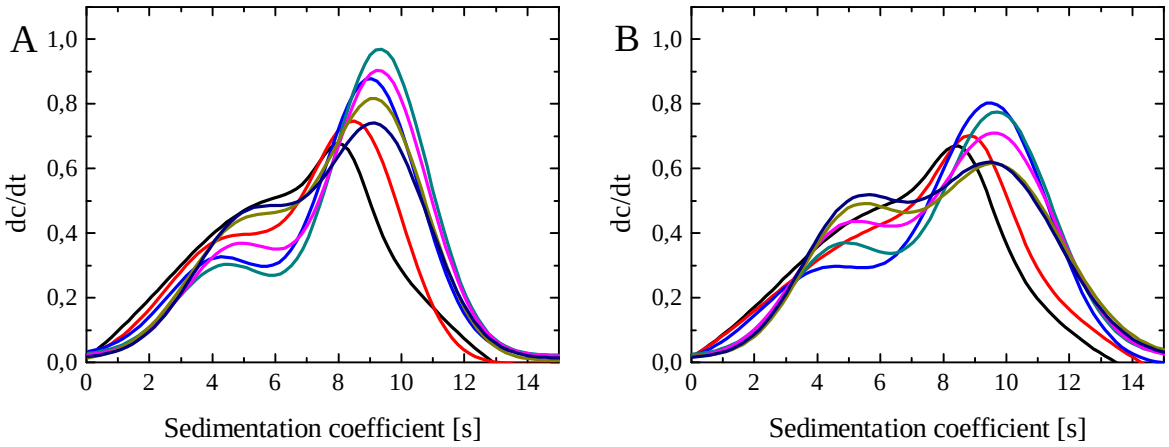

Figure 2.16: Formation of ternary complexes between labeled yHsp70, yHsp90 and increasing concentrations of Sti1 wildtype (A) and linker deleted Sti1 (B) monitored by analytical ultracentrifugation. 0.5 µM labeled yHsp70 with 3 µM yHsp90 under addition of 0.5 µM (black), 1 µM (red), 2 µM (blue), 3 µM (dark cyan), 4 µM (magenta), 6 µM (dark yellow) and 8 µM (navy) Sti1 variant. For clarity, only bi-Gaussian fits are depicted of which the standard errors were below 1%.

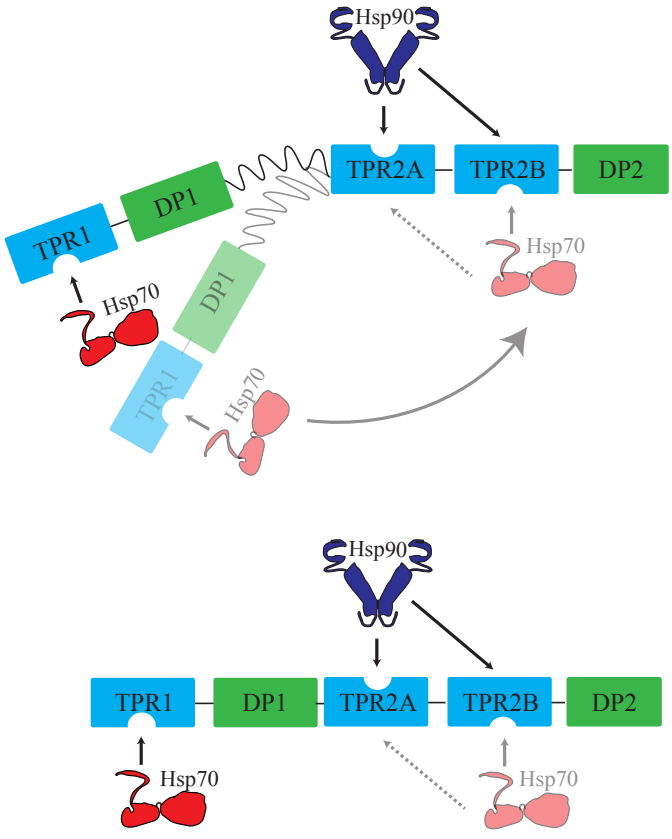

Figure 2.17: The linker regulates the interaction with Hsp70. Top: In Sti1 wildtype, the flexible linker is supposed to allow transfer of Hsp70 between TPR1 and TPR2B. Bottom: After deletion of the linker, this is not possible anymore.

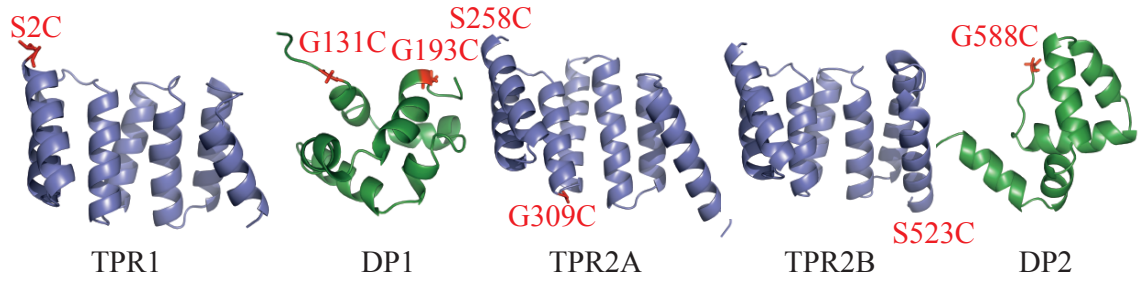

Figure 2.18: Position of introduced cysteines in Sti1 for smFRET experiments. Cysteines are highlighted in red. S258C, located at the very N-terminus of TPR2A, and S523C at the very C-terminus of TPR2B are not resolved in the structures. Used structures: Homology model of Sti1 TPR1 based on Hop TPR1 (PDB: 1ELW) with SWISS-MODEL, DP1 (PDB: 2LLV), TPR2A-TPR2B (PDB: 3UQ3), DP2 (PBD: 2LLW).

In conclusion, the linker deletion does not affect the interaction with Hsp90. This is in line with the finding that TPR2A-TPR2B is the Hsp90 interacting module of Sti1 [Schmid et al., 2012]. Instead, the deletion of the linker leads to enhanced affinity for Hsp70 which indicates that the linker, or another part of the protein which is influenced by the linker, normally partly blocks binding of Hsp70. This is accompanied by an altered equilibrium between binary and ternary complexes which together may explain the loss of function *in vivo*.
Deletion of only the linker reduced *in vivo* activity stronger than complete deletion of the first module including the linker (TPR2A-TPR2B-DP2) implying a crosstalk between the two TPR-DP modules connected by the linker. Without the linker, TPR1-DP1 may represent a 'dead end' which is still capable of binding Hsp70 via TPR1, but Hsp70, together with the client, cannot be transferred to TPR2B only where activation can occur (Figure 2.17). In summary, this demonstrates that the linker plays a key role for the function of Sti1.

2.5 Intramolecular FRET analysis to study dynamics of Sti1

The last sections have illustrated that the flexible linker connecting the two TPR-DP modules is of central importance for the function of Sti1. In order to analyze the conformational dynamics that the linker conveys, intramolecular FRET experiments were performed. To this end, Sti1 double cysteine mutants were generated, each with one cysteine N-terminally and the other one C-terminally of the linker. These could be labeled with two different dyes suitable for single molecule FRET analysis. On the one hand, this could serve for the estimation of distances within the domains of Sti1 and on

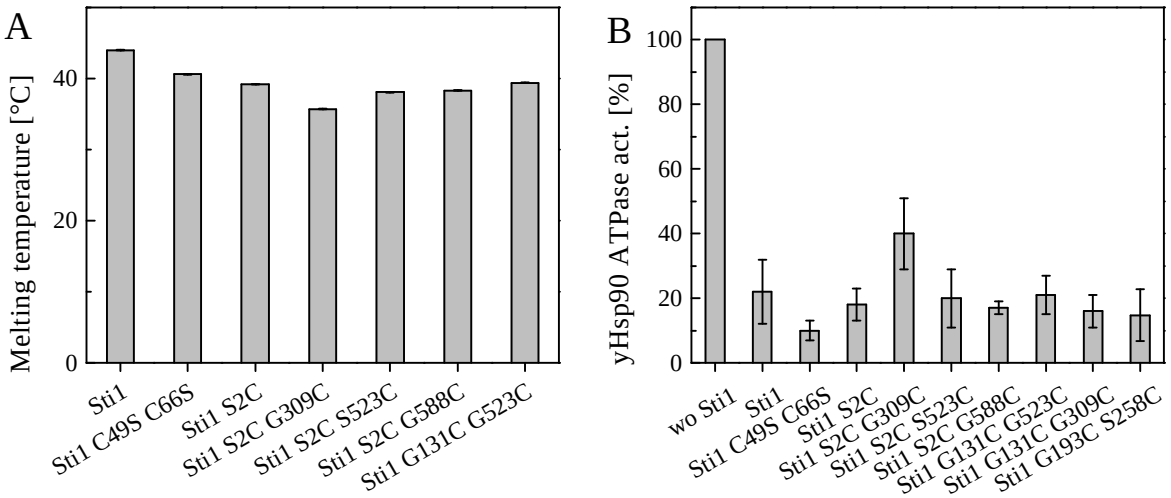

Figure 2.19: Effects of cysteine replacements on the stability and function of Sti1. A: Thermal transition temperatures measured at 220 nm. B: Effects on the inhibition of the ATPase activity of yHsp90. Means of values at equimolar concentrations of yHsp90 and Sti1 variant and their standard deviations are shown, determined in at least three independent end-point measurements.

the other hand to detect factors that would induce conformational changes within Sti1. In principle, this approach is similar to recent studies on the conformational dynamics of different Hsp70 homologs [Marcinowski et al., 2011, Sikor et al., 2013].

The first mutants were generated and labeled by Monika Herrmann (Master's Thesis). For this approach, the native cysteines were replaced by serines first (C49S, C66S, C453S). Then, for the replacement by cysteine, residues in exposed loops, if possible serine or a second best alternative glycine, were chosen (Figure 2.18).
After standard purification, the mutants were tested for their stability and function via CD spectroscopy and ATPase assays (Figure 2.19). The variants showed similar characteristics like the wildtype indicating that the various mutations did not hamper the structure of the protein drastically. The mutants were statistically labeled with ATTO 532 and ATTO 647.

The smFRET measurements were performed in cooperation with Dr. Jelle Hendrix and Daniela Wengler (Prof. Don Lamb, Department of Physical Chemistry, LMU Munich). To detect putative large conformational changes within Sti1, first three mutants were tested which contained labeled cysteines that were far apart in the primary sequence. These three (S2C-G588C, S2C-S523C, G131C-S523C) exhibited very low FRET efficiencies with a mean of around 0.05 (Figure 2.20, A-C). This shows that the labels in the N-terminus of the protein do not come in close contact with the C-terminal labels. For a second round of mutants with the C-terminal label located in the middle of TPR2A (S2C-G309C, G131C-G309C), the mean FRET efficiencies (aprox. 0.1) were a bit higher but still too low for accurate estimation of distances (Figure 2.20, D

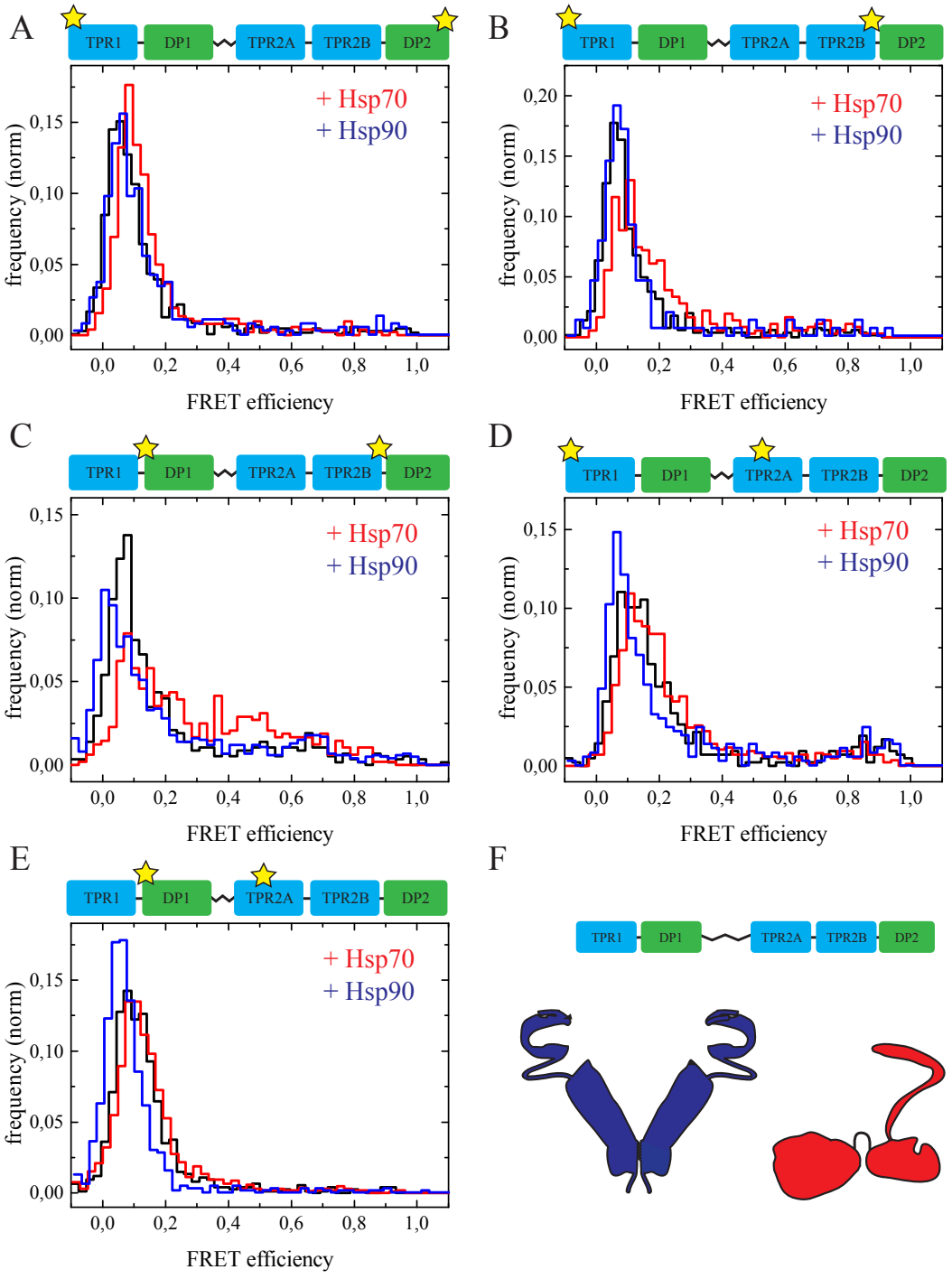

Figure 2.20: Single molecule FRET analysis of low FRET Sti1 mutants in the absence and presence of Hsp90 and Hsp70. Histograms of the probability distribution analysis. Sample preparations with yHsp90 (blue) and yHsp70 (red) were performed under high excess of the unlabeled proteins during the incubation and in the dilution steps. A: Sti1 S2C-G588C. B: Sti1 S2C-S523C. C: Sti1 G131C-S523C. D: Sti1 S2C-G309C. E: G131C-G309C. F: Schematic representation of analyzed proteins in their relative sizes (roughly estimated from the crystal and NMR structures).

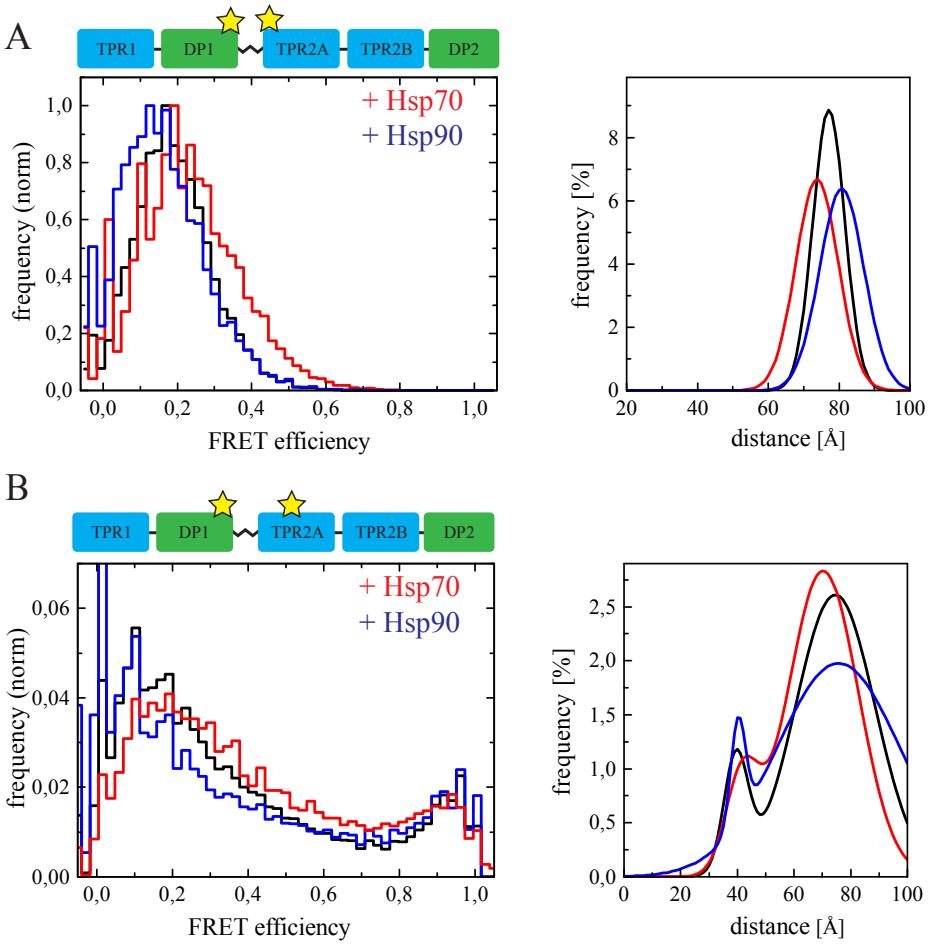

Figure 2.21: Single molecule FRET analysis of intermediate FRET Sti1 mutants in the absence and presence of Hsp90 and Hsp70. Histograms of the probability distribution analysis (left) and distance distributions (right). Sample preparations with yHsp90 (blue) and yHsp70 (red) were performed under high excess of the unlabeled proteins during the incubation and in the dilution steps. A: Sti1 G193C-G309C. B: Sti1 S258C-G309C.

and E). Also in this case, the labels were more than 80 Å apart. Upon the addition of yHsp90 and yHsp70, altered FRET efficiencies were observed. Although this was a slight change, it was reproducible and came up for all of the low FRET mutants. Hsp70 shifted the histograms towards higher FRET efficiencies going along with a smaller distance between the dyes, whereas Hsp90 had the opposite effect leading to larger distances of the dyes.

In conclusion, the attached labels are not only far apart in the sequence but also in the tertiary structure of Sti1. The different mutants were affected by the presence of Hsp90 and Hsp70 in the same manner indicating a general compression by Hsp70/decompression by Hsp90 rather than a rearrangement of specific domains.

In a third round, Sti1 mutants (G193C-G309C, S258C-G309C) were generated with labels located at the boundaries of the linker allowing the observation of the dynamics of the linker itself (Figure 2.21). These exhibited higher FRET efficiencies applicable to an evaluation of the distances. In the case of the mutant with the labels directly at the linker boundaries (S258C-G309C), an intermediate low FRET efficiency was observed which correlates to a distance of about 70 to 80 Å. Again, the FRET signal was influenced by the presence of Hsp90 and Hsp70. The addition of Hsp90 lowered FRET efficiencies resulting from a larger distance between the dyes, whereas Hsp70 increased the FRET signal speaking for an approaching of the dyes.
For G193C-G309C, the first measurements indicated the appearance of two FRET efficiencies, an intermediate low (aprox. 0.2) and a high FRET (aprox. 0.9) signal which translates to distances of about 80 and 40 Å. This suggests the presence of two distinct positions of the labels relative to each other. Interestingly, the addition of Hsp70 shifted the intermediate low peak to higher values like observed before for the low FRET mutants. Both Hsp70 and Hsp90 shifted the population of these two conformations as the amplitudes were influenced by the chaperones. While with Hsp70, Sti1 preferably adopted the intermediate low FRET state, Hsp90 favored the population of the high FRET state. However, the results of the last mutant need to be reproduced and the final results are not available yet.

In conclusion, the end-to-end distance of the 60 amino acid linker is 70 to 80 Å minus contributions of the labels. Therefore, it is elongated compared to the compact structured domains with diameters of 20 to 40 Å.

Assuming a random coil structure, the end-to-end distance of the linker should follow $D_{ee} = \sqrt{\langle \vec{R}^2 \rangle} = \sqrt{4 \cdot p \cdot L}$, where $\vec{R}$ is the end-to-end vector, L is the contour length, and p is the persistence length [Ohashi et al., 2002]. The contour length represents the maximally extended conformation and can be calculated with $L = N \cdot b$, where N is the number of amino acids and b the average size of an amino acid. With b = 0.4 nm for an amino acid [Ainavarapu et al., 2007] and a persistence length of around 0.4 to 0.66 nm [Ohashi et al., 2002], this would equal 6.2 to 8 nm for the end-to-end distance of the linker in Sti1. In another study [Kohn et al., 2004], a common relationship for the radius of gyration R_G of unfolded proteins and the amino acid number is described which translates into a R_G of the linker in Sti1 of 2.3 nm. With the rough estimation of the end-to-end distance for an ideal chain $D_{ee} = \sqrt{6} \cdot R_G$, this ends up in 5.6 nm. In summary, the theoretical distances are slightly below or in the range of the measured distances between the dyes at the linker boundaries.

The addition of Hsp90 loosens the linker, whereas Hsp70 tightens the linker. This fits into a model in which the linker mediates the transfer of Hsp70 from TPR1 to TPR2B, with TPR1 delivering Hsp70 to TPR2B where client activation can proceed. Hsp70 leads to a bending of the linker inducing the proximity of the two TPR domains so that

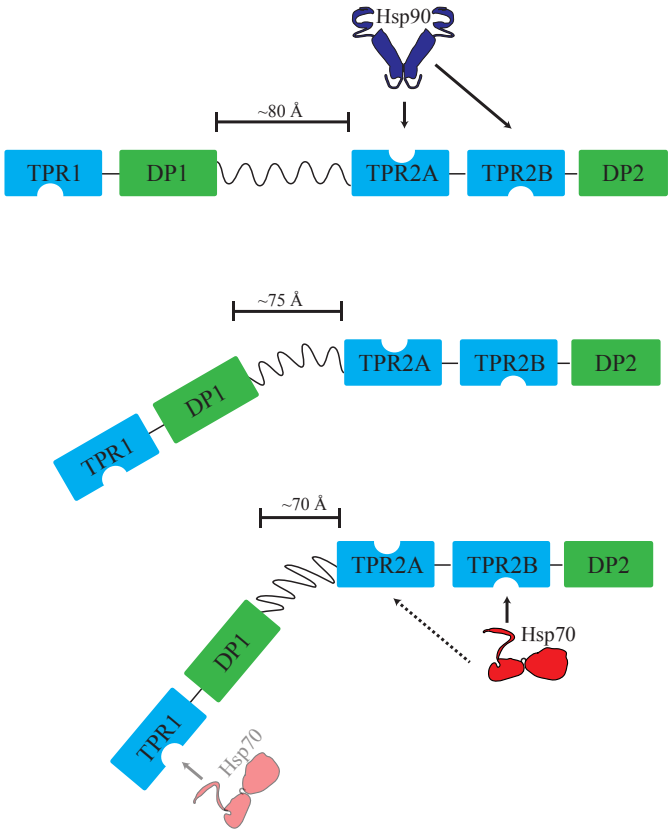

Figure 2.22: Possible scenario to explain observed effects of Hsp70 and Hsp90 on intramolecular FRET measurements. In the presence of Hsp90, the linker is stretched. In the presence of Hsp70, the linker bends to enable transfer of Hsp70 between TPR1 and TPR2B.

Hsp70 can be transferred. Hsp90 instead induces a more relaxed conformation where TPR1 connected by the linker has enough space to bind free Hsp70 (Figure 2.22).

Further experiments are planned in order to strengthen this interpretation. Sti1 variants with labels at positions G193C-G309C in addition to either mutated TPR1 or mutated TPR2B, as well as mutants comprising cysteines in other parts of TPR1 in combination with a label in TPR2A were generated and will be analyzed in this ongoing cooperation.

2.6 Intermolecular FRET experiments

A major part of this work addresses the interaction between Sti1, Hsp90 and Hsp70 with *in vitro* techniques. A tool to monitor the interaction under various conditions would be an intermolecular FRET system between two of the proteins. FRET assays between Hsp90 and Sti1 have been reported before using randomly labeled Sti1 [Li

et al., 2010, Lee et al., 2012]. Yet with these systems it is not possible to locate binding regions of Sti1. A FRET system between Hsp70 and Sti1 has never been described to my knowledge.
Using site-specific labeled Sti1, on the one hand, the FRET system between Hsp90 and Sti1 should be improved and influences of the addition of Hsp70 analyzed. On the other hand, FRET experiments to monitor the interaction of Sti1 with Hsp70 were conducted. By the use of different label positions, the putative switch of Hsp70 between different binding sites within Sti1 should be addressed. To this end, single cysteine mutants of Sti1 were generated by replacing the three native cysteines by serines (C49S, C66S, C453S) and afterwards introducing new cysteines at positions used in section 2.5. Variants containing these mutations showed no significant difference in their stability and inhibition of Hsp90 ATPase activity compared to wildtype Sti1 (Figure 2.19) and are therefore suitable for these experiments.

2.6.1 FRET assay to monitor binding of Sti1 to Hsp90

The different single cysteine mutants of Sti1 were labeled with ATTO 550 and yHsp90 was randomly labeled with ATTO 488. No specific FRET signal between Sti1 and Hsp90 was detected with Sti1 S2C, Sti1 G309C, Sti1 G588C, Sti1 C453 (native cysteine) or randomly labeled Sti1. Only with Sti1 S523C, FRET was observed as indicated by an increase of acceptor signal (576 nm) and a decrease of donor signal (523 nm) upon addition of labeled Sti1 (Sti1*) to labeled Hsp90 (Hsp90*) (Figure 2.23, A). This effect was reversible by adding excess of unlabeled Hsp90 or unlabeled Sti1. As controls, addition of the unlabeled protein to the labeled component did not influence the spectra and no FRET-like behavior was detected after addition of Hsp90 ATTO 550 to Hsp90 ATTO 488 (Figure 2.23, B).

Having established this system, it was used for a kinetic analysis of the formation of Sti1-Hsp90 complexes (Figure 2.24). The complexes formed rapidly within a few seconds as can be seen by the simultaneous, fast increase of acceptor and decrease of donor signal. The addition of unlabeled Hsp90 abolished the FRET signal in a similar time frame.
This shows that the binding of Hsp90 to Sti1 can be monitored using this system. Stopped-flow measurements for a deeper evaluation of the kinetics demonstrated that the binding is a multistep process [Lee et al., 2012]. The fact that only one of the single cysteine mutants of Sti1 worked in this setup illustrates that FRET is highly dependent on the exact position of the label. S2C and G588C at the very C- and N-terminal ends of Sti1 are far away from the Hsp90 binding module TPR2A-TPR2B explaining that no FRET was detected. The other three label positions are all located in the Hsp90 binding region (Figure 2.25). C453 is buried in a helix of TPR2B and

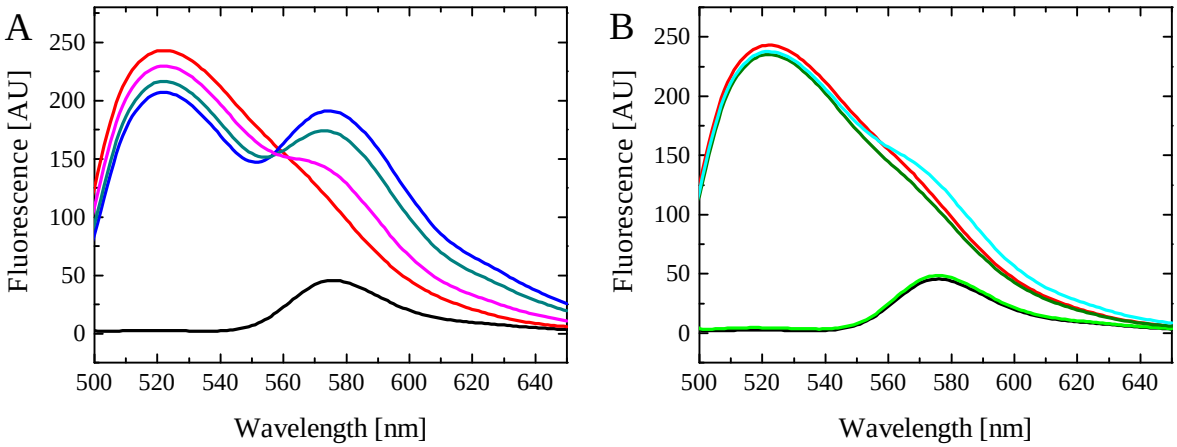

Figure 2.23: FRET between Hsp90 and Sti1 S532C. Wavelength scans with an excitation wavelength of $\lambda = 488\,\text{nm}$ were recorded using 100 nM randomly labeled Hsp90 ATTO 488 (red) and 100 nM specifically labeled Sti1 S532C ATTO 550 (black). A: Mixing of the two proteins (blue) resulted in an increase of the acceptor signal (576 nm) and a decrease of the donor signal (523 nm). Addition of a 10-fold excess of unlabeled Sti1 (dark cyan) or Hsp90 (magenta) lead to a decrease of the FRET signal. B: Corresponding controls adding unlabeled Hsp90 to Sti1 S532C ATTO 550 (green), unlabeled Sti1 to Hsp90 ATTO 488 (olive) and Hsp90 ATTO 550 to Hsp90 ATTO 488 (cyan).

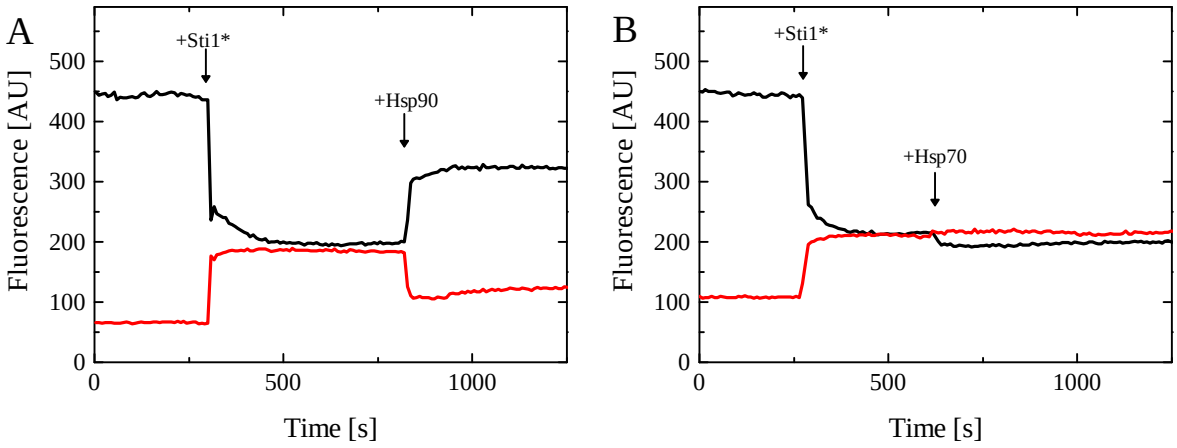

Figure 2.24: Kinetics of FRET between Hsp90* and Sti1* under the influence of unlabeled Hsp90 and Hsp70. Measurement of emission at donor wavelength $\lambda = 523\,\text{nm}$ (black) and acceptor wavelength $\lambda = 576\,\text{nm}$ (red) after excitation with $\lambda = 488\,\text{nm}$ using 300 nM randomly labeled Hsp90 ATTO 488. After 250 sec, 300 nM specifically labeled Sti1 S532C ATTO 550 were added. A: FRET signal after addition of excess unlabeled Hsp90. B: FRET signal after addition of 10-fold excess of Hsp70.

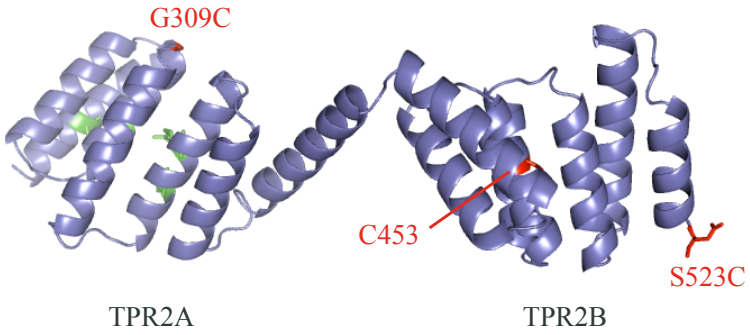

Figure 2.25: Positions of cysteines in TPR2A-TPR2B used for FRET experiments. Crystal structure of TPR2A-TPR2B (PDB: 3UQ3) with cysteines in red. G309C and S523C are located on different sides of the module. C453 is buried in a helix of TPR2B. In green, the carboxylate clamp and residues involved in electrostatic interactions of TPR2A with the Hsp90 peptide are depicted.

probably not accessible. G309C is part of a loop in TPR2A not far from the binding site of the C-terminal EEVD of Hsp90. S523C is located at the C-terminus of TPR2B which comes in close contact to Hsp90-M. G309C and S523C are positioned on opposite sides of TPR2A-TPR2B (Figure 2.25). As FRET was only detected with Sti1 S523C, this is a hint that Hsp90 contacts TPR2A-TPR2B from this side. This confirms the localization of Hsp90-MC towards TPR2A-TPR2B deduced from NMR [Schmid et al., 2012].

Using this system, the impact of Hsp70 on the interaction of Hsp90 with Sti1 was assessed. Upon addition of unlabeled Hsp70, no dramatic change in the fluorescence of the donor as well as of the acceptor was observed. This demonstrates that Hsp70 does not influence the interaction of Sti1 with Hsp90 in this setup and is in line with the unaffected affinities between Hsp90 and Sti1 by Hsp70 [Hernández et al., 2002].

2.6.2 Approaches to establish a Sti1-Hsp70 FRET system

The goal was to establish a FRET system between Hsp70 and Sti1 in order to detect influences on this interaction especially in combination with TPR1 or TPR2B defective mutants and under the addition of Hsp90. However, no specific FRET signal was monitored for a variety of constructs and conditions. Different specifically labeled (single cysteine variants) and randomly labeled Sti1 were tested in combination with randomly labeled yHsp70 (Ssa1) as well as with the substrate binding domain of yHsp70 (SBD) specifically labeled at E632C. Some experiments were also performed with maleimide-labeled yHsp70 (three native cysteines), randomly labeled hHsp70 and FAM-labeled yHsp70 which was used in analytical ultracentrifugation experiments before. Because of the comparably low affinity between Sti1 and Hsp70, a broad range of concentrations

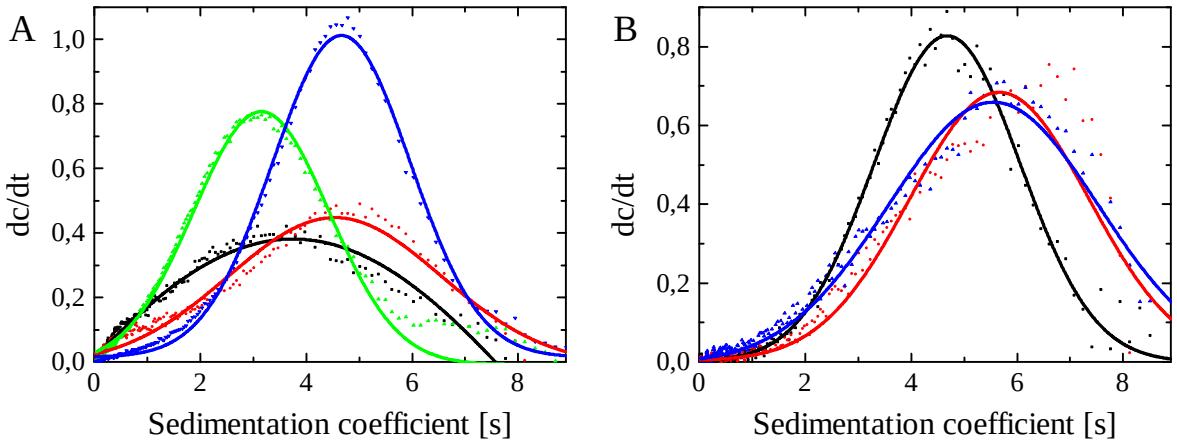

Figure 2.26: Labeled components used in FRET experiments form binary complexes analyzed by analytical ultracentrifugation. A: yHsp70 Atto 488 alone (black) and in complex with unlabeled Sti1 (red). yHsp70 SBD Atto 488 alone (green) and in complex with unlabeled Sti1 (blue). B: Sti1 S2C Atto 550 alone (black) and in complex with unlabeled yHsp70 (red). Sti1 C49S C66S Atto 550 in complex with unlabeled yHsp70 (blue). The data was fitted with Gaussian functions.

was applied (50 nM to 4 µM) and factors which might enhance the interaction like Hsp90, Hsp40 (Ydj1) or ADP were added.
A loss of interaction due to labeling was excluded as the labeled proteins were able to form binary complexes as detected by analytical ultracentrifugation (exemplary in Figure 2.26). Also, labeled Hsp70 still exhibited ATPase activity although some of the labeled variants displayed lower rates of ATP hydrolysis. This proves that the labeling does not completely delete functionality of Hsp70.

The most probable reason why no FRET was detected with the randomly labeled full-length Hsp70 is because the distance between the positions is too large in the complex. Introducing specific cysteines into Ssa1 was omitted because the replacement of one of the cysteines by serine (C15S) leads to instability and loss of function [Wang et al., 2012]. Moreover, the three cysteines are conserved and buried deeply in the secondary structure elements (Figure 2.27). Nevertheless, cysteine labeling via the three native cysteines was tested in combination with the different Sti1 variants but no FRET was observed. The three native cysteines are located in the N-terminal nucleotide binding domain (NBD), far away from the C-terminal EEVD motif explaining why they are not suited for a FRET system between Hsp70 and Sti1.

A good alternative was found by generating the Hsp70 SBD constructs (no native cysteines) in which a specific cysteine was introduced, only a few amino acids behind the EEVD (Figure 2.27, E632C). This position was chosen on the one hand because it is very close to the binding site of Sti1 and on the other hand, because a similar single cysteine variant of the ER Hsp70 homolog BiP (position 636) was suited to detect

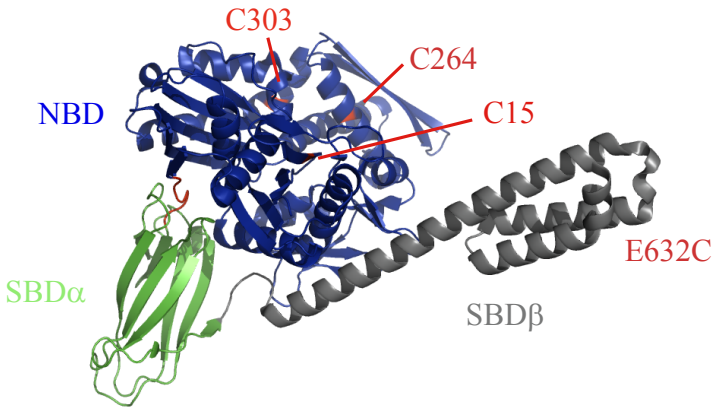

Figure 2.27: Positions of cysteines in Ssa1. Crystal structure of DnaK (PDB: 4B9Q) with positions which correspond to the native cysteines of Ssa1 in red. The introduced cysteine in the SBD is indicated but not resolved in the structure.

FRET with a labeled substrate [Marcinowski et al., 2011]. As this variant still bound to Sti1 as shown by analytical ultracentrifugation experiments (Figure 2.26, B), it can be excluded that the label is so close to the binding site that it interrupts the interaction. In Sti1, various positions have been tested in combination with Hsp70 SBD: the N-terminal end of TPR1 (S2C), positions in DP1 and TPR2A (G131C, G193C, S258C, G309C) and at the C-terminal end of TPR2B and DP2 (S523C, G588C).

Taken together, the conducted experiments prove that the C-terminal EEVD of Hsp70 does not come in close contact to the tested positions of Sti1. To overcome the difficulties in establishing a Sti1-Hsp70 FRET system, it might be promising to generate mutants with cysteines in the inner loops of TPR1 or TPR2B and test them in combination with single cysteine yHsp70 SBD. Once established, this could lead to a more detailed picture of the dynamic interaction of Sti1 with Hsp70 and especially on the function of two alternative Hsp70 binding sites.

2.7 Structural analysis of Sti1 by SAXS

2.7.1 Conformation of TPR2A-TPR2B

In the crystal structure of the two-domain-construct TPR2A-TPR2B together with the Hsp90 peptide, the linker connecting the two domains is structurally well defined [Schmid et al., 2012]. It fixes the two domains in a way that the two peptide binding grooves are oriented in opposite directions (Figure 2.28, left). This arrangement is mainly stabilized by the cation-π interaction between the side chain of R425 and the

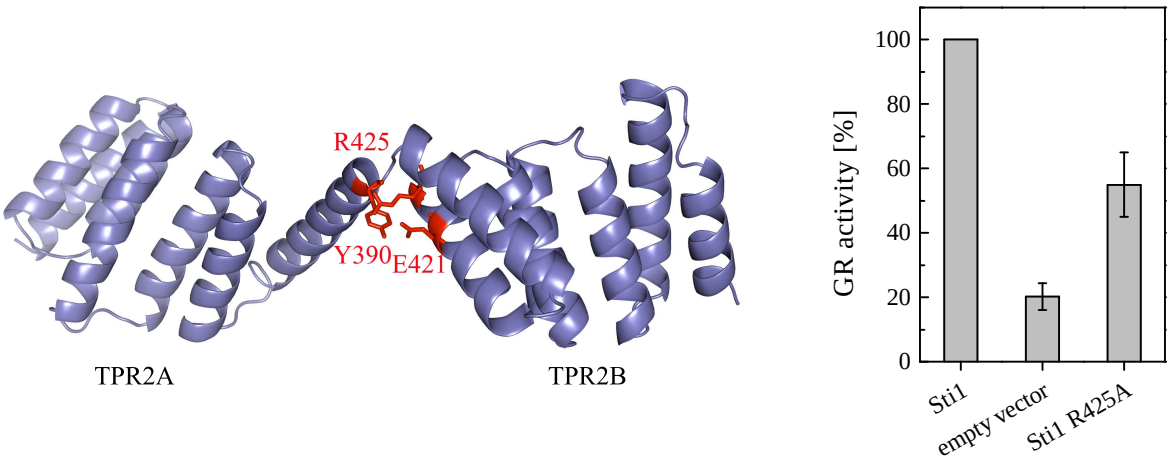

Figure 2.28: Domain arrangement of TPR2A-TPR2B. Left: Crystal structure of TPR2A-TPR2B (PDB: 3UQ3). The two domains are rotated against each other. The residues fixing this arrangement are highlighted in red. Right: Effects of mutation of one of the fixing residues on GR activation in *S. cerevisiae*. Means of at least three independent experiments are shown with their standard deviation.

aromatic ring of Y390. Hydrogen bonds between R425 and E421 as well as between Y390 and E421 further contribute to this. These three residues are strictly conserved among different Sti1 homologs.

To address the *in vivo* role of this conformation, the main fixing residue R425 was mutated to alanine and assayed for GR activation in yeast (Figure 2.28, right). It reconstituted only about 50% of the GR activation of wildtype Sti1 which highlights the importance of this special interface.

To investigate the arrangement of the two domains in solution, the fragment TPR2A-TPR2B was subjected to small angle X-ray scattering (SAXS) in the absence of peptides. The measurements and analysis were performed in cooperation with Dr. Tobias Madl (TU München). The data was evaluated with SASREF [Petoukhov and Svergun, 2005] using the crystal structure of TPR2A-TPR2B. The fit of the computed scattering data and the experimental data aligned very well (Figure 2.29, left). Rigid body modeling revealed that also in solution and in the absence of the Hsp90 peptide, the two domains are rotated to one another with their peptide binding grooves pointing towards opposite sides (Figure 2.29, right). This serves as a basis for SAXS experiments with larger fragments and full-length Sti1.

Taken together, this demonstrates that the twisted conformation of TPR2A and TPR2B exists under different conditions and is important *in vivo*. This suggests that in the ternary complex, Hsp90 and Hsp70 are located on opposite sides of Sti1.

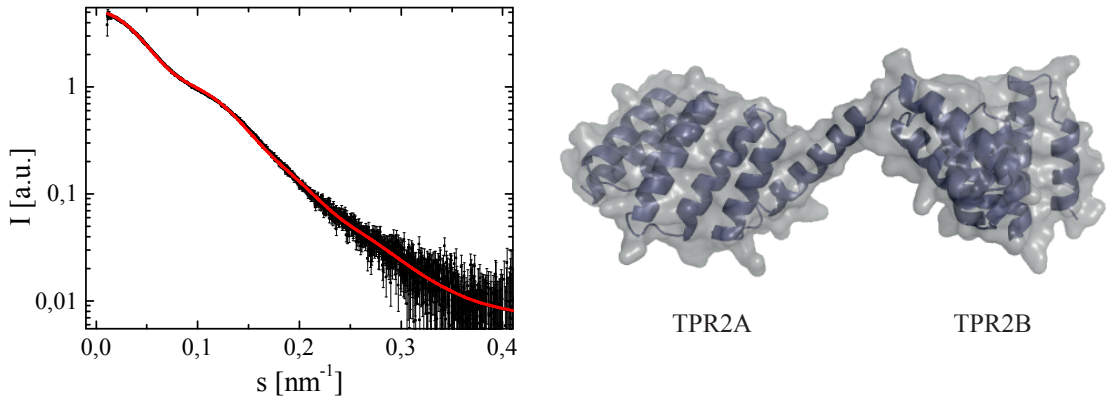

Figure 2.29: Evaluation of the SAXS data of TPR2A-TPR2B. Left: Fit of the scattering curve computed from the crystal structure (red) versus the experimental data (black) with $\chi = 1.399$. Right: Rigid body modeling of the SAXS data (surface) accommodates the crystal structure (cartoon) very well.

2.7.2 Arrangement of Sti1 domains

The structures of the individual domains of Sti1 have been resolved [Scheufler et al., 2000, Schmid et al., 2012] but the overall arrangement of the domains in full-length Sti1 remained largely unknown. Earlier studies have implemented that Sti1 exists in an elongated shape [Yi et al., 2010]. Approaches to determine the shape of full-length Hop by SAXS have been taken but at this time only for two of the domains high resolution structures were available [Onuoha et al., 2008, Romano et al., 2009].
With the additional structural input from our recent publication [Schmid et al., 2012], a comprehensive analysis of the structure of Sti1 with SAXS experiments was now possible. For this purpose, scattering curves of deletion variants and full-length Sti1 were recorded in standard gelfiltration buffer for several solute concentrations from 1 to 10 mg/ml. Rigid body modeling against multiple scattering curves was performed with CORAL [Petoukhov et al., 2012] with the input of the single domain structures and in the case of TPR2A-TPR2B the two domain crystal structure. In principle, the program places and rotates the atomic models of individual domains under certain constraints like the length of the interconnecting linkers. The optimal arrangements are calculated by minimizing the discrepancy between the experimental scattering data and the curves calculated from the respective assemblies.

Of about 50 calculated models, the five fitted structures with the lowest median deviation from the data representing the most probable arrangements are shown in Figure 2.30. For full-length Sti1, six models are shown in detail (Figure 2.31) as among the fitted structures also an alternative arrangement was found which was not represented in the five best fits. For better comparability, TPR2A-TPR2B has been set in the center of the view. In the different models, the long linker connecting DP1 with TPR2A shows

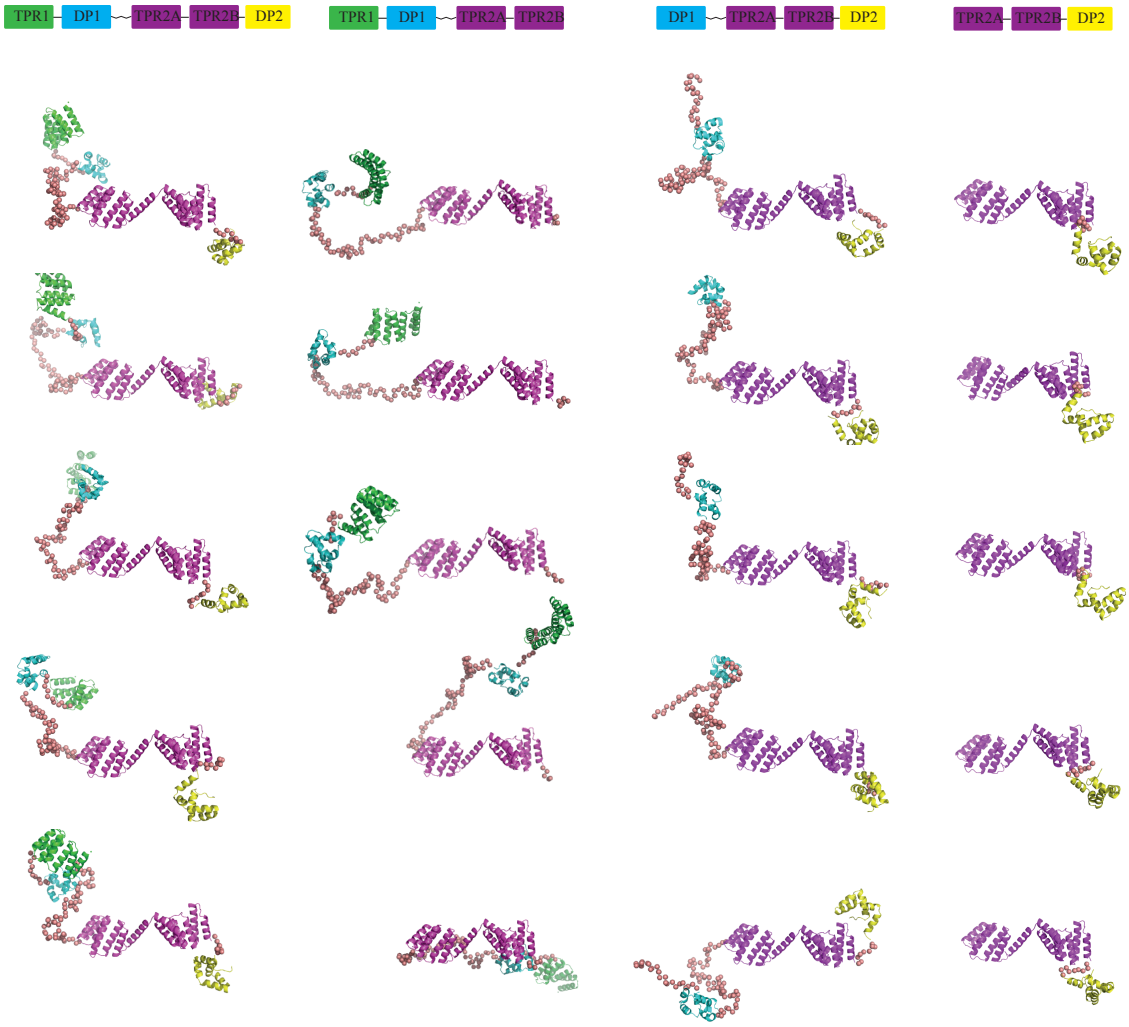

Figure 2.30: Overview of the SAXS models of Sti1 full-length and fragments. Structures from the rigid body modeling of the SAXS data with the lowest χ values are represented. Linkers are depicted as interconnected 'dummy' residues. From left to right: Sti1 full-length, ΔDP2, ΔTPR1, ΔTPR1-DP1.

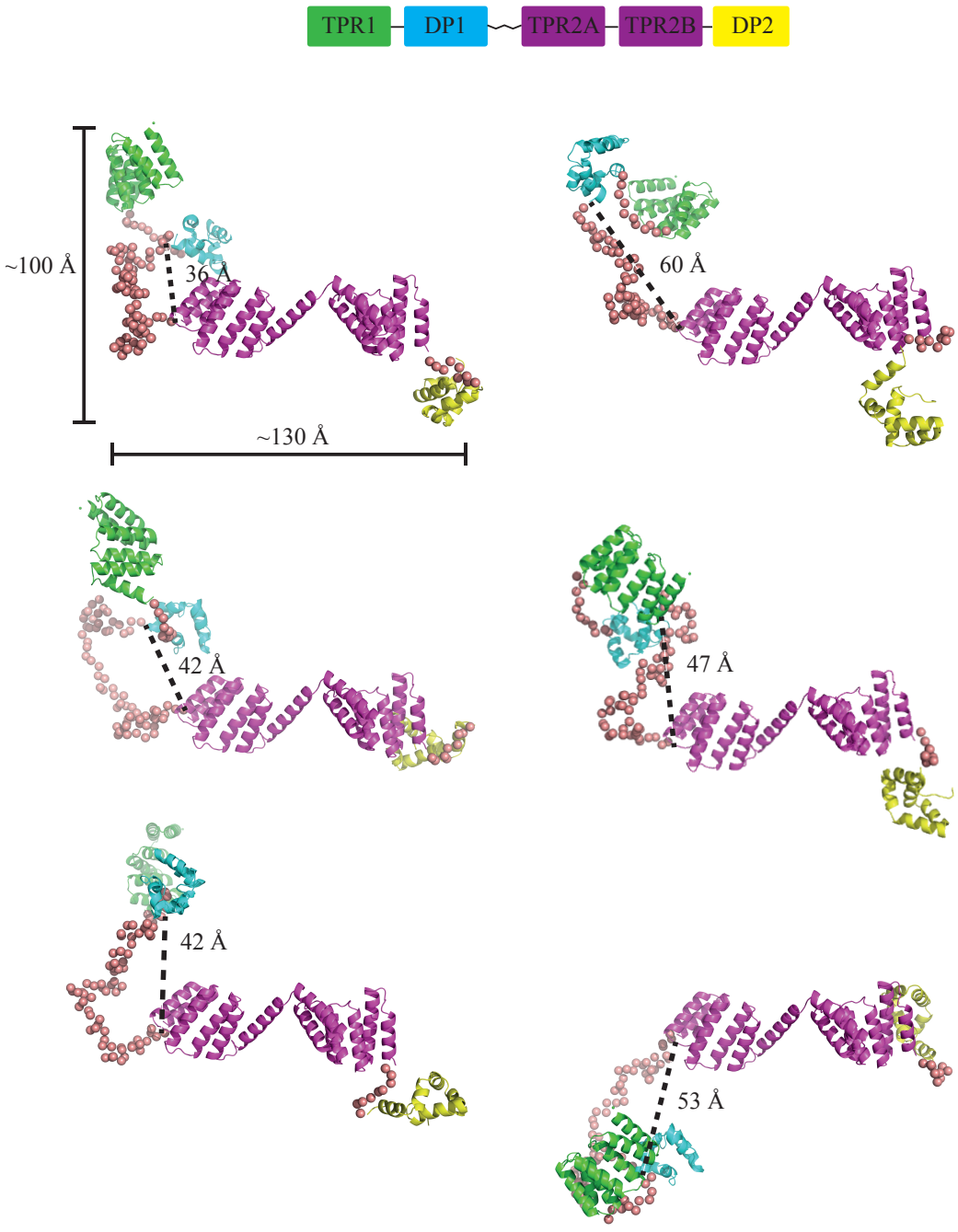

Figure 2.31: SAXS models of full-length Sti1. Structures from the rigid body modeling of the SAXS data with the lowest χ values are represented. Distances of linker boundaries and approximate side lengths are indicated. Linkers are depicted as interconnected 'dummy' residues.

different arrangements but it mostly kinked. Consequently, the overall structures are elongated but not entirely stretched. TPR1 and DP1 are not directly attached to any other domain but are relatively apart from the other rest of the protein. In different models, they are positioned in different angles and distances with respect to TPR2A-TPR2B. This strongly argues for them being detached and only flexibly linked to the rest of the protein.
DP2, in constrast, is not completely mobile as it is more closely attached to TPR2B. DP2 consistently is kinked to the opposite side as TPR1-DP1 is, and except for two models, this is also one particular side relative to TPR2A-TPR2B (in this view to the 'bottom'). However, to evaluate if this is indeed statistically relevant, a larger number of models has to be compared. The residues at the boundaries of the linker in Sti1 full-length are 36 to 60 Å apart.

In conclusion, the Sti1 full-length models suggest that TPR1 and DP1 are detached and far apart from the rest of the protein inducing a mostly elongated shape. Especially the long linker is highly flexible. This encourages the idea of the linker being the versatile element of Sti1 which allows Hsp70 to switch from one to another TPR domain. DP2 is fixed towards TPR2B to some extent which may be important for the interaction with Hsp70 and the client.

The orientation of the domains of Sti1 presented here sheds light on the results from the smFRET experiments in section 2.5. Means and standard deviation of the distances of the introduced cysteines in the different Sti1 full-length models are given in table 2.1. In the first three combinations, distances above 100 Å have been derived from the SAXS models. This is above the maximum distance detectable with FRET and explains why the FRET efficiencies of these variants were very low.
In contrast, mean distances between the other residue combinations are in the range of 47 to 70 Å. The used label pair has a Förster radius of 60 Å and this commonly serves as a orientation for which distances the dyes are applicable (Instructions of the manufacturer of the labels, AttoTec). Therefore, the distances lie in the range of detection arguing for their suitability for this approach. For G131-G309, G193-G309 and G193-S258, even though the number of amino acids in between is different, the SAXS models suggest very similar distances of around 50 Å. This explains why the FRET efficiencies between these three labeled residues were also similar to each other. However, the FRET measurements detected distances of 70-80 Å. The 20-30 Å discrepancy might be explained by the orientation and the length of the linker of the attached dye.
The structural information obtained here will now allow the design of more suitable mutants for smFRET experiments. Furthermore, SAXS measurements with full-length Hsp90, Hsp70 and fragments thereof are currently ongoing and will provide information on the organization of the complexes. This will in addition improve the selection of positions for specific labeling for the intermolecular FRET measurements.

	Mean	SD
S2-G588	136 Å	18 Å
S2-S523	129 Å	16 Å
G131-S523	110 Å	10 Å
S2-G309	70 Å	13 Å
G131-G309	49 Å	13 Å
G193-G309	50 Å	16 Å
G193-S258	47 Å	9 Å

Table 2.1: Distances between residues used in smFRET experiments from the six selected SAXS models of Sti1 full-length. Means and standard deviation (SD) are given.

2.8 Electron microscopy of the Hsp90-Sti1-Hsp70 complex

A TEM-based structural analysis of the ternary Hsp90-Sti1-Hsp70 complex was realized in collaboration with Sara Alvira from the group of Prof. Jose Valpuesta (CSIC, Madrid). Protein complexes were isolated using GraFix, a method in which the complexes are separated by a glycerol gradient and simultaneously mildly crosslinked with glutaraldehyde [Kastner et al., 2007]. After negative staining, electron microscopy was performed and particles were selected from the electron micrographs, classified and used for 3D reconstructions. Complexes of the human homologs were investigated with the same procedure. Similar volumes were obtained arguing for the reliability of the method for these particular complexes (Figure 2.32).
For the attribution of the densities to individual proteins, Hsp90 was also analyzed alone and in the presence of Sti1/Hop only. Analogy with the human complexes was assumed for the positioning of the single domains. For the human system, the NBD and SBDα of Hsp70 as well as Hop-DP2 were localized with the help of immunomicroscopy. The contributions of TPR1-DP1 were determined with deletion variants of Hop. Additional input was the interaction of Hsp90-C with TPR2A. With this information, high resolution structures of single proteins or domains were docked into the reconstructions (Figure 2.32, bottom).

In these docking models, the ternary complex adopts a rather compact structure. The crystal structure of closed Hsp90 was docked into the center of the density. Sti1 and Hsp70 are asymmetrically positioned towards the Hsp90 dimer, mainly located at one of the two monomers. TPR2A is located close to the C-terminal domain of Hsp90

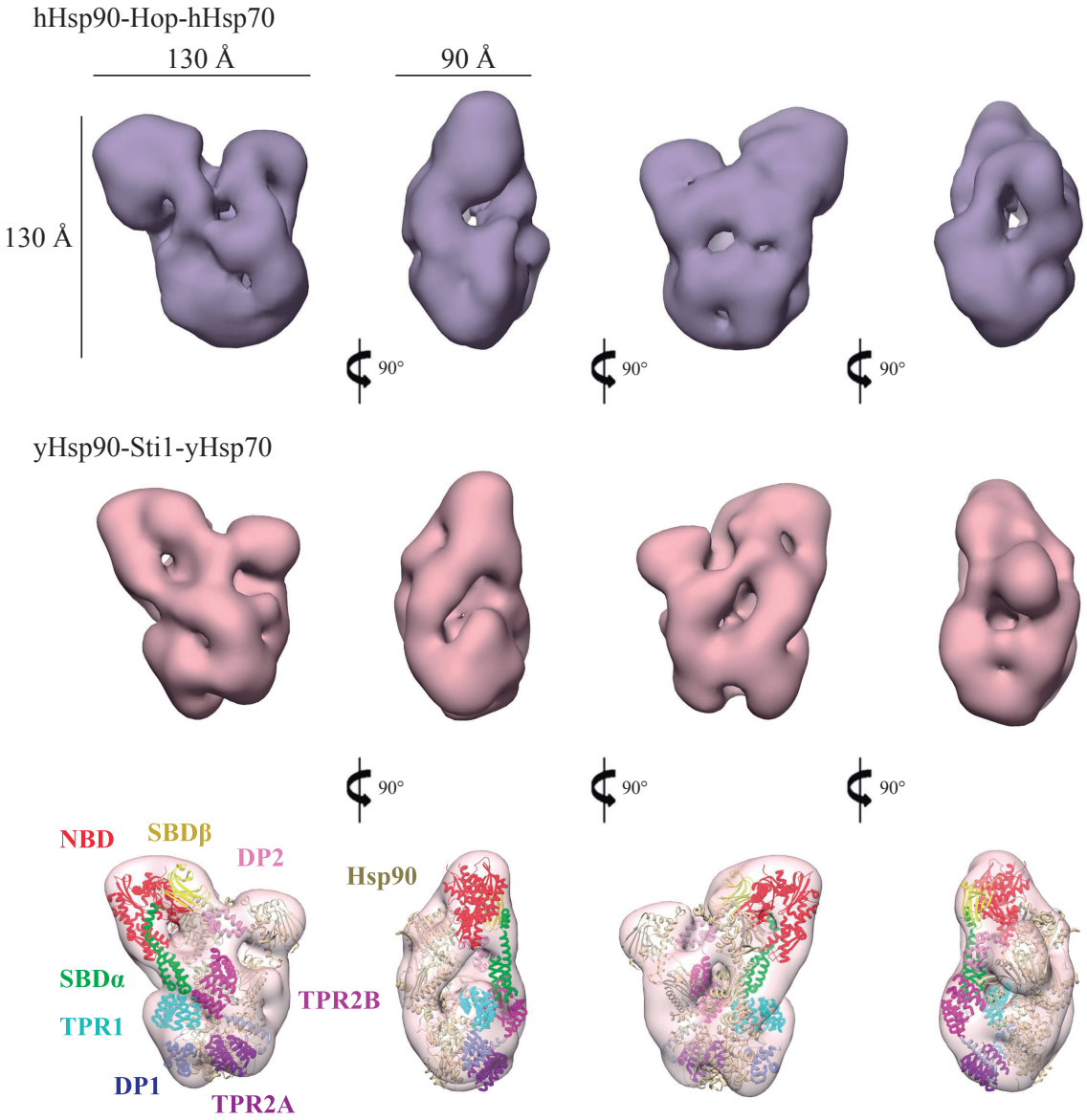

Figure 2.32: 3D reconstructions of the ternary Hsp90-Sti1-Hsp70 complex. Top row: Orthogonal views of the human ternary complex (violet, 21 Å resolution). Middle row: Orthogonal views of the yeast ternary complex (pink, 21 Å resolution). Bottom row: Docking of the protein and domain structures into the yeast 3D reconstruction analogous to the docking of the human complex. The following PDB structures were used: Hsp90 (2CG9), Hsp70 (1YUW), TPR1 (1ELW), DP1 (2LLV), TPR2A (1ELR), TPR2B (3UPV), DP2 (2LLW).

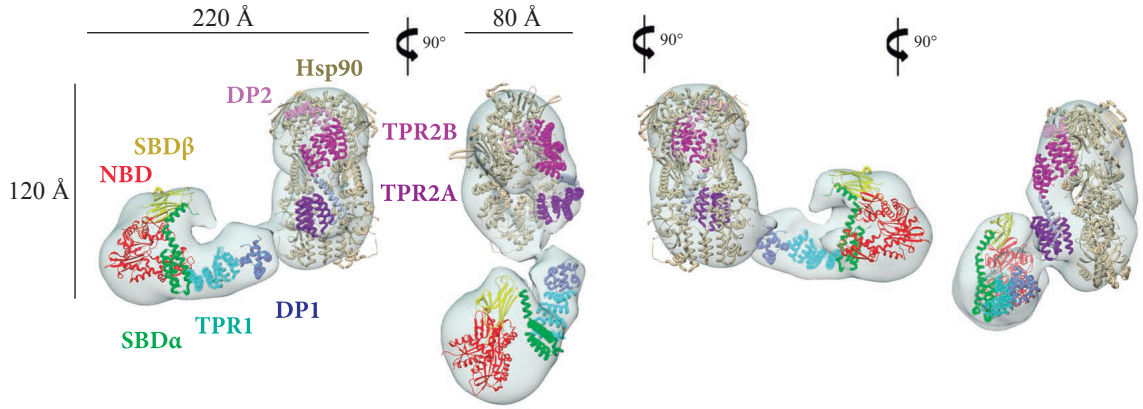

Figure 2.33: 3D reconstructions of the alternative Hsp90-Sti1-Hsp70 ternary complex. Orthogonal views of the complex comprising TPR2B defective Sti1 (R469A), Hsp70 and Hsp90 (26 Å resolution). Docking according to suggested positions: As the crystal structure of Hsp90 only fits into the major mass and TPR2A-TPR2B-DP2 are supposed to associate with Hsp90, the rest of the volume should correspond to TPR1-DP1 and Hsp70.

while TPR2B associates with Hsp90-M. DP2 is attributed to a mass in between the two Hsp90 N domains where it is also close to Hsp70. According to the docking, Sti1 bends like a jackknife with the linker being the center of the motion. This induces a close proximity of the two Hsp70 binding TPR domains, TPR1 and TPR2B. The C-terminal lid of Hsp70 (SBDα) is positioned directly in between these two. The NBD of Hsp70 is located in a bulge near the N-domains of one of the Hsp90 subunits.

Interestingly, about 15 % of the particles displayed a different topology and exhibited an elongated shape. We suspected that this was correlated to the presence of two Hsp70 binding sites in Sti1 and tested complexes with a Sti1 construct with mutated TPR2B binding site (R469A). Intriguingly, this forced the complex into the elongated conformation so that the 3D reconstruction of this alternative state was possible (Figure 2.33). In the alternative state, the structures of the single components have been docked at suggested positions without directly being localized by immunomicroscopy: The crystal structure of Hsp90 only fits into the major mass and is presumed to be associated with TPR2A-TPR2B. As TPR2B of Sti1 R469A is defective for Hsp70 binding, Hsp70 must be bound to TPR1 which, together with DP1, are suggested to fill the additional mass.

In conclusion, the main population of the ternary complex adopts a compact shape where Hsp90 and Hsp70 are in intimate contact. The crystal structure of closed Hsp90 was used for the docking. This may seem to be in contrast to Sti1 stabilizing the open conformation of Hsp90 [Richter et al., 2003, Hessling et al., 2009]. Sti1 shifts the equilibrium between open and closed Hsp90 towards the open state but may not completely prevent the closing reaction. The crosslinker which is added to the complexes

after formation could trap this rarely occuring closed state as it randomly links residues which come in close contact. This argues against this conformation being mainly an artifact.
The location of TPR2A-TPR2B fits the expected positions from previous structural studies [Schmid et al., 2012]. The bent linker brings the two Hsp70 binding domains, TPR1 and TPR2B, in close contact enclosing the C-terminal lid of Hsp70. It is easy to imagine how this could facilitate the transfer of Hsp70 between these two domains. In an alternative elongated conformation, the module TPR1-DP1, together with Hsp70, is suggested to be farer apart from Hsp90 and the rest of Sti1 mediated by a more elongated conformation of the linker. Considering that the Sti1 mutant used in this complex did not support GR activation *in vivo*, it is likely that the intimate contact of Hsp90 and Hsp70 is required for the transfer of client. In the compact reconstruction where Hsp70 is supposedly bound to TPR2B, DP2 is in close proximity to Hsp70 while in the alternative reconstruction, where Hsp70 must be bound to TPR1, DP1 is close to Hsp70. This indicates that the DP domains may lead to a stabilization of the interaction with Hsp70.
TPR2A-TPR2B-DP2 adopts a similar conformation in both reconstruction, while the differences seem to be conveyed by the flexible linker. The arrangement of the domains in the alternative conformation fits better to the SAXS models of Sti1 than in the compact structure. This indicates that either the presence of Hsp90 and/or Hsp70 induces the compact conformation or that the crosslinker 'freezes' the intimate contact. It is noteworthy that both methods, SAXS and EM, do not allow determination of the exact orientation of domains. Considering that in the smFRET experiments a tightening of domains attached by the linker was observed upon addition of Hsp70, it is likely that the binding of Hsp70 induces the compact conformation of Sti1.

In a recent study, another group has assessed the structure of the human Hsp90-Hop complex by cryo EM [Southworth and Agard, 2011]. They concluded that Hsp90 adopts an 'alternate open state' in the presence of Hop. The analysis shown here represents an improvement to this study: Southworth and Agard were only able to obtain complexes when, in addition to fixation by glutaraldehyde, Hsp90-C and Hop TPR2A were specifically crosslinked via a disulfide bond leading to a more artificial complex. Moreover, in these complexes, Hsp90 and Hop are found in a 2:2 stoichiometry which is in contrast to ratios determined by others [Li et al., 2010, Yi et al., 2010, Schmid et al., 2012]. Another shortcoming of the work is the docking of the single components. No experimental localization has been performed here and only two of the five domains of Hop are represented in the final model.

Taken together, this structural analysis suggests that Sti1 adopts two conformations in the ternary complex. One is compact with a bent linker and Hsp70 bound to TPR2B in close proximity to Hsp90. The other one is elongated and here, Hsp70 is bound to TPR1 relatively far apart from Hsp90.

2.9 Comparison of yeast Sti1 and human Hop

Sti1 from *S. cerevisiae* and human Hop share large sequence and structural similarity. Both comprise the same domain arrangement of two TPR-DP modules with the connecting linker exhibiting the lowest degree of conservation. In GR activation assays in yeast, Hop can complement for Sti1 and the domains important for this function are the same: TPR1 is dispensable and DP2 is essential in this respect (Andreas Schmid, PhD Thesis). However, differences have been reported in regard to their regulation of Hsp90. This is why a more detailed comparison of the two homologs was of interest.

2.9.1 Inhibition of the ATPase activity of Hsp90

Sti1 from *S. cerevisiae* is a potent inhibitor of the Hsp90 ATPase activity [Prodromou et al., 1999, Richter et al., 2003]. For the human system, only one study addressed this issue finding no inhibitory effect of Hop on the basal ATPase rate of human Hsp90 (hHsp90) [McLaughlin et al., 2002] despite the high structural similarity and sequence conservation of the two homologs. McLaughlin et al. only observed an inhibition of the client-stimulated ATPase activity of hHsp90 after addition of Hop.

To analyze these differences closer, we tested the inhibitory potential of Sti1 and Hop on Hsp90 in physiological and mixed combinations (Evelyn Bender, Master's Thesis). To our surprise, Hop and Sti1 inhibited the ATPase activity of yHsp90 and hHsp90 in both scenarios (Figure 2.34). For each combination, maximal inhibition was reached at an equimolar concentration of Hsp90 and the inhibitor. The ATPase activity of yHsp90 was almost completely inhibited by Sti1 and Hop (around 15 %), while the ATPase activity of hHsp90 was inhibited to a smaller degree (around 30-40 %). For both, Sti1 and Hop, the central element TPR2A-TPR2B was already sufficient for inhibition of the yHsp90 ATPase activity.

This implies that both homologs in principle regulate Hsp90 in the same manner and that the minimal fragment responsible for inhibition is conserved from yeast to man. Some species-specific differences exist, as hHsp90 was inhibited about half as efficiently as yHsp90. This might be correlated to the fact that hHsp90 on its own is already a much weaker ATPase [Richter et al., 2008]. In consequence, the measurement of the ATPase activity of hHsp90 can be easily influenced by contaminant ATPases which could account for the reported differences in the previous study [McLaughlin et al., 2002]. Impurities in their protein preparations could have overlaid the inhibitory effect of Hop. To avoid this, in this work, contaminant ATPases were largely removed from the protein solutions by a Hydroxyapatite column, radicicol controls were evaluated carefully and the inhibitor preparation was assessed individually for its ATPase activity.

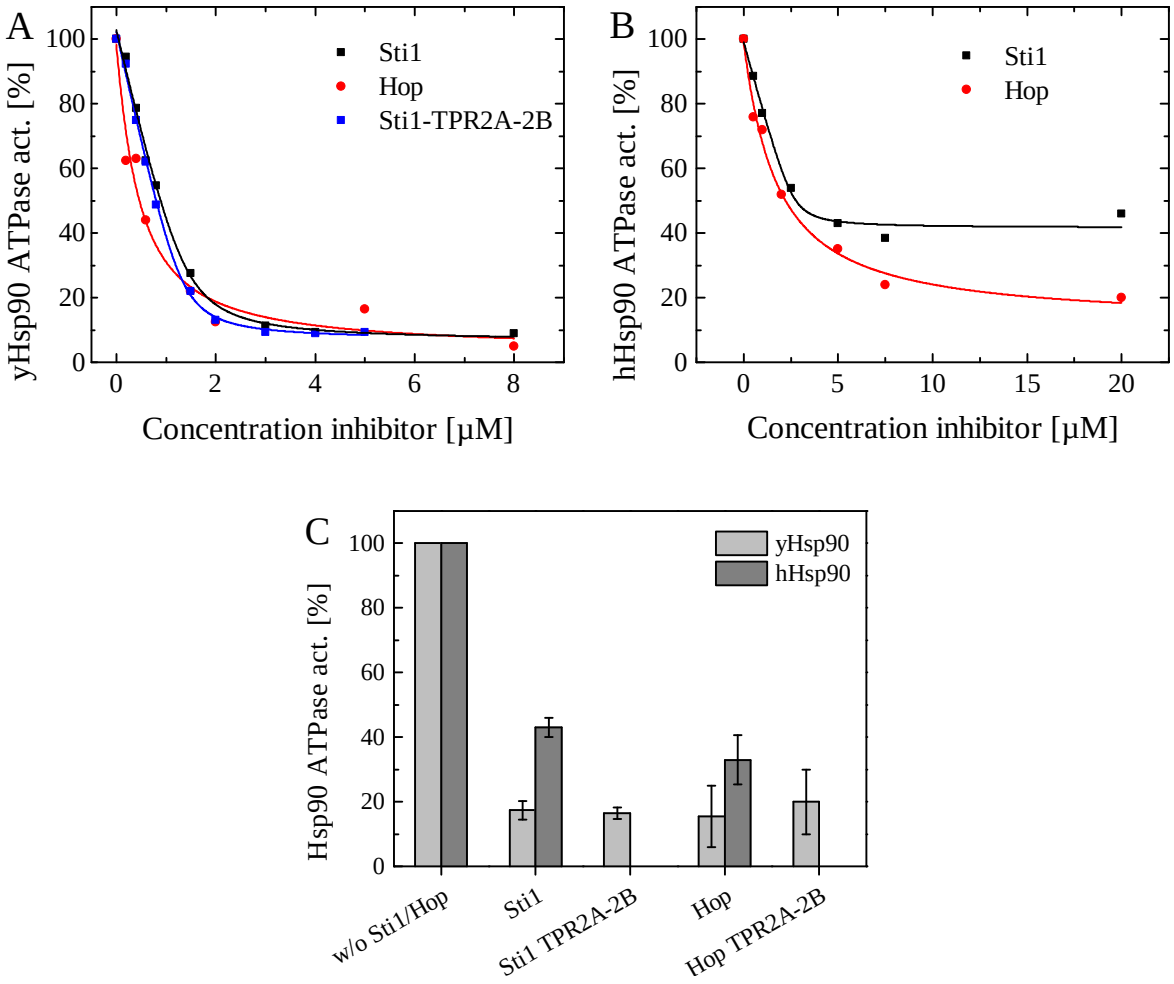

Figure 2.34: Effects of Sti1, Hop and TPR2A-TPR2B on the ATPase activity of yeast and human Hsp90. ATPase assays with yHsp90 were performed at 30 °C, those with hHsp90 at 37 °C. Titration of Sti1, Hop and Sti1 TPR2A-TPR2B to 2 µM yHsp90 (A) and to 5 µM hHsp90 (B). Means of three independent experiments were fitted as described in 4.6.1. C: Values at equimolar concentrations of Hsp90 and Sti1/Hop variant derived from the fit with their standard deviations are shown. Inhibition with Hop TPR2A-TPR2B was determined in three independent end-point measurements.

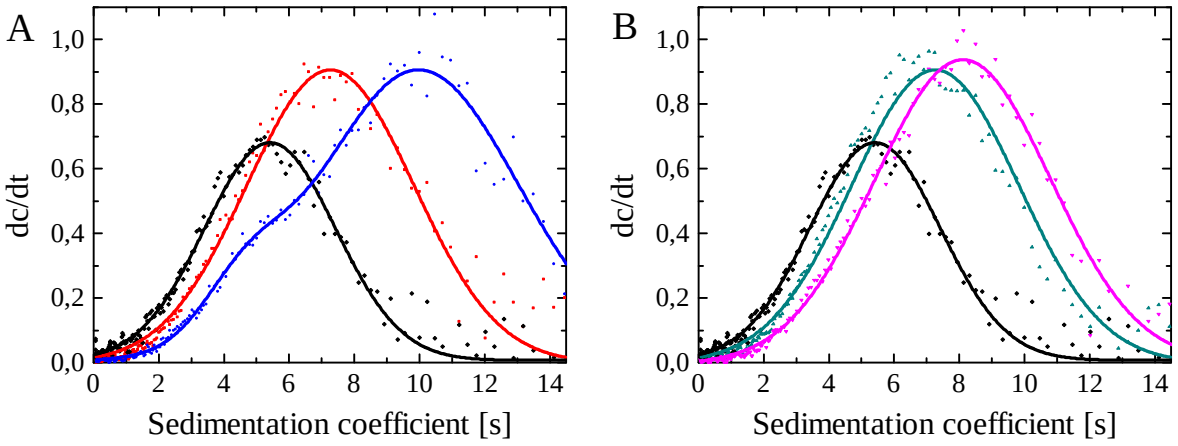

Figure 2.35: Complexes by labeled hHsp70 with Hop variants and hHsp90 analyzed by analytical ultracentrifugation. A: Complexes formed by labeled hHsp70 (hHsp70 alone: black) with Hop (red) and after addition of hHsp90 (blue). B: hHsp70 in the presence of Hop TPR2A-TPR2B (dark cyan) and after addition of hHsp90 (magenta). The data was fitted with (bi-) Gaussian functions.

2.9.2 Interaction of Sti1 versus Hop with Hsp90 and Hsp70

Sti1 and Hop were probed for their interaction towards Hsp90 and Hsp70, again in the physiological and in the mixed system via SPR analysis and analytical ultracentrifugation experiments.
Sti1 and Hop exhibited affinities towards both Hsp90 homologs in the same order of magnitude, although yHsp90 bound stronger to Sti1 and Hop than hHsp90 (Figure 2.36). The affinities towards the Hsp90 homologs were consistent with the degree of inhibition (Figure 2.34). Also the two Hsp70 homologs bound Sti1 and Hop with similar affinities with yHsp70 being the slightly stronger interactor.
As shown before in section 2.1, binary and ternary complexes can be visualized by analytical ultracentrifugation with proteins from the yeast system. With labeled hHsp70, the analogous complexes were formed with the human proteins (Figure 2.35). Ternary complexes were also observed using Hop TPR2A-TPR2B.

In conclusion, Sti1 from *S. cerevisiae* and human Hop interact with Hsp90 and Hsp70 similarly, both inhibit the ATPase activity of Hsp90, and the homologs are in principle interchangeable in these respects. Together with the observation that the same domains of Sti1 and Hop are important for *in vivo* GR activation, this indicates that the bridging of substrates between Hsp90 and Hsp70 is conserved from yeast to man. However, species-specific differences exist in the affinities between the components of the complex. Generally, the yeast system seems to require slightly higher affinities. This may be correlated to each organism comprising a different set of cochaperones [Johnson and Brown, 2009].

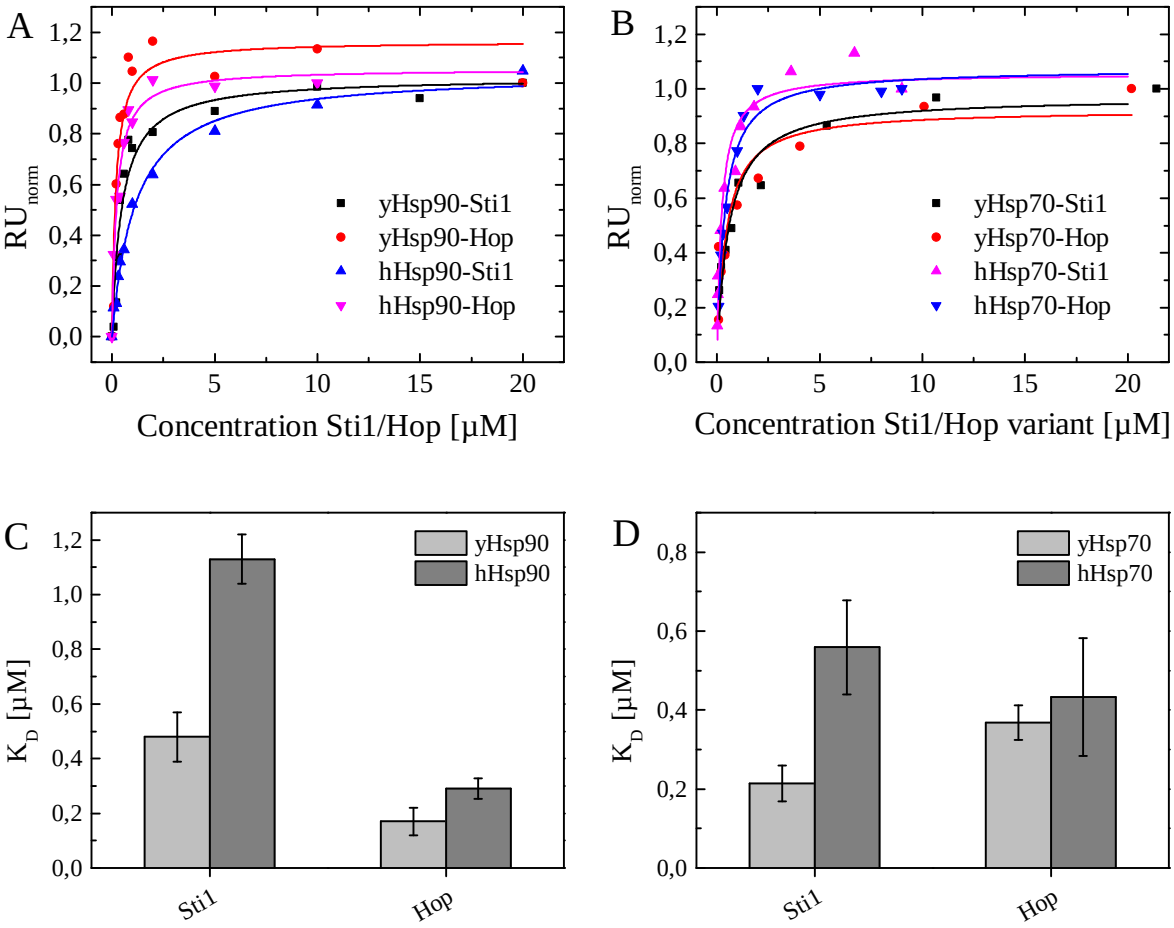

Figure 2.36: Affinities of Sti1 and Hop towards Hsp90 and Hsp70 determined by SPR using Hsp90/Hsp70-coupled chips. Titration of Sti1 and Hop to yHsp90 or hHsp90 (A) and yHsp70 or hHsp70 (B) fitted as described in section 4.5.7. C and D: Derived K_D values for the different interactions with the fitting error are shown.

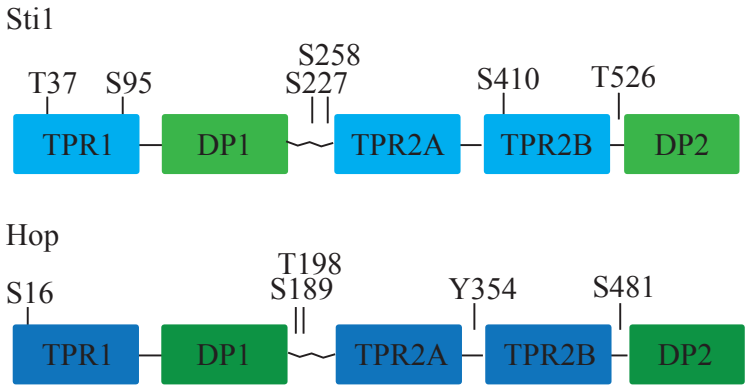

Figure 2.37: Location of phosphorylation sites in Sti1 and Hop. The phosphorylation sites are broadly distributed with hotspots at the Hsp70 binding domains TPR1 and TPR2B and the linker.

2.10 Phosphorylation of Sti1 and Hop

In mammalian Hop, five conserved phosphorylation sites have been identified by mass spectrometry: S16, S189, T198, Y354, S481 (Figure 2.37, www.phosphosite.org). A few studies investigated the role of phosphorylation at S189 and T198 in mouse Hop which were found to control nuclear localization of the protein [Lässle et al., 1997, Longshaw et al., 2004, Daniel et al., 2008]. The other sites in contrast have never been analyzed in detail. Especially Y354 (corresponds to Sti1 Y390) is interesting as it is located directly at the domain contact of TPR2A and TPR2B. This region has been shown to exhibit a crucial role for client activation (see section 2.7.1).
For Sti1, a global phosphorylation screen of yeast proteins has recently identified six phosphorylation sites: T37, S95, S227, S258, S410, T526 (Figure 2.37) [Schreiber et al., 2012]. Only one of these regulatory sites is conserved compared to mammalian Hop (S481 in Hop, T526 in Sti1). In Sti1, except S95, all of the phosphorylation sites are located in loop regions or unfolded regions. In both Hop and Sti1, phosphorylation sites are broadly distributed but hotspots occur in the Hsp70 binding TPR domains (TPR1 and TPR2B) and in the linker.

To test for the effects of phosphorylation, phospho-mimicking variants of Sti1 and Hop using glutamate replacements were generated. Glutamate is a good replacement for phosphorylated serine or threonine as they have a similar size and are both negatively charged. In the case of tyrosine with its bulky aromatic ring, glutamate does not mimic the phosphorylated state as well. However, it is still the best and most widely used natural amino acid substitution [Xu et al., 2012]. Plasmids were constructed for recombinant purification as well as for *in vivo* yeast assays.

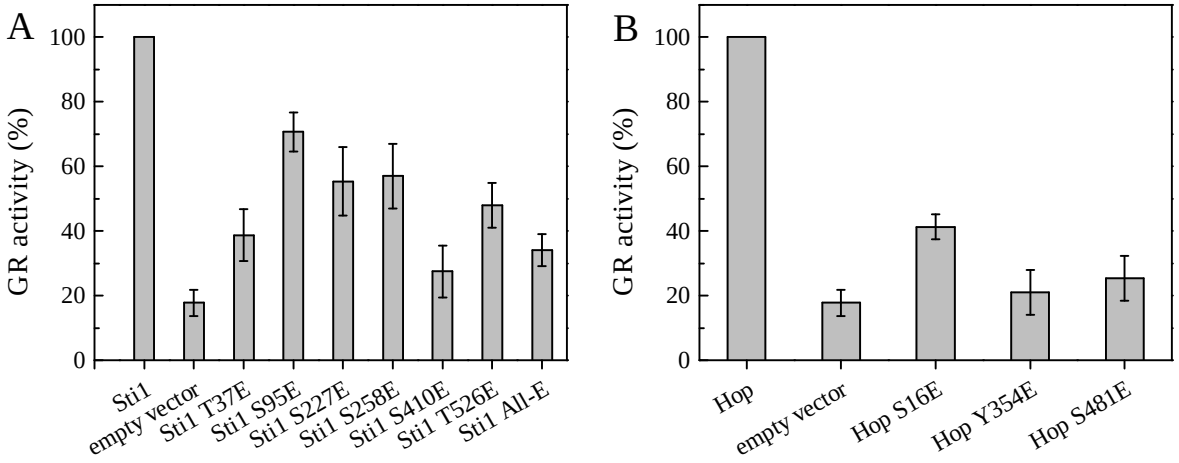

Figure 2.38: Effects of phospho-mimicking mutations in Sti1 (A) and Hop (B) on GR activation in *S. cerevisiae*. Means of at least three independent experiments are shown with their standard deviation. The phospho-mimics generally reduce GR activation.

2.10.1 In vivo effects of phospho-mimicking mutations

In the GR activation assay, the phospho-mimics generally showed a decrease in substrate activation (Figure 2.38). For Sti1, the most striking effects were caused by mutations at positions T37 and S410, located in the two Hsp70 binding TPR domains of Sti1. Replacement of all of the residues with glutamate (Sti1 All-E) did not lead to a stronger reduction of GR activation than the single replacements which indicates that the effect of the phospho-sites is not additive. Mimicking the phosphorylation in Hop also dramatically reduced GR activation. S16E, located in TPR1, and S481E, at the boarder of TPR2B, diminish client activation as well as Y354E at the domain contact of TPR2A and TPR2B.

Taken together, this shows that especially phosphorylation in or close to the Hsp70 binding TPR domains affects client activation. Although deletion of TPR1 did not influence levels of GR activation (see section 2.1), the single point mutations in TPR1 tested here, did. This proves that TPR1, if present, has an impact on client activation. Furthermore, the strongly affected activity upon mutation of Y354 highlights again the special role of the contact between TPR2A and TPR2B.

2.10.2 In vitro effects of phospho-mimicking mutations

The initial *in vitro* characterization of the phospho-mimicking mutants, the CD spectroscopy and ATPase assays of Sti1 mutants, was performed by Evelyn Bender in her Master's Thesis supervised by myself. The introduction of phospho-mimicking residues

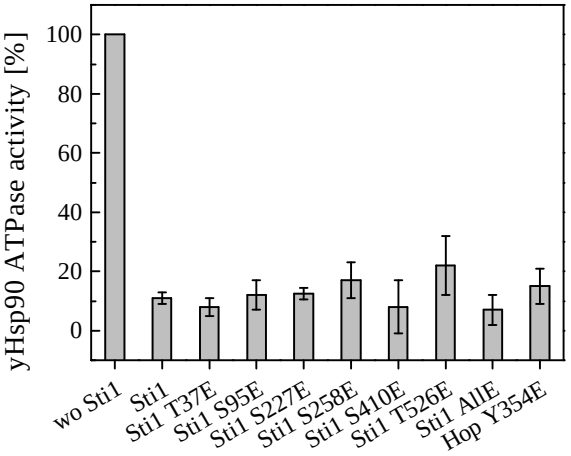

Figure 2.39: Effects of phospho-mimicking mutations in Sti1 and Hop on inhibition of the ATPase activity of Hsp90. Means of values at equimolar concentrations of yHsp90 and Sti1 variant and their standard deviations are shown, determined in three independent experiments. The phospho-mimics inhibit the ATPase activity like wildtype Sti1.

did not influence secondary structure or stability of the proteins. Thermal transitions for all of the mutants occurred between 45 °C and 47 °C as it was the case for Sti1 wildtype (primary data see Master's Thesis of Evelyn Bender). Moreover, the glutamate mutants were able to inhibit the ATPase activity of Hsp90 like wildtype Sti1 indicating that phosphorylation does not interfere with Hsp90 interaction (Figure 2.39).

Next, the interaction of the phospho-mimics with Hsp70 was probed. SPR analysis showed that the phospho-mimicking mutations generally decreased affinities for Hsp70 (Figure 2.40, A). The effect was strongest for Sti1 S410E and Hop Y354E. As only slight differences in the dissociation constants were observed, the results were confirmed by the complex formation monitored by analytical ultracentrifugation. Here, the phospho-mimics were titrated to a constant concentration of labeled Hsp70 and the sedimentation coefficients of the resulting complexes were plotted against the Sti1/Hop concentration. Multiple runs were performed, each time Sti1 wildtype served as reference and values were normalized to levels of the first measurement (Figure 2.40, B-D). With this method, the tendency of the phospho-mimics for lower affinities towards Hsp70 was backed up.

This allows the conclusion that phosphorylation of Sti1 and Hop negatively effects the interaction with Hsp70. The strongest effects were observed for Sti1 S410E and Hop Y354E which also had the most pronounced impact on *in vivo* activity. This suggests a direct connection between affinity towards Hsp70 and *in vivo* client activation, both regulated by phosphorylation. In addition, other factors may play a role. The interaction of the multichaperone complex with the client may also be affected by phosphorylation of Sti1/Hop but this could not be addressed yet as *in vitro* handling

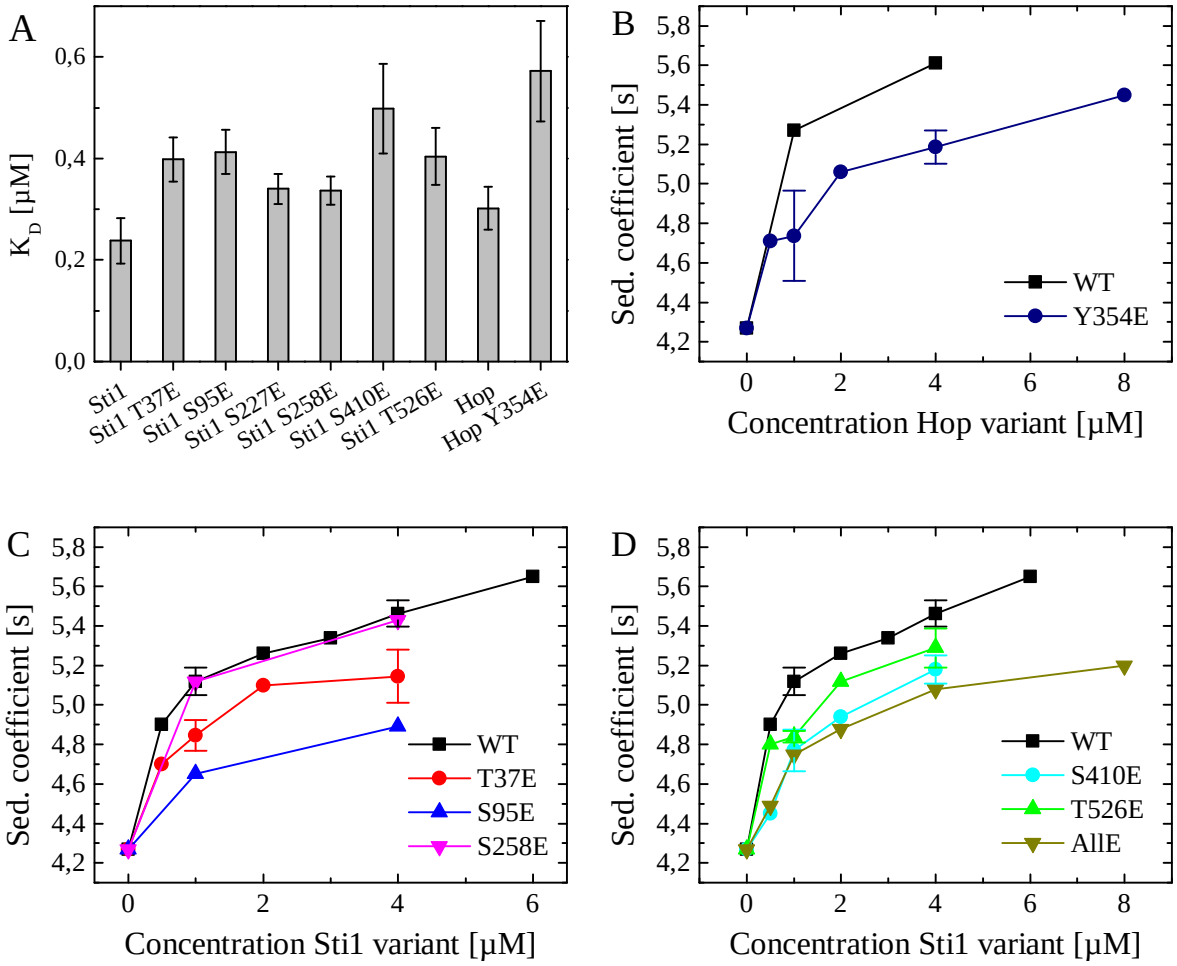

Figure 2.40: Effects of phospho-mimicking mutations in Sti1 and Hop on interaction with Hsp70. A: SPR analysis with a yHsp70 coupled chip. Error bars indicate fitting error. B-D: Comparison of sedimentation coefficients of Hsp70-Sti1/Hop-complexes for different concentrations of the Sti1/Hop variants. If multiple measurements have been performed, the error bars indicate standard deviation. The continuous line serves only as a guide for the eye. Hop phospho-mimics (B): Hop wildtype (black), Hop Y354E (navy). Sti1 phospho-mimics (C and D): Sti1 wildtype (black), Sti1 T37E (red), Sti1 S95E (blue), Sti1 S258E (magenta), Sti1 S410E (cyan), Sti1 T526E (green), Sti1 AllE (dark yellow).

of the clients is not fully established. To rule out secondary effects of the amino acid mimics, non-phosphoryable alanine replacements need to be tested.

Clearly, phosphorylation dramatically affects the function of the adaptor protein *in vivo*. Not only in the case of Sti1/Hop, but also for other components of the Hsp90 chaperone machinery, evidence accumulated in the past years that regulation by phosphorylation plays an important role here. Hsp90 itself is highly phosphorylated and this affects its ATPase activity, but also cochaperone binding and *in vivo* function [Soroka et al., 2012]. In this context, it is interesting that one of the Hsp90 cochaperones, Ppt1, is a Ser/Thr phosphatase. Ppt1 is able to dephosphorylate Hsp90 but also the cochaperone Cdc37 which is phosphorylated at multiple sites [Vaughan et al., 2008, Wandinger et al., 2006]. Phosphorylation of Cdc37 has been studied in quite some detail [Xu et al., 2012]. Different phosphorylation events on Cdc37 and Hsp90 enhance association or dissociation of single components of the Hsp90-cochaperones-client-complexes. A specific serie of these events may introduce directionality to the chaperone cycle. However, the studies so far cover only a tiny fraction of the possible modifications, thus a comprehensive understanding of this kind of regulation cannot be expected in the near future.

2.11 Synthetic lethal screen of Sti1

Sti1 participates in the maturation of key regulatory proteins by mediating the transfer of clients between Hsp70 and Hsp90. As neither Sti1 is essential nor the EEVD of Hsp90 [Nicolet and Craig, 1989, Louvion et al., 1996], this suggests the presence of proteins which compensate for Sti1 or have at least partly redundant functions. To identify such potential compensators, seven hits from a synthetic lethal screen of Sti1 (Sylvia Welker, TU München) were further analyzed in this work (Table 2.2).

The genes were first checked for reported interactions with chaperones with the *S. cerevisiae*-specific database chaperone DB [Gong et al., 2009]. Each one of the hits, except Sae3 and Nca3, was previously found in physical interactions with at least one of the Hsp70 isoforms. Additionally, for Sno1 and Set6, interactions are described with the two cytosolic isoforms of Hsp90. Set6 is particularly interesting as physical interactions with five Hsp70 and the two Hsp90 isoforms have been detected. None of the hits contain TPR domains.

Single knockouts of these genes were assessed with the help of Hsp90 substrate activity assays *in vivo* (Figure 2.41). For two of the genes, namely *sae3* and *nca3*, no effect on GR activity was observed. These are the genes for which no interaction with Hsp70 or Hsp90 was described in the database. Knockout of the other five genes enhanced

Gene	Annotated function of protein product	Interactors
sno1	Protein of unconfirmed function, involved in pyridoxine metabolism; expression is induced during stationary phase; forms a putative glutamine amidotransferase complex with Snz1p, with Sno1p serving as the glutaminase	Ssb1^{p}, Hsc82^{g}, Hsp82^{g}
sae3	Meiosis specific protein involved in DMC1-dependent meiotic recombination, forms heterodimer with Mei5p; proposed to be an assembly factor for Dmc1p	
set6	Protein of unknown function; deletion heterozygote is sensitive to compounds that target ergosterol biosynthesis, may be involved in compound availability	Ssa1^{p}, Ssa2^{p}, Ssb1^{p}, Sse1^{p}, Ssz1^{p}, Hsc82^{p}, Hsp82^{p}
nca3	Protein that functions with Nca2p to regulate mitochondrial expression of subunits 6 (Atp6p) and 8 (Atp8p) of the Fo-F1 ATP synthase; member of the SUN family	
ade17	Enzyme of 'de novo' purine biosynthesis containing both 5-aminoimidazole-4-carboxamide ribonucleotide transformylase and inosine monophosphate cyclohydrolase activities, isozyme of Ade16p; *ade16 ade17* mutants require adenine and histidine	Ssa1^{p}, Ssa2^{p}, Ssb1^{p}, Sse1^{p}, Ydj1^{p}
cem1	Mitochondrial beta-keto-acyl synthase with possible role in fatty acid synthesis; required for mitochondrial respiration	Ssb1^{p}, Ydj1^{p}
leu9	Alpha-isopropylmalate synthase II (2-isopropylmalate synthase), catalyzes the first step in the leucine biosynthesis pathway; the minor isozyme, responsible for the residual alpha-IPMS activity detected in a *leu4* null mutant	Ssa1^{p}, Ssb1^{p}

Table 2.2: Hits of the synthetic lethal screen of Sti1 with their annotated function (Saccharomyces genome database) and selected genetic (g) and physical (p) interactors.

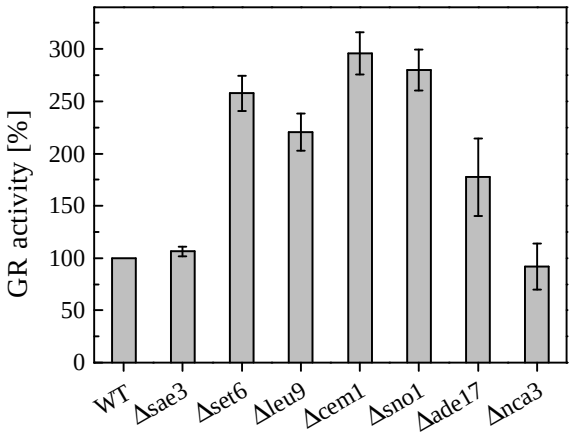

Figure 2.41: GR activation in wildtype yeast and knockouts of Sti1 interactors (SL screen). Means of at least three independent experiments are shown with their standard deviation. Except for *sae3* and *nca3*, knockouts of the hits positively influence GR activation.

GR activity compared to wildtype yeast. Interestingly, they show the reverse effect of a *sti1* knockout where GR activity is reduced by 80 %.
For V-Src activity, no difference of the knockout strains compared to wildtype could be observed. In this assay, a higher substrate activity leading to higher toxicity cannot be assessed, as the cells already die of the toxic amount of activated V-Src in wildtype yeast.

Taken together, the five hits for which interactions with Hsp70 and/or Hsp90 have been found in the database affected GR activation and therefore influence the Hsp90-Hsp70 chaperone machinery. Of these, Sno1 and Set6 have been found in complexes with Hsp90 and Hsp70 homologs. As a result, they represent putative compensators for Sti1 that may be able to bind both chaperones via surfaces other than a TPR domain. The other three hits, Nca3, Ade17 and Leu9 are likely to be associated with Hsp70. *In vitro* characterization of these proteins is planned but so far failed because of their insolubility after *E. coli* expression and standard purification.

CHAPTER 3

CONCLUSIONS

In the following sections, I will summarize the most important conclusions for the individual parts of Sti1 acquired in this study and bring them into context with each other and with findings from previous studies. Then, the structure of Sti1 and its complexes next to the similarities and differences between the yeast and human system are discussed. Based on these results, I will in the end present a comprehensive model of how clients are transferred from Hsp70 to Hsp90 via Sti1.

3.1 TPR2A-TPR2B: the central element of Sti1

The main function of Sti1 is to connect the Hsp70 and the Hsp90 chaperone machinery, the two major chaperone components of eukaryotes [Chen and Smith, 1998]. By simultaneously binding them and by slowing down the ATPase activity of Hsp90, it facilitates the transfer of clients between the two systems [Prodromou et al., 1999]. For these purposes, TPR2A-TPR2B is the main platform of Sti1. One the one hand, this part of Sti1 fully enables the interaction and regulation of Hsp90. While Hsp90-C interacts with TPR2A in the typical TPR-EEVD mode, Hsp90-M additionally binds to regions of TPR2A-TPR2B distinct from the peptide binding site [Schmid et al., 2012]. On the other hand, this work showed by fragmentation and mutagenesis of Sti1 in combination with interaction studies that TPR2A-TPR2B is the crucial region for the interaction with Hsp70 as well (section 2.1 and 2.2). It was demonstrated that the peptide binding groove of TPR2B is still accessible for Hsp70 even if Hsp90 is bound to TPR2A-TPR2B. This allows the formation of ternary complexes between Hsp90, Hsp70 and TPR2A-TPR2B.

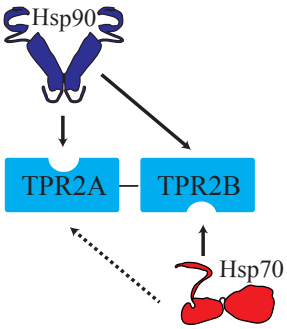

Figure 3.1: TPR2A-TPR2B is the main adaptor platform. Both Hsp90 and Hsp70 can be bound simultaneously via the peptide binding groove of TPR2A and TPR2B, respectively. Additional interactions occur between Hsp90-M and surfaces of TPR2B distinct from the peptide binding groove and between Hsp70 and TPR2A.

Importantly, TPR2A and TPR2B do not seem to function well individually but rather to synergistically form a joint binding site for Hsp90 and for Hsp70 as SPR analysis indicated (section 2.2.1). This most probably is related to the orientation of these two domains which is defined by the region connecting them. In the crystal structure, TPR2A and TPR2B are rotated so that their peptide binding grooves are oriented in opposite directions [Schmid et al., 2012]. The residues fixing the domains are conserved from yeast to man and were identified as critical *in vivo* in this work (section 2.7). This conformation was furthermore confirmed in solution with SAXS experiments and suggests that in the ternary complex, Hsp90 and Hsp70 are positioned on opposite sides of Sti1. The conclusions drawn in this section are schematically depicted in Figure 3.1.

3.2 Two alternative Hsp70 binding TPR-DP modules

The interaction between Sti1 and Hsp70 is of complex nature as multiple domains are involved. With the help of peptide binding groove defective mutants of Sti1, it was shown that Hsp70 can contact TPR2B via its C-terminal tail and that this is the critical contact in the absence of Hsp90 and for client activation *in vivo* (section 2.1 and 2.2.1). However, TPR1 also contributed to the interaction with Hsp70 especially when Hsp90 was present (section 2.2). Apparently, Hsp70 can use TPR1 and TPR2B alternatively and the different domains have to communicate for this. This implies that Hsp70 can switch between these two positions and that TPR1 exhibits a more latent function. This can also explain why certain homologs like *C. elegans* Hop lack TPR1-DP1 but are still functional [Gaiser et al., 2009]. Thus, TPR1 seems to act as a 'deliverer' or 'storage' for Hsp70.
The two Hsp70 binding TPR domains are each followed by a DP domain. Both DP domains contribute to client activation, but DP2 which follows the crucial TPR2B is

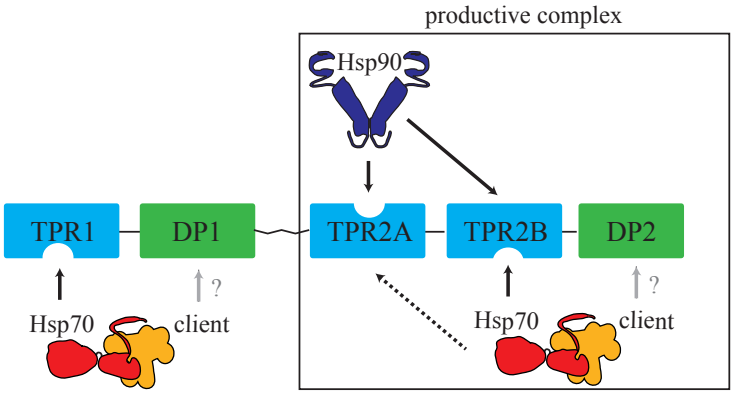

Figure 3.2: Hsp70 can contact two alternative Hsp70 binding sites. In the productive complex, Hsp70 is bound to TPR2B. TPR1 is an alternative binding site for Hsp70. The DP domains may stabilize the client.

absolutely essential in this process (section 2.3). This suggests that a TPR domain and a DP domain form a module which mediates the interaction with Hsp70 and the client. Reconstructions of the ternary Hsp90-Sti1-Hsp70 complex based on electron microscopy indicate that the DP domains are in close proximity to Hsp70 (section 2.8). However, no direct interaction between Hsp70 and the isolated DP domains has been detected. Possibly, the DP domains associate with the client. This interaction may be transient or may only occur if Hsp70 is also bound as Sti1 is not a chaperone on its own [Bose et al., 1996, Freeman et al., 1996].
Structurally, DP1 and DP2 are very similar [Schmid et al., 2012]. Two of their helices which are in particular sensitive to mutation form a groove which was identified as a potential binding site for clients (section 2.3). In DP1, an additional small helix blocks this groove which could explain why they are not interchangable. Generally, the exact composition of DP2 seems to be crucial as already the replacement with the very similar Hop DP2 lead to reduced levels of client activation. Combined conclusions from the first two sections are represented in Figure 3.2.

3.3 The linker regulates the interaction with Hsp70

The two TPR-DP modules of Sti1 are connected through a 60 amino acid flexible linker. In this study, experiments using a linker-deleted variant of Sti1 showed that the linker is important *in vivo* although its sequence is the least conserved region of the protein (section 2.4). *In vitro*, deletion of the linker shifted the equilibrium between binary (Sti1-Hsp70) and ternary complexes (Hsp90-Sti1-Hsp70) towards the binary complex. This came along with an increased affinity towards Hsp70. Considering that TPR2A-TPR2B and TPR2A-TPR2B-DP2 also displayed enhanced interaction with

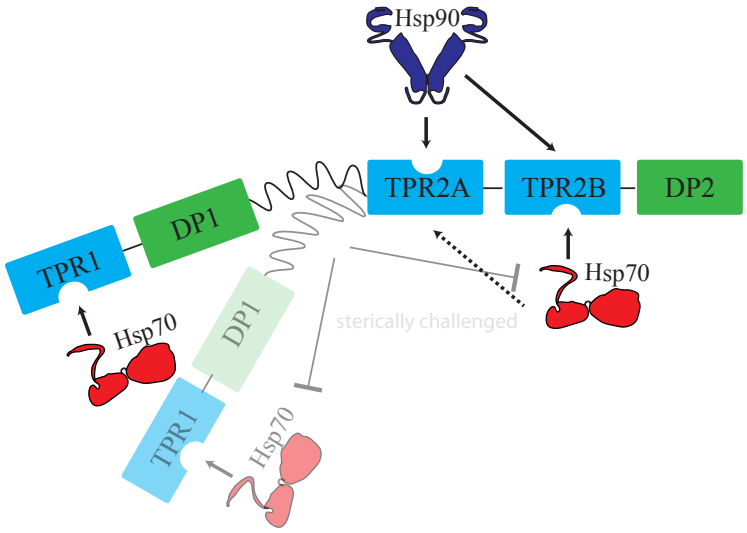

Figure 3.3: The flexible linker regulates the interaction with Hsp70. The long linker allows bending of Sti1. The affinity towards Hsp70 is probably influenced by the linker as the attached TPR1-DP1, if not bent away completely from TPR2A-TPR2B-DP2, sterically challenges the interaction with Hsp70.

Hsp70 compared to wildtype Sti1, it is reasonable to assume that TPR1-DP1, when the linker is present, partly prevents binding of Hsp70. This may be conveyed by sterical hindrance between the two Hsp70 binding regions as the linker allows them to approach each other.

The presence of two alternative Hsp70 binding sites with only TPR2B being necessary for final activation of the client has lead to the idea that during client transfer Hsp70 switches from TPR1 to TPR2B. Besides the mere location of the linker, a number of results presented here encourage the hypothesis that the linker mediates the transfer of Hsp70 between these two domains.

One, the linker is flexible and substantially contributes to the length of Sti1 (section 2.5 and 2.7). Two, the linker clearly impacts the interaction with Hsp70 and ternary complex formation (section 2.4.1). Three, the presence of Hsp90 and Hsp70 affects the end-to-end distance of the linker (section 2.5). Four, both low resolution structural methods observe a bending of the linker. The electron microscopy studies further indicate that this leads to the close proximity of TPR1 and TPR2B and that the C-terminal lid of Hsp70 containing the EEVD motif is located directly in between (section 2.8). Obviously, this would facilitate transfer of Hsp70 between TPR1 and TPR2B. Apart from that, it would explain why client activation upon linker deletion was reduced to a larger extent than upon deletion of the complete first module TPR1-DP1-linker (section 2.4). In this construct, TPR1-Hsp70 would be trapped as without the linker, Sti1 binds Hsp70 with higher affinity and no transfer to TPR2B is possible which would prevent client activation. These conclusions are schematically presented in Figure 3.3.

3.4 Overall structure of Sti1 and its complexes

This work has contributed substantially to the knowledge on the overall topology of Sti1 and the ternary complex via different cellular, structural and biophysical methods. As deduced from SAXS and FRET experiments, Sti1 adopts a rather elongated conformation with a long flexible linker (section 2.5 and 2.7). TPR1-DP1 is 'disconnected' from the rest of the protein, but also TPR1 and DP1 are flexible towards each other, allowing a variety of conformations. With electron microscopy, two distinct conformations of the module TPR1-DP1 towards TPR2A-TPR2B have been recovered: a compact one with TPR1-DP1 in close proximity to TPR2A-TPR2B and an elongated one with the modules being relatively far apart (section 2.8). At the same time, Hsp70 is either brought in intimate contact with Hsp90-N or in the alternative structure, Hsp70 is far apart from Hsp90. TPR2A and TPR2B form a rigidly linked platform also in solution. FRET experiments confirmed that Hsp90 approaches TPR2A-TPR2B from one specific side (section 2.6). Because of the rotation of the two TPR domains, Hsp70 is suspected to contact the module from the respectively opposite direction. The EM reconstructions support this notion. SAXS models indicate that DP2 is attached to TPR2B and not as flexible as DP1 towards TPR1, again highlighting that they have concerted functions.

3.5 Sti1 and Hop: same task - different regulation

Sti1 from *S. cerevisiae* and human Hop share large sequence and structural homology but differences have been reported with regards to the regulation of the ATPase activity of Hsp90 [McLaughlin et al., 2002]. For this reason, the two homologs have been compared concerning their interactions with Hsp90 and Hsp70 in their physiological and in mixed systems (section 2.9). Here, Sti1 and Hop behaved relatively similar although generally, they exhibited higher affinities for the yeast chaperones. Surprisingly, the two homologs both inhibited the ATPase activity of yeast Hsp90 as well as human Hsp90 even if hHsp90 was not inhibited to the same degree.
Together with the fact that the *in vivo* activity depends on the same domains of Sti1 and Hop and the similar EM structure of ternary complexes (section 2.8), this indicates that the bridging of substrates between Hsp90 and Hsp70 is conserved from yeast to man. However, some species-specific differences exist, as the replacement of DP2 in Sti1 by the DP2 domain of human Hop lead to reduced activity (section 2.3). This indicates that the single domains are adjusted precisely to one another.
A major difference was found to be conveyed by phosphorylation of the two homologs. Sti1 and Hop are both phosphorylated at multiple regions with hotspots in the Hsp70 binding domains TPR1 and TPR2B and in the linker. However, except for one residue,

unique sites are affected. By analyzing the effects of phospho-mimetic mutations, it was demonstrated that phosphorylation of both homologs efficiently regulates their activity *in vivo* (section 2.10). In Sti1 and Hop, it generally leads to reduced client activation levels which is accompanied by reduced affinity for Hsp70 *in vitro*. In the case of Sti1, the most striking *in vivo* effects were caused by phospho-mimicking positions in the Hsp70 binding TPR domains (T37E and S410E). If the different phospho-mimicking mutations were combined this did not further decrease its activity indicating that the modifications do not function additively.
In Hop, all of the tested phospho-mimicking mutations (in TPR1, and at the C- and N-terminal boarders of TPR2B) reduced client activation similarly. Of special consequence may be the phosphorylation of Y354 which is part of the residues fixing the domain arrangement of TPR2A and TPR2B. Taken together, the analysis and the location of the phosphosites highlights a special role of the phosphorylation for regulating the interaction with Hsp70 which in turn influences client transfer.

3.6 Model for the transfer of clients mediated by Sti1

It was demonstrated that the activation of different clients is dependent on the same domains of Sti1 and that this connection is also conserved for different organisms (section 2.1.2 and 2.9). This suggests that there is a general mechanism for how Sti1 mediates the transfer of clients from Hsp70 to Hsp90. The discussed results and conclusions lead to the following model for this transfer (Figure 3.4).
In the absence of Hsp90, client-bound Hsp70 binds to Sti1 via the joint binding platform TPR2A-TPR2B mainly through the interaction of the Hsp70 C-terminal EEVD with the peptide binding groove of TPR2B. Meanwhile, the closely attached DP2 domain may participate in the stabilization of the client. In this state, TPR1 is not accessible very well for Hsp70, presumably because the binding site of TPR1 is blocked due to how it is arranged by the linker. Hsp90 associates with the complex via its middle and C-terminal domain which bind to the central block of Sti1, TPR2A-TPR2B. With Hsp70 and Hsp90 brought in intimate contact, the client can be transferred and at some point after that, activation of the client occurs.
Under these conditions, another client-bound Hsp70 molecule can be bound to TPR1 which is separated from the rest of the protein via the long linker. This may be enabled by the loosening effect of Hsp90 on the linker. At the same time, Hsp90 displaces the first Hsp70 from TPR2B. This is assumed because such ternary complexes were preferred *in vitro* (section 2.2). Bending of the linker induces a more compact conformation of Sti1 which leads to the close proximity of TPR1 and TPR2B. Now, transfer of the second Hsp70-bound client to TPR2B is possible where further transfer of the client to Hsp90 occurs.

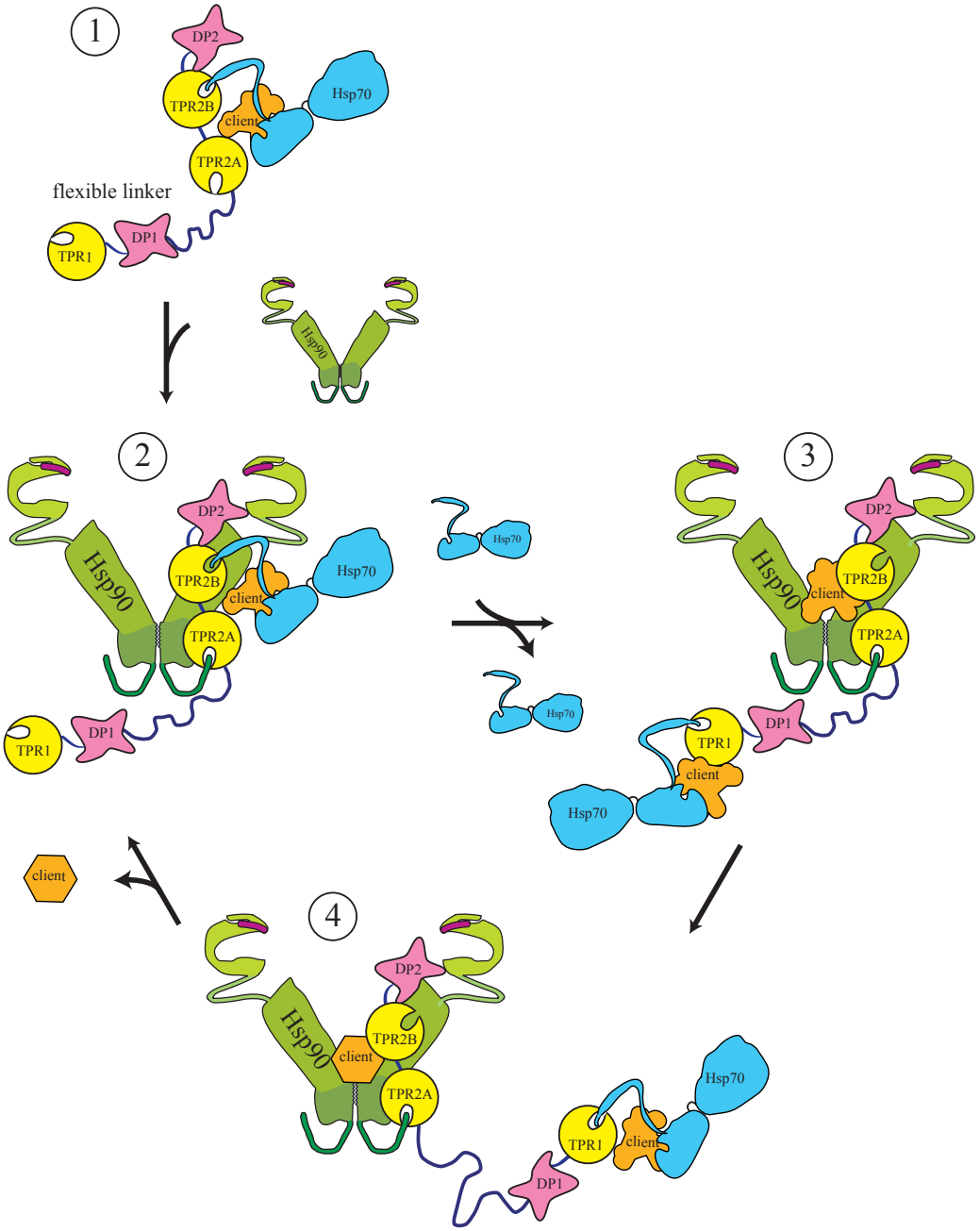

Figure 3.4: Model for the transfer of clients mediated by Sti1. (1) Client-bound Hsp70 binds mainly via TPR2B to Sti1. (2) Hsp90 associates with this complex via interaction with TPR2A-TPR2B. The client can now be transferred from Hsp70 to Hsp90 and afterwards Hsp70 is released. (3) Another client-bound Hsp70 molecule may be bound to TPR1 in the presence of Hsp90. (4) Bending of the linker induces the close proximity of TPR1 and TPR2B which enables the hand-over of Hsp70 from TPR1 to TPR2B. Again, the client can be transferred to Hsp90.

Such a complex mechanism with TPR1-DP1 acting as a delivery or storage system for Hsp70 may be justified by the unequal proportion of the single components *in vivo*. In eukaryotes, Hsp90 and Hsp70 are highly abundant whereas cochaperones are much more weakly expressed. More precisely, in *S. cerevisiae* under normal conditions, the cytosolic Hsp90 variants are present in about the same concentration as the different cytosolic Ssa variants. In comparison, Sti1 is ten times less abundant [Ghaemmaghami et al., 2003]. As shown in this thesis, the ratios between Sti1, Hsp90 and Hsp70 do influence which complexes are formed *in vitro*.

As an outlook, the presented insight into the complex interaction of Sti1/Hop with Hsp90 and Hsp70 may have implications for the development of novel drugs. All three components are overexpressed in tumor cells and promote the progression of cancer [Ruckova et al., 2012]. Hsp90 inhibitors are in clinical trials for anti-cancer therapy but have the drawback that they in turn induce overexpression of Hsp70 [Alarcon et al., 2012]. As a consequence, the interaction of Hop with Hsp90 or Hsp70 is considered to be an interesting drug target [Pimienta et al., 2011, Walsh et al., 2011, Horibe et al., 2012]. The mechanism proposed here may contribute to rationally design specific, more advanced inhibitors of this interaction.

CHAPTER 4

MATERIALS AND METHODS

4.1 Materials

Chemicals not listed were purchased from Merck (Darmstadt, Germany). For preparation of buffers, Millipore-filtered water was used (Millipore, Bedford, USA).

Chemical	**Origin**
Acrylamide (38 %, 2 % Bisacrylamide)	Roth (Karlsruhe, Germany)
Agarose, ultra pure	Roth (Karlsruhe, Germany)
Amino acids	Sigma-Aldrich (St. Louis, USA)
Ammoniumperoxodisulfate (APS)	Roche (Mannheim, Germany)
Ampicillin	Roth (Karlsruhe, Germany)
Adenosyl-imidodiphosphate (AMP-PNP)	Roche (Mannheim, Germany)
Adenosin-5'-diphosphate (ADP) disodium salt	Roche (Mannheim, Germany)
Adenosin-5'-triphosphate (ATP) disodium salt	Roche (Mannheim, Germany)
Bacto Agar	Difco (Detroit, USA)
Bacto Tryptone	Difco (Detroit, USA)
Bacto Yeast Extract	Difco (Detroit, USA)
Bromphenolblue S	Serva (Heidelberg, Germany)
Coomassie Brilliant-Blue R-250	Serva (Heidelberg, Germany)
Desoxycorticosterone (DOX)	Sigma-Aldrich (St. Louis, USA)
Desoxynucleotide triphosphates (dNTPs)	Roche (Mannheim, Germany)
DNA stain G	Serva (Heidelberg, Germany)
1,4-Dithiothreitol (DTT)	Roth (Karlsruhe, Germany)
Ethylendiamintetraacidic acid (EDTA)	Merck (Darmstadt, Germany)
Glycerol 99 %	ICN (Costa Mesa, USA)

Glycine	Roth (Karlsruhe, Germany)
N-(2-Hydroxyethyl)-piperazin-N'2-ethansulfonic acid (HEPES)	ICN (Costa Mesa, USA)
Isopropanol	Roth (Karlsruhe, Germany)
Isopropyl-β-D-thiogalactopyranosid (IPTG)	Roth (Karlsruhe, Germany)
Kanamycin	Roth (Karlsruhe, Germany)
β-Mercaptoethanol, pure	Merck (Darmstadt, Germany)
2-Nitrophenyl-β-D-galactopyranosid (ONPG)	Sigma-Aldrich (St. Louis, USA)
NADH	Roche (Mannheim, Germany)
Phosphoenol pyruvate	Roche (Mannheim, Germany)
Protease Inhibitor Mix HP	Serva (Heidelberg, Germany)
Radicicol	Sigma-Aldrich (St. Louis, USA)
Salmon Sperm DNA	Sigma-Aldrich (St. Louis, USA)
Sodiumdodecylsulfat (SDS)	Roth (Karlsruhe, Germany)
N,N,N',N'-Tetramethylethylendiamin (TEMED)	Roth (Karlsruhe, Germany)
Tris-(Hydroxymethyl)-aminomethan (Tris)	ICN (Costa Mesa, US)
Tween 20	Merck (Darmstadt, Germany)
Yeast Nitrogen Base (YNB)	Difco (Detroit, USA)

Size Marker/kit	**Origin**
BiaCore amine coupling kit	BiaCore Inc. (Uppsala, Sweden)
Wizard® Plus SV Mini-Preps DNA purification	Promega (Madison, USA)
Wizard® SV Gel and PCR Clean-Up System	Promega (Madison, USA)
PeqGold 1 kb DNA ladder	PeqLab (Erlangen, Germany)
Low-Range-molecular weight marker	Biorad (München, Germany)

Enzyme	**Origin**
Pfu Polymerase	Promega (Madison, USA)
Restriction enzymes	Promega (Madison, USA)
T4 Ligase	Promega (Madison, USA)
DNAse I	Roche (Mannheim, Germany)
Pyruvate Kinase (PK)	Roche (Mannheim, Germany)
L-Lactate dehydrogenase (LDH)	Roche (Mannheim, Germany)

Fluorescence label	**Origin**
ATTO 488 maleimide	AttoTec (Siegen, Germany)
ATTO 488 NHS ester	AttoTec (Siegen, Germany)
ATTO 550 maleimide	AttoTec (Siegen, Germany)
ATTO 532 maleimide	AttoTec (Siegen, Germany)
ATTO 647 maleimide	AttoTec (Siegen, Germany)
5-(and-6)-Carboxyfluorescein (FAM) NHS	Invitrogen (La Jolla, USA)

Equipment	Origin
Analytical balances	
BP 121 S	Sartorius (Göttingen, Germany)
BL310	Sartorius (Göttingen, Germany)
Centrifuges	
Avanti J25 (JA-10 and JA-25.50 rotor)	Beckman (Fullerton, USA)
Rotina 420R	Hettich (Tuttlingen, Germany)
Eppendorf Centrifuge 5415 C	Eppendorf (Hamburg, Germany)
Beckman ProteomeLab XL-A (TI-50 rotor)	Beckman (Fullerton, USA)
Gel electrophoresis devices	
Hoefer Mighty Small II	GE Healthcare (Freiburg, Germany)
Power amplifiers	
LKB-GPS 200/400	GE Healthcare (Freiburg, Germany)
Pharmacia EPS 3500, 301, 1001	GE Healthcare (Freiburg, Germany)
Chromatographic devices	
ÄKTA FPLC	GE Healthcare (Freiburg, Germany)
Jasco HPLC system	Shimadzu (Munich, Germany)
Spectroscopic devices	
Varian Cary 50/100 Bio UV-Vis-Spectrometer	Varian (Palo Alto, USA)
Biotech Ultrospec 3000 UV-Vis-Spectrometer	Amersham (Uppsala, Sweden)
Jasco J715 with PTC 343 Peltier device	Jasco (Groß-Umstadt, Germany)
FluoroMaxIII spectrofluorimeter	Jobin Ivon (Edison, USA)
BiacoreX	Biacore (Uppsala, Sweden)
Fluorescence detection system (aUC)	Aviv Biomedical (Lakewood, USA)
Additional equipment	
Quartz Cuvettes	Hellma (Müllheim, Germany)
Incubator	Haake (Karlsruhe, Germany)
pH Meter WTW	WTW (Weilheim, Germany)
Eppendorf Thermomixer	Eppendorf (Hamburg, Germany)
Thermocycler Primus	MWG (Ebersberg, Germany)
Cell disruption machine Basic Z model	Constant Systems (Warwick, England)
Mixer Mill MM 400	Retsch (Haan, Germany)

Chromatographic material	Origin
HiLoad FF Ni-NTA 5 ml	GE Healthcare (Freiburg, Germany)
Ressource Q	GE Healthcare (Freiburg, Germany)
Hydroxyapatite	Biorad (München, Germany)
Superdex 75 prep grade (16/60)	GE Healthcare (Freiburg, Germany)
Superdex 200 prep grade (26/60)	GE Healthcare (Freiburg, Germany)
HiPrep 26/10 Desalting	GE Healthcare (Freiburg, Germany)
PD10 desalting column	GE Healthcare (Freiburg, Germany)

Miscellaneous material	Origin
Amicon Centrifugal Filter Units	Amicon (Witten, Germany)
Cellulose acetate filters, 0.45 µm	Sartorius (Göttingen, Germany)
Sensor Chip CM5 Research Grade	GE Healthcare (Freiburg, Germany)

Software & Web-based tools	Source
Adobe CS	Adobe Systems (San Jose, USA)
ApE Plasmid Editor 2.0.36	M. Wayne Davis (Univ. Utah, USA)
Chaperone DB	[Gong et al., 2009]
Clustal W sequence alignment	[Thompson et al., 1994]
NetPhos	[Blom et al., 1999]
Origin 8	OriginLab (Northhampton, USA)
PhosphoSite	[Li et al., 2002]
ProtParam Tool	[Gasteiger et al., 2005]
Pymol	Schrödinger LLC (New York, USA)
Saccharomyces genome database	[Cherry et al., 2012]
SedView	[Hayes and Stafford, 2010]
SWISS-MODEL	[Arnold et al., 2006]

4.2 Cultivation of organisms

4.2.1 Cultivation of E. coli strains

E. coli One-Shot® Mach1™ was used for cloning. *E. coli* BL21 (DE3) Cod+ (T7 promoter) and *E. coli* HB101 (T5 Promoter) were used for protein expression.

Strain	Genotype	Origin
E. coli One-Shot® Mach1™	F- ϕ80*lac*ZΔM15 Δ*lac*X74 *hsd*R(rK-mK+) Δ*rec*A1398 *end*A1 *ton*A	Invitrogen (Groningen, Netherlands)
E. coli BL21 (DE3) Cod+	F- *omp*T *hsd*SB (rB-mB-) *dcm*+ Tetr *gal* I (DE3) *end*A Hte [*argU ileY leuW* CamR]	Stratagene (La Jolla, USA)
E. coli HB101	F- *hsd*S20 (rB-mB-) xyl5 λ- *rec*A13 *gal*K2 *leu*B6 *ara*14 *sup*E44 *pro*A2 *lac*Y1 *rps*L20(strR) mtl-1	Sigma Aldrich (St. Louis, USA)

Streaked *E. coli* cultures were incubated on lysogeny broth (LB) plates or liquid culture with the adequate antibiotic (100 µg/ml Ampicillin or 50 µg/ml Kanamycin) at 37 °C for 16 hours. Liquid cultures up to 10 ml were incubated in a test tube roller, larger volumes in a culture shaker. Growth was monitored photometrically at a wavelength of 600 nm (OD_{600} = 1 correlates to about 8 x 10^8 cells). For long-term storage, 700 µl of the culture were mixed with 300 µl 50 % glycerol, frozen using liquid nitrogen and stored at -80 °C.

4.2.2 Cultivation of yeast strains

Wildtype *Saccharomyces cerevisiae* and knockout strains were purchased from Euroscarf with the strain background BY4741 (*MATa his3Δ1 leu2Δ0 met15Δ0 ura3Δ0*).

Acc.no (Euroscarf)	**Deletion**
Y00000 (wildtype)	–
Y01803 (Δ*sti1*)	YOR027w
Y06535 (Δ*sno1*)	YMR095c
Y02087 (Δ*set6*)	YPL165c
Y01907 (Δ*sae3*)	YHR079c
Y06197 (Δ*nca1*)	YMR064w
Y02364 (Δ*leu9*)	YOR108w
Y06561 (Δ*ade17*)	YMR120c
Y00198 (Δ*cem1*)	YER061c

Pichia pastoris strain KM71H (genotype: *aox1::ARG4 arg4*) was purchased from Invitrogen, Groningen, Netherlands. Streaked cultures of *S. cerevisiae* or *P. pastoris* were incubated on Yeast Extract Peptone Dextrose (YPD) or Complete Supplement Mixture (CSM) plates or liquid culture at 30 °C for two or three days. Growth was monitored photometrically at a wavelength of 600 nm (OD_{600} = 1 correlates to about 2 x 10^7 cells). For long-term storage, 700 µl of the culture were mixed with 300 µl 50 % glycerol, frozen using liquid nitrogen and stored at -80 °C.

Complete Supplement Mixture	
YNB	6.7 g
Selective amino acid mix	2.0 g
Glucose/Raffinose/Galactose	20 g
1 M NaOH	1 ml
H_2O	Ad 1 l
For plates: Agar	20 g

4.3 Molecular biology

4.3.1 DNA isolation and purification

Plasmid DNA was isolated from 4 ml overnight cultures with the Wizard® Plus SV Mini-Preps DNA purification. PCR products and restricted fragments were purified with the Wizard® SV Gel and PCR Clean-Up System. DNA was stored in nuclease-free H_2O at -20 °C. Sequencing of plasmid DNA with a concentration of 50 to 100 ng/µl was performed by GATC Biotech AG, Konstanz or Eurofins MWG Operon, Ebersberg.

4.3.2 Polymerase chain reaction

Polymerase chain reaction (PCR) was performed using Pfu polymerase with the provided buffer, generally following the instructions of the manufacturer. The polymerase was added at the initial 95 °C step.

Standard Mix

Template DNA	1 µl
10x Pfu buffer	5 µl
dNTP mix (each 10 mM)	1 µl
Each Primer (100 pmol/ µl)	1 µl
Pfu Polymerase	1 µl
H_2O	ad 50 µl

PCR conditions

1x	95 °C	2 min
30-35x	95 °C	30 sec
	50-55 °C	30 sec - 1 min
	72 °C	2 min/kb
1x	72 °C	10 min

Quick change mutagenesis was performed after the protocol of the QuikChange® Site-Directed Mutagenesis Kit (Stratagene, La Jolla) with slight modifications. PCR was performed under standard conditions with primers with a concentration of 10 pmol/µl. The PCR product was treated with 1 µl Dpn1 for 1 hour at 37 °C and afterwards directly transformed into competent cells. In the case of linker PCRs, the first two PCR products were purified prior to adding them 1:1 in the third PCR.

Primer	Sequence
Sti1-BamHI fwd	gatcataggatccatgtcattgacagccgatgaatacaaac
Sti1-XhoI-rev	gatcctcgagttattagcggccagtccggatgatac
p425-Hop-SpeI-1-fwd	gatctgaactagtggatccatggagcaggtcaatgagctgaagg
Hop BamHI fwd	gatcataggatccatggagcaggtcaatgagctgaag
Hop XhoI rev	gatcctcgagtcaccgaattgcaatcagaccca
Sti1 SAGA linker 1 fwd	atttaaacagtgcaggtgcagactctaaaattgaggccgacaagg
Sti1 SAGA linker 2 rev	gagtctgcacctgcactgtttaaatcaacccccatcaatgtagcc
pET-Hsp90-BamHI	gatctcggatcccgcggcatggccagtgaaacttttgaatttc
Hsp90-FL-XhoI	gatctgctcgagttaatctacctcttccatttcggtgtcag
Hsp90-NM-XhoI	gatctgctcgagttattcgaaatctttagtaatgtcaaccaaag
Set6 HindIII fwd	gatcaagcttatgactattgatggagac
Set6 XhoI rev	gatcctcgagctaatggacagattgca
Sno1 BamHI fwd	gattggatccatgcacaaaacccacag
Sno1 Xho1 rev	gagcctcgagttaattagaaacaaactg
Sti1 T37E fwd	aagctattgaagtttctgaagaaccaaaccatgttttatattc
Sti1 T37E rev	gaatataaaacatggtttggttcttcagaaacttcaatagctt
Sti1 S95E fwd	cgacgaagctgaagaaaactacaaaaaag
Sti1 S95E rev	ctttttgtagtttcttcagcttcgtcg
Sti1 S227E fwd	gaaagatgctgaaccacaagaagattccactacgagcaagg
Sti1 S227E rev	ccttgctcgtagtggaatcttcttgtggttcagcatctttc
Sti1 S258E fwd	ggaagttgatgaagatgacgaaaaaattgaggccgacaagg
Sti1 S258E rev	ccttgtcggcctcaatttttcgtcatcttcatcaacttcc
Sti1 S410E fwd	ggtaaggaatattttaccaaggaagactggccgaatgctgttaag
Sti1 S410E rev	cttaacagcattcggccagtcttccttggtaaaatattccttacc
Sti1 T526E fwd	caacctggtaccagtaacgaagaaccagaagaaacctatcaaagg
Sti1 T526E rev	cctttgataggtttcttctggttcttcgttactggtaccaggttg
Sti1 C49S fwd	ccatgttttatattctaacaggtccgcc
Sti1 C49S rev	ggcggacctgttagaatataaaacatgg
Sti1 C66S fwd	gtgacgcattgaatgatgctaatgaa
Sti1 C66S rev	ttcattagcatcattcaatgcgtcac
Sti1 G193C fwd	catcatggctacattgatgtgcgttgatttaaacatggatg
Sti1 G193C rev	catccatgtttaaatcaacgcacatcaatgtagccatgatg
Sti1 S258C fwd	ttgatgaagatgactgcaaaattgaggccgac
Sti1 S258C rev	gtcggcctcaattttgcagtcatcttcatcaa
Sti1 G309C fwd	gctgctgaatacgaaaaatgcgaatacgagacagctatttctacc
Sti1 G309C rev	ggtagaaatagctgtctcgtattcgcatttttcgtattcagcagc
Hop S16E fwd	gaaaggcaacaaggccctggaagtgggtaacatcgatgatg
Hop S16E rev	catcatcgatgttacccacttccagggccttgttgcctttc
Hop Y354E fwd	agcggctggccgaaataaaccccga
Hop Y354E rev	tcggggtttatttcggccagccgct
Hop S481E fwd	gtacaaccggcacgacgaacccgaagatgtgaagc
Hop S481E rev	gcttcacatcttcgggttcgtcgtgccggttgtac

4.3.3 Restriction digest and ligation

For preparative restriction digest, enzymes and the appropriate 10x reaction buffer were used. For a final volume of 20 µl, 1 µg of DNA and 0.5 µl of the restriction enzymes (10 u/µl) were incubated at 37 °C for 4-12 hours following the instructions of the manufacturer.

Ligation was performed with 100 ng of vector and the appropriate amount of insert for a ratio of 1:3 to 1:5 (vector:insert). Incubation in standard buffer varied from 4 °C over night to 16 °C or room temperature for 3 h. Using quick ligation buffer, the ligation was performed at 25 °C for 5 min.

Quick ligation buffer	
Tris-HCl, pH 7.5	50 mM
$MgCl_2$	10 mM
ATP	1 mM
DTT	10 mM

4.3.4 Transformation of plasmids in E. coli

E.coli cells were made competent according to [Sambrook et al., 1989]. 100 ml LB were inoculated with a fresh overnight culture until growth reached an OD_{600} of 0.5 to 0.8. Then, 2 ml sterile 1 M $MgCl_2$ were added and further incubated at 37 °C for 10 min. The cells were then chilled on ice for 1 hour and centrifuged for 10 min at 4 °C at 4500 g. The sediment was resuspended in 20 ml Solution A and again chilled on ice for 1 hour. Subsequently, cells were centrifuged again and resuspended in 2 ml Solution A with 15 % glycerol (v/v). 100 µl Aliquots were frozen with liquid nitrogen and stored at -80 °C. For transformation, the competent cells were briefly thawed on ice, and mixed with 1 µl of plasmid DNA (or 10 to 20 µl of a ligation reaction or mutagenesis PCR). After incubation on ice for 15 to 30 min, the cells were heat-shocked for 1 min at 42 °C. Afterwards, the cells were incubated with 1 ml of LB_0 at 37 °C for regeneration. Cells were centrifuged and the sediment was resuspended in 100 µl of medium and plated on plates containing the respective antibiotic.

Solution A	
3 M NaAc, pH 5.5	13 ml
1 M $CaCl_2$	100 ml
2.8 M $MnCl_2$	25 ml
H_2O	862 ml

4.3.5 Transformation of plasmids in S. cerevisiae

An exponentially growing yeast culture (100 ml) with an OD_{600} of 2 to 2.5 was centrifuged at room temperature for 5 min at 3000 g. The sediment was washed with 25 ml sterile H_2O. This step was repeated and the final sediment was resuspended in 1 ml sterile H_2O. 100 µl aliquots were centrifuged again and the sediment was resuspended in 320 µl transformation solution (0.1 M Lithium acetate, 33 % PEG-3350, 0.3 mg/ml single-stranded DNA carrier in water). 1-5 µl of plasmid DNA were added, mixed and incubated at 42 °C for 40 min. After heat shock, the cells were centrifuged and resuspended in 1 ml sterile H_2O. 100 µl were plated on the respective CSM selection plates [Gietz and Schiestl, 2007].

4.3.6 Agarose gel electrophoresis

For separation of DNA, 1 % (w/v) agarose gels with 2 µl DNA stain G in 1x TAE buffer were used. Electrophoresis was performed with a constant voltage of 120 V for 20 min for 500 to 3000 bp DNA and 30 to 60 min for longer DNA fragments.

TAE (50x)	
Tris/acetate, pH 8.0	2 M
EDTA, pH 8.0	50 mM

Gel loading buffer (10x)	
Glycerol	50 % (v/v)
EDTA, pH 8.0	10 mM
Bromphenole blue	0.2 % (w/v)
Xylencyanole	0.2 % (w/v)

4.3.7 Plasmids

Plasmid	**Cloning site**	**Origin**
pET28-yHsp82	NdeI/XhoI	Klaus Richter
pETSUMO-yHsp82	BamHI/XhoI	This work
pETSUMO-yHsp82-NM	BamHI/XhoI	This work
pETSUMO-yHsp82-MC (aa274-709)	BamHI/XhoI	Andreas Schmid
pET28-yHsp82-M	NdeI/XhoI	Marco Retzlaff
pETSUMO-yHsp82-C (aa529-709) E698C	BamHI/XhoI	This work
pET28-hHsp90β	BamHI/XhoI	Oliver Lorenz

pICZA-6xHis-Ssa1	NheI/XhoI	Andreas Schmid
pETSUMO-Ssa1-SBD (aa392-642) E632C	BamHI/XhoI	This work
pETSUMO-hHsc70		Oliver Lorenz
pETSUMO-Sti1	BamHI/XhoI	Andreas Schmid
pETSUMO-Sti1 C49S C66S	BamHI/XhoI	This work
pETSUMO-Sti1 C49S C66S C453S	BamHI/XhoI	This work
pETSUMO-Sti1* S2C	BamHI/XhoI	Monika Herrmann
pETSUMO-Sti1* S2C G309C	BamHI/XhoI	Monika Herrmann
pETSUMO-Sti1* S2C S523C	BamHI/XhoI	Monika Herrmann
pETSUMO-Sti1* S2C G588C	BamHI/XhoI	Monika Herrmann
pETSUMO-Sti1* G131C G309C	BamHI/XhoI	Monika Herrmann
pETSUMO-Sti1* G131C S523C	BamHI/XhoI	Monika Herrmann
pETSUMO-Sti1* G193C S258C	BamHI/XhoI	This work
pETSUMO-Sti1* G193C G309C	BamHI/XhoI	This work
pETSUMO-Sti1* G193C G309C N39A	BamHI/XhoI	This work
pETSUMO-Sti1* G193C G309C N435A	BamHI/XhoI	This work
pETSUMO-Sti1* G309C S523C	BamHI/XhoI	This work
pETSUMO-Sti1* G309C	BamHI/XhoI	This work
pETSUMO-Sti1* G588C	BamHI/XhoI	Monika Herrmann
pETSUMO-Sti1 T37E	BamHI/XhoI	This work
pETSUMO-Sti1 S95E	BamHI/XhoI	This work
pETSUMO-Sti1 S227E	BamHI/XhoI	This work
pETSUMO-Sti1 S258E	BamHI/XhoI	This work
pETSUMO-Sti1 S410E	BamHI/XhoI	This work
pETSUMO-Sti1 T526E	BamHI/XhoI	This work
pETSUMO-Sti1 AllE	BamHI/XhoI	This work
pETSUMO-Sti1 Linkerdeletion	BamHI/XhoI	Monika Herrmann
pETSUMO-Sti1-TPR1	BamHI/XhoI	Andreas Schmid
pETSUMO-Sti1-TPR1-DP1	BamHI/XhoI	Andreas Schmid
pETSUMO-Sti1-TPR1-TPR2A	BamHI/XhoI	Andreas Schmid
pETSUMO-Sti1-TPR1-TPR2B	BamHI/XhoI	Andreas Schmid
pETSUMO-Sti1-DP1	BamHI/XhoI	Andreas Schmid
pETSUMO-Sti1-DP1-TPR2A	BamHI/XhoI	Andreas Schmid
pETSUMO-Sti1-DP1-TPR2B	BamHI/XhoI	Andreas Schmid
pETSUMO-Sti1-DP1-DP2	BamHI/XhoI	Andreas Schmid
pETSUMO-Sti1-TPR2A	BamHI/XhoI	Andreas Schmid
pETSUMO-Sti1-TPR2A-TPR2B	BamHI/XhoI	Andreas Schmid
pETSUMO-Sti1-TPR2A-DP2	BamHI/XhoI	Andreas Schmid
pETSUMO-Sti1-TPR2B	BamHI/XhoI	Andreas Schmid
pETSUMO-Sti1-TPR2B-DP2	BamHI/XhoI	Andreas Schmid
pETSUMO-Sti1 N435A	BamHI/XhoI	Stephan Lagleder
pETSUMO-Sti1 R465A	BamHI/XhoI	Stephan Lagleder
pETSUMO-Sti1 R469A	BamHI/XhoI	Stephan Lagleder
pETSUMO-Sti1-DP1-DP2 N435A	BamHI/XhoI	Stephan Lagleder

pETSUMO-Sti1-DP1-DP2 R465A	BamHI/XhoI	Stephan Lagleder
pETSUMO-Sti1-DP1-DP2 R469A	BamHI/XhoI	Stephan Lagleder
pETSUMO-Sti1-TPR2A-TPR2B N435A	BamHI/XhoI	Stephan Lagleder
pET28-Hop (no Histag)		Klaus Richter
pET28-Hop Y354E (no Histag)		This work
pETSUMO-Hop-TPR2A-TPR2B	BamHI/XhoI	This work
pETSUMO-Hop-TPR2A-TPR2B Y354D	BamHI/XhoI	This work
pETSUMO-Sno1	BamHI/XhoI	This work
pETSUMO-Set6	HindIII/XhoI	This work
pET28-SUMO Protease		Oliver Lorenz
p425-Sti1 T37E	BamHI/XhoI	This work
p425-Sti1 S95E	BamHI/XhoI	This work
p425-Sti1 S227E	BamHI/XhoI	This work
p425-Sti1 S258E	BamHI/XhoI	This work
p425-Sti1 S410E	BamHI/XhoI	This work
p425-Sti1 T526E	BamHI/XhoI	This work
p425-Sti1 AllE	BamHI/XhoI	This work
p425-Sti1	BamHI/XhoI	Andreas Schmid
p425-Sti1-TPR1	BamHI/XhoI	Andreas Schmid
p425-Sti1-TPR1-DP1	BamHI/XhoI	Andreas Schmid
p425-Sti1-TPR1-TPR2A	BamHI/XhoI	Andreas Schmid
p425-Sti1-TPR1-TPR2B	BamHI/XhoI	Andreas Schmid
p425-Sti1-DP1	BamHI/XhoI	Andreas Schmid
p425-Sti1-DP1-TPR2A	BamHI/XhoI	Andreas Schmid
p425-Sti1-DP1-TPR2B	BamHI/XhoI	Andreas Schmid
p425-Sti1-DP1-DP2	BamHI/XhoI	Andreas Schmid
p425-Sti1-TPR2A	BamHI/XhoI	Andreas Schmid
p425-Sti1-TPR2A-TPR2B	BamHI/XhoI	Andreas Schmid
p425-Sti1-TPR2A-DP2	BamHI/XhoI	Andreas Schmid
p425-Sti1-TPR2B	BamHI/XhoI	Andreas Schmid
p425-Sti1-TPR2B-DP2	BamHI/XhoI	Andreas Schmid
p425-Sti1 N435A	BamHI/XhoI	Stephan Lagleder
p425-Sti1 R465A	BamHI/XhoI	Stephan Lagleder
p425-Sti1 R469A	BamHI/XhoI	Stephan Lagleder
p425-Sti1-DP1-DP2 N435A	BamHI/XhoI	Stephan Lagleder
p425-Sti1-DP1-DP2 R465A	BamHI/XhoI	Stephan Lagleder
p425-Sti1-DP1-DP2 R469A	BamHI/XhoI	Stephan Lagleder
p425-Sti1-DP1-DP2 N435A R465A	BamHI/XhoI	Stephan Lagleder
p425-Sti1-DP1-DP2 N435A R469A	BamHI/XhoI	Stephan Lagleder
p425-Sti1 T578A	BamHI/XhoI	Stephan Lagleder
p425-Sti1 Q557A	BamHI/XhoI	Stephan Lagleder
p425-Sti1 I584A	BamHI/XhoI	Stephan Lagleder
p425-Sti1 V540A	BamHI/XhoI	Stephan Lagleder
p425-Sti1 Q564A	BamHI/XhoI	Stephan Lagleder

p425-Sti1 L553A	BamHI/XhoI	Stephan Lagleder
p425-Sti1 R425A	BamHI/XhoI	Stephan Lagleder
p425-Sti1-DP swap	BamHI/XhoI/PstI	Stephan Lagleder
p425-Sti1-Hop DP2	BamHI/XhoI/PstI	This work
p425-Sti1-Linkerdeletion	BamHI/XhoI	Monika Herrmann
p425-Hop	SpeI/XhoI	Andreas Schmid
p425-Hop Y354E	SpeI/XhoI	Evelyn Bender
p413-GPD-hGR		Andreas Schmid
pUCΔss26x		JF Louivion
p416-Gal-vSrc		Julia Rohrberg

Abbreviations: * stands for C49S C66S C453S.

4.4 Protein purification

Proteins were purified according to methods developed at the chair of biotechnology (TU München). Purification was performed with an ÄKTA FPLC system at around 4 °C. Purity of the proteins was analyzed by SDS-PAGE. Final protein solutions were concentrated to about 100 µM, frozen in liquid nitrogen and stored in 50 µl aliquots at -80 °C.

4.4.1 Protein expression

For standard protein expression, *E. coli* BL21 DE3 cod+ were used. 2 to 10 l of LB medium with the respective antibiotic were inoculated with an overnight culture (50 ml per 2 l) and incubated at 37 °C. At an OD_{600} of 0.5 to 0.8, protein expression was induced with 1 mM IPTG. Cells were incubated at 30 °C overnight and then harvested at 8000 rpm for 10 min at 8 °C (Beckman Avanti J25, JA10 rotor).

Ssa1 was expressed in *P. pastoris* KM71H. 6 l of YNB/Sorbitol medium (per liter: 13.4 g YNB, 20 g Sorbitol, pH 7.0) were inoculated with an overnight culture of *P. pastoris* KM71H and incubated at 30 °C. 24 hours later, expression was induced with 10 % methanol (v/v). Another 24 hours later, again 10 % methanol (v/v) were added as the methanol evaporates. The next day, the cells were harvested at 8000 rpm for 10 min at 8 °C (Beckman Avanti J25, JA10 rotor).

4.4.2 Cell disruption and preparation of protein lysate

Cell pellets were thoroughly resuspended in 100 ml lysis buffer containing 500 µl Protease Inhibitor Mix HP and a tip of a spatula of DNAse I. As lysis buffer, buffer A of the first chromatographic technique was used, usually Ni-NTA A. Then cells were disrupted with 1.8 kbar (*E. coli*) or 2.6 kbar (*P. pastoris*) in a Basic Z model cell disruption system. The lysate was cleared by centrifugation at 40,000 g for 45 min at 8 °C.

4.4.3 Chromatographic buffers

Ni-NTA buffers	
Sodium phosphate, pH 7.5	40 mM
NaCl	500 mM
Imidazole	A: 10 mM
	B: 300 mM

Ni-NTA (Ssa1) buffers	
HEPES, pH 7.5	40 mM
NaCl	350 mM
KCl	150 mM
$MgCl_2$	20 mM
Glycerol	5 % (v/v)
β-Mercaptoethanol	2 mM
ATP	1 mM
Imidazole	A: 10 mM
	B: 300 mM

Resource buffers	
Tris, pH 8.5	50 mM
KCl	A: 20 mM
	B: 1 M

Hydroxyapatite buffers	
Potassium phosphate, pH 7.0	A: 10 mM
	B: 300 mM

Gelfiltration buffer	
HEPES, pH 7.5	40 mM
KCl	150 mM
$MgCl_2$	5 mM

4.4.4 Purification steps

For most of the proteins purified (Sti1 and Hop variants as well as some of the Hsp90 fragments), the pETSUMO vector was used for expression. Here, the lysate was first loaded on a preequilibrated HiLoad FF Ni-NTA. After washing steps with Ni-NTA A and 5 % Ni-NTA B, the protein was eluted with Ni-NTA B (step elution). The protein was then diluted 1:5 with Millipore-H_2O and 200 µl 0.8 mg/ml SUMO protease were added. Cleavage of the His-tag was performed over night at 4 °C.
After buffer exchange with the Desalting column 26/10 in Ni-NTA A, the protein was again loaded on a preequilibrated HiLoad FF Ni-NTA and the flow-through was collected. The flow-through was concentrated with Amicon Centrifugal Filter Units to a volume of about 1 to 2 ml. Gelfiltration buffer was added to a final volume of 5 ml and the protein was loaded on a preequilibrated gelfiltration column (Superdex 75 or Superdex 200). In the case of cysteine mutants, 2 mM DTT was added to every purification buffer.

For purification of full-length Hsp90, the vector pET28 was used for expression. In this case, after affinity purification with a HiLoad FF Ni-NTA column, yHsp90 was not digested as it contains an internal thrombin cleavage site. Instead, it was loaded on a Resource Q 5 ml column preequilibrated with Resource A. After washing with Resource A, the protein was eluted with a gradient over 200 ml Resource B. Subsequently, yHsp90 was diluted 1:5 into Hydroxyapatite buffer A and loaded onto a Hydroxyapatite column. After elution with a gradient over 200 ml Hydroxyapatite buffer B, the protein was concentrated and finally purified via gelfiltration.

In the case of Ssa1, first a HiLoad FF Ni-NTA was run for affinity chromatography but special Ni-NTA (Ssa1) buffers containing ATP and β-Mercaptoethanol were used. The His-tag was not cleaved. Ssa1 was further purified via Hydroxyapatite and gelfiltration columns.

SUMO protease was purified via HiLoad FF Ni-NTA and gelfiltration. After gelfiltration, the protein was stored in 25 mM Tris, pH 8.0, 1 % Igepal (v/v), 250 mM NaCl, 500 µM DTT and 50 % glycerol.

4.5 Protein analytical methods

4.5.1 SDS polyacrylamide electrophoresis

For separation of proteins, biphasic gels were used of which the separating gel contained 10 % to 15 % of acrylamide depending on the size of the proteins [Laemmli et al., 1970].

Polymerization was induced by addition of TEMED and APS. Probes for SDS-PAGE were laced with 5x Laemmli loading buffer and heated at 95°C for 5 min. The gels were run in SDS PAGE buffer at 30 mA per gel for 30 to 60 min and afterwards, they were stained with Coomassie Blue R.

10-15 % Separating gel	
40 % Acrylamide 38:2 (w/v)	2.5 - 3.75 ml
4x SDS-Buffer	2.5 ml
(0.8 % SDS, 1.5 M Tris, pH 8.8)	
H_2O	Ad 10 ml

5 % Stacking gel	
40 % Acrylamide 38:2 (w/v)	0.625 ml
2x SDS-Buffer	2.5 ml
(0.4 % SDS, 0.25 M Tris, pH 6.8)	
H_2O	1.875 ml

SDS-PAGE buffer (10x)	
Tris	250 mM
Glycine	2 M
SDS	1 % (w/v)

Laemmli loading buffer (5x)	
SDS	10 % (w/v)
Glycerol	50 % (w/v)
Tris	300 mM
Bromphenole blue	0.05 % (w/v)
β-Mercaptoethanol	5 % (v/v)

4.5.2 Analytical ultracentrifugation

Analytical ultracentrifugation was used to investigate formation of protein complexes [Laue and Stafford III, 1999]. In sedimentation velocity experiments, the rate of sedimentation of the complexes under a strong centrifugal force is observed from which sedimentation coefficients are calculated. This method has the advantage that protein protein interactions can be observed without interactions with any matrix or surface. The experiments were carried out together with Dr. Klaus Richter in a Beckman ProteomeLab XL-A equipped with a fluorescence detection system. Sedimentation analysis was performed at 42,000 rpm in a TI-50 rotor at 20 °C. Usually, 500 nM of the labeled species and 3 µM of unlabeled proteins were applied. To determine the size of the complexes, the raw data were converted to dc/dt profiles as described before [Gaiser et al., 2010] and then fitted with (bi-)Gaussian functions.

4.5.3 Protein labeling

Proteins were either labeled at cysteine residues using maleimide-coupled ATTO dyes (thioether product) or at lysine residues using NHS-coupled dyes (amide product). In the case of cysteine labeling, prior to the labeling reaction, the accessibility of the cysteines was determined by an Ellman assay [Ellman, 1959]. 2 µM protein were mixed with 200 µg DTNB and incubated for 20 min at RT. The absorption was determined at $\lambda = 412$ nm and the concentration of accessible thiol groups was calculated with Lambert Beer's Law.

Proteins were first separated from DTT with a PD10 desalting column. Standard gelfiltration buffer (pH 7.5) was used for the labeling reaction. A three-fold excess of label (dissolved in DMSO) was added to the protein (about 500 µl of 100 µM) and incubated for 1 h at RT. In the case of FAM-labeled Ssa1, the labeling reaction was performed at 16 °C over night. For statistical double-labeling with two different dyes, three-fold excess of both dyes was added simultaneously. The reaction was afterwards quenched using 10-fold excess of DTT or cysteine and free label was separated using a PD10 desalting column. The degree of labeling (DOL) was determined according to the equation:

$$DOL = \frac{A_{dye} \cdot \varepsilon_{dye}}{(A_{280} - A_{dye} \cdot CF_{dye}) \cdot \varepsilon_{protein}}$$

with the absorption at 280 nm (A_{280}) and at the wavelength of maximal absorption of the dye (A_{dye}), the extinction coefficients ε_{dye} and $\varepsilon_{protein}$ [$M^{-1}cm^{-1}$] and correction factors CF_{dye} provided by the manufacturer of the labels.

4.5.4 UV absorption spectroscopy

To determine protein concentration, UV absorption of the aromatic amino acids at 280 nm was used according to the law of Lambert-Beer:

$$A_{280} = \varepsilon_{protein} \cdot c \cdot d$$

with the absorbance at 280 nm (A_{280}), the molar extinction coefficient ε [$M^{-1}cm^{-1}$], the protein concentration c [M] and the thickness of the sample d [cm].

The absorbance was measured in quartz glass cuvettes. Proteins were diluted to an absorption of 0.2 to 1 to ensure linearity of Lambert-Beer's law. Extinction coefficients were calculated using the ProtParam tool.

4.5.5 CD spectroscopy

Circular dicroism (CD) spectroscopy is used for the structural characterization of proteins [Greenfield, 2007]. Proteins are optically active molecules which absorb left and right circularly-polarized light with different intensity. The optical active parts of proteins are the peptide backbone and the side chains of the aromatic amino acids. The ellipticity θ is a quantitative measure for circular dicroism.
Depending on the used wavelength, different levels of structural information can be addressed. Near UV (250-300 nm) allows prediction of the tertiary structure of a protein, as in this region, the aromatic amino acids are responsible for the CD signal. Their optical activity is determined by their environment composed of the tertiary structure. In the far UV region (170-250 nm), the peptide backbone conformation results in a characteristic CD signal. α-helices have minima at 208 nm and 222 nm, whereas β-sheets exhibit a minimum at 218 nm. This enables analysis of the secondary structure of a protein.

In this work, far UV spectra were recorded to ensure folding of proteins and to measure thermal stability of different mutants. Measurements were carried out in quartz glass cuvettes in 10 mM potassium phosphate buffer, pH 7.5. For thermal stability measurements at a specific wavelength, samples were heated from 20 °C to 80 °C with a heating rate of 20 °C/h and afterwards cooled down again. All recorded spectra were buffer corrected and normalized to the molar ellipticity θ_{MRW} according to the equation:

$$\theta_{MRW} = \frac{\theta \cdot 100 \cdot M}{c \cdot d \cdot N_{AS}}$$

θ is the ellipticity [mdeg], M is the molecular weight of the protein [kDa], c is the protein concentration [mg/ml], d is the thickness of the sample [cm] and N_{AS} is the

number of amino acids. In thermal stability experiments, the transition points of the melting curves were determined by a Boltzmann fit.

Parameters for far UV spectra	
Start wavelength	260 nm
End wavelength	190 to 200 nm
Resolution	0.1 nm
Scan Speed	20 nm/min
Response	4.0 s
Band width	1.0 nm
Accumulations	10
Cuvette thickness	0.1 cm
Protein concentration	0.1 mg/ml

4.5.6 Fluorescence spectroscopy

Fluorescence is the emission of light by a substance that has been excited with electromagnetic radiation. Usually, a part of the absorbed energy is lost to the environment. Therefore, the emitted light has a longer wavelength than the absorbed light. This is referred to as Stokes shift [Lakowicz, 2009].
In more detail, when a substance absorbs a photon, it is excited from the ground state S_0 to a higher singulett state S_n which is metastabile. Following internal conversion, the excited state with the lowest energy level S_1 is reached. As the substance drops down to the ground state again, a photon may be emitted. If this happens in a time range of 10^{-9} to 10^{-7} s, it is called fluorescence. Phosphorescence and radiationless deactivation are alternative pathways of the excited states.

Förster Resonance Energy Transfer (FRET) is the transfer of energy of an excited donor to an acceptor dye. The quantum yield of the energy transfer transition, the FRET efficiency E, is dependent on the distance between the dyes according to the equation:

$$E = \frac{1}{(1 + (r/R_o)^6}$$

with the donor-acceptor distance r and the Förster distance of this pair R_0. Because of this relationship, it can be used as a molecular ruler as well as for the analysis of protein-protein interaction and conformational changes within proteins [Stryer, 1978]. For FRET experiments in this work, synthetic fluorophores were coupled to proteins (Table 4.1).

	λ_{ex} [nm]	λ_{em} [nm]
ATTO 488	501	523
ATTO 550	554	576
ATTO 532	532	550
ATTO 647	645	669

Table 4.1: Atto dyes used for FRET experiments and their excitation and emission wavelengths

Ensemble FRET measurements

For monitoring the complex formation between two different proteins, the proteins were labeled with two different dyes of a FRET pair. Ensemble FRET measurements were performed in quartz cuvettes using a Spex FluoroMaxIII spectrofluorimeter at 20 °C or 30 °C. Usually, 100 nM of labeled donor and acceptor were mixed and excited with the donor excitation wavelength. The emission was recorded at the acceptor emission wavelength. Control experiments were performed with only donor, only acceptor and by displacing one of the labeled proteins with the unlabeled variant.

Single molecule FRET measurements

To monitor conformational changes within one protein, the two dyes of a FRET pair were attached to different positions in the protein. ATTO 532 and ATTO 647 were used in this set of experiments. These experiments were performed in cooperation with Dr. Jelle Hendrix and Daniela Wengler (Prof. Don Lamb, Department of Physical Chemistry, LMU Munich) using a custom built two color confocal system based on an Eclipse TE2000 (Nikon, Tokio, Japan) with pulsed interleaved excitation and multiparameter detection. 10 pM of double labeled Sti1 variants and 10 to 25 µM of ligands were used.

4.5.7 Surface plasmon resonance spectroscopy

Surface plasmon resonance spectroscopy is used to analyze protein-protein interactions [Willander and Al-Hilli, 2009]. Basis of this method is a optical sensor consisting of a glass surface coated with an electrically conducting gold layer. A protein is immobilized on the sensor (ligand) and the second protein is passed under continuous flow (analyte). Polarized light is directed on the sensor where it leads to the excitation of surface

plasmons at a certain angle. This angle changes depending on the amount of bound protein and this can be measured as resonance units (RU).
In this work, a BiaCore X system was used and proteins were bound to a CM5 SPR chip employing amine-coupling reagents. 50 mM NHS and 200 mM EDC were used to activate the chip, the ligand was then applied in 20 mM potassium phosphate pH 4-5. Blocking was performed with ethanolamine. The analyte was flushed over the chip in 40 mM Hepes, 20 mM KCl, 5 $MgCl_2$, 0.005 % Tween (v/v) with a constant flow of 20 µl/min at a temperature of 20 °C.
The maximum SPR signal upon injection was plotted against the analyte concentration and fitted with the equation:

$$RU = RU_{Max} - \frac{RU_{Max} \cdot K_D}{c + K_D}$$

with the maximum SPR signal RU_{Max}, the dissociation constant K_D [M] and the analyte concentration c [M].

4.6 Activity assays

4.6.1 ATPase activity assay

An ATP-regenerative assay was used to assess the ATPase activity of Hsp90 and Hsp70 in the presence of different cochaperones or other factors [Richter et al., 2003]. In this coupled enzyme assay, the decrease of NADH is monitored at a wavelength of 340 nm. The assays were performed in a Cary 50 Bio UV/Vis spectrometer at 30 °C for yeast proteins (37 °C for human proteins). For each assay, 100 µl of premix, 1 to 4 µM Hsp90 or Hsp70, varying concentrations of cochaperones, and 2 mM ATP were mixed in a total volume of 140 µl in quartz cuvettes. In the case of Hsp90, 500 µM radicicol were added after the measurement to substract the residual ATPase activity of contaminant ATPases.

ATPase assay buffer	
HEPES pH 7.5	50 mM
KCl	50 mM
$MgCl_2$	10 mM

ATPase Premix	
ATPase assay buffer	8.656 ml
100 mM NADH	48 µl

100 mM PEP	240 µl
PK	12 µl
LDH	44 µl

The hydrolysis rates were calculated according to:

$$K_{hyd} = \frac{m}{(d \cdot \varepsilon_{NADH} \cdot c)}$$

with the slope m, the thickness of the sample d [cm], the extinction coefficient of NADH $\varepsilon_{\mathrm{NADH}}$ [$M^{-1}cm^{-1}$] and the concentration of the enzyme c [M].

Titration curves were fitted according to:

$$y = v_{max} + [2M_{tot}(v_{max} - v_0) \cdot (x + K_D - M_{tot} - \sqrt{(x + K_D - M_{tot})^2 + 4M_{tot}K_D}]^{-1}$$

with the rate of ATP hydrolysis in the beginning and maximally inhibited v_{max} and v_0 respectively, the concentration of the ATPase M_{tot} [M], and the dissociation constant K_D.

4.6.2 V-Src activity assay

V-Src expression is toxic to yeast due to hyperphosphorylation of the proteome [Brugge et al., 1987]. Maturation and activation of v-Src are dependent on the Hsp90 machinery including some of the cochaperones. In cells lacking Sti1, v-Src cannot be activated hence viability is restored [Lee et al., 2002]. Substituting Sti1 variants in Δ*sti1* yeast cells and monitoring their growth enables the measurement of the functionally of Sti1 variants towards client activation *in vivo*. Sti1 variants on p425 plasmids were introduced in a Δ*sti1* yeast strain harboring the p416-GPD-v-Src expression plasmid. V-Src expression was induced by transferring the cells onto medium containing galactose. 3 ml raffinose CSM were inoculated with a single colony and incubated at 30 °C overnight. Cells with an OD of 1 were diluted in 1:10 dilution series in sterile H_2O. Of each dilution, 3 µl were spotted onto galactose CSM plates and onto glucose CSM plates as a control and incubated for three days at 30 °C.

4.6.3 GR activity assay

To assess the ability of different yeast strains to support GR activation, a β-Galactosidase assay was used [Johnson and Craig, 2000]. To this end, the cells were transformed with the GR expression vector p413-GPD-hGR and the reporter vector pUCΔss26x.

In order to investigate effects of Sti1/Hop variants, Δ*sti1* yeast were additionally transformed with a p425-GPD vector containing Sti1 or Hop variants.
Single clones were inoculated in 3 ml CSM medium and incubated overnight at 30 °C. Cells were then diluted to an OD_{600} of 0.3 in a total volume of 10 ml, induced with 10 µM Deoxycorticosterone and grown for 12 hours at 30°C.
1 ml cells were harvested and the sediment was resuspended in 200 µl Z buffer. After addition of glass beads, the cells were disrupted in the Mixer Mill MM 400. 100 µl of the cleared lysate were added to 1 ml Z buffer with 0.8 mg/ml ONPG and incubated at 30 °C for 5 to 10 min. The reaction was stopped with 400 µl 1 M $CaCO_3$ and the absorption measured at 420 nm. These values were normalized with a Bradford assay of the samples. The relative activity values were obtained by setting the absolute value of the Sti1 wildtype sample to 100 %. At least three independent experiments were performed per variant.

Z buffer	
Na_2HPO_4	60 mM
NaH_2PO_4, pH 7.0	40 mM
KCl	10 mM
$MgSO_4$	1 mM
β-Mercaptoethanol	0,27 % (v/v)

4.7 Structural methods

4.7.1 Electron microscopy

The electron microscopy was performed by Sara Alvira and Prof. Jose Valpuesta (CSIC, Madrid). The complexes were isolated with the GraFix protocol [Kastner et al., 2007] and afterwards applied onto carbon-coated copper grids and stained with 2% uranyl acetate. Micrographs were taken on Kodak SO-163 film with a JEOL JEM1200EXII microscope (JEOL, Tokio, Japan) operated at 100 kV and a magnification of 60000. Particle selection, classification and 3D reconstruction was performed as published elsewhere [Peña et al., 2012].

4.7.2 Small angle X-ray scattering

The SAXS data was recorded by Dr. Tobias Madl (TU München) using an in-house SAXS instrument (SAXSess mc^2, Anton Paar, Graz, Austria) equipped with a Kratky camera, a sealed X-ray tube source and a two-dimensional Princeton Instruments PI-

SCX:4300 (Roper Scientific, Sarasota, USA) CCD detector. The scattering patterns were measured for several solute concentrations in the range from 1 to 10 mg/ml. The data was analyzed with the package ATSAS (version 2.5). Structure modeling was performed with the input of the single domain high resolution structures.

BIBLIOGRAPHY

[Ainavarapu et al., 2007] Ainavarapu, S. R. K., Brujić, J., Huang, H. H., Wiita, A. P., Lu, H., Li, L., Walther, K. A., Carrion-Vazquez, M., Li, H. and Fernandez, J. M. (2007). Contour length and refolding rate of a small protein controlled by engineered disulfide bonds. Biophysical Journal *92*, 225–233.

[Alarcon et al., 2012] Alarcon, S., Mollapour, M., Lee, M.-J., Tsutsumi, S., Lee, S., Kim, Y., Prince, T., Apolo, A., Giaccone, G., Xu, W. et al. (2012). Tumor-intrinsic and tumor-extrinsic factors impacting Hsp90-targeted therapy. Current Molecular Medicine *12*, 1125–1141.

[Ali et al., 2006] Ali, M. M., Roe, S. M., Vaughan, C. K., Meyer, P., Panaretou, B., Piper, P. W., Prodromou, C. and Pearl, L. H. (2006). Crystal structure of an Hsp90-nucleotide-p23/Sba1 closed chaperone complex. Nature *440*, 1013–1017.

[Anfinsen, 1973] Anfinsen, C. B. (1973). Principles that govern the folding of protein chains. Science *181*, 223–230.

[Arnold et al., 2006] Arnold, K., Bordoli, L., Kopp, J. and Schwede, T. (2006). The SWISS-MODEL workspace: a web-based environment for protein structure homology modelling. Bioinformatics *22*, 195–201.

[Barends et al., 2010] Barends, T. R., Werbeck, N. D. and Reinstein, J. (2010). Disaggregases in 4 dimensions. Current Opinion in Structural Biology *20*, 46–53.

[Barent et al., 1998] Barent, R. L., Nair, S. C., Carr, D. C., Ruan, Y., Rimerman, R. A., Fulton, J., Zhang, Y. and Smith, D. F. (1998). Analysis of FKBP51/FKBP52 chimeras and mutants for Hsp90 binding and association with progesterone receptor complexes. Molecular Endocrinology *12*, 342–354.

[Blom et al., 1999] Blom, N., Gammeltoft, S. and Brunak, S. (1999). Sequence and structure-based prediction of eukaryotic protein phosphorylation sites. Journal of molecular biology *294*, 1351–1362.

[Bose et al., 1996] Bose, S., Weikl, T., Bügl, H. and Buchner, J. (1996). Chaperone function of Hsp90-associated proteins. Science *274*, 1715–1717.

[Brady et al., 2011] Brady, C. A., Jiang, D., Mello, S. S., Johnson, T. M., Jarvis, L. A., Kozak, M. M., Broz, D. K., Basak, S., Park, E. J., McLaughlin, M. E. et al. (2011). Distinct p53 transcriptional programs dictate acute DNA-damage responses and tumor suppression. Cell *145*, 571–583.

[Brugge et al., 1987] Brugge, J., Jarosik, G., Andersen, J., Queral-Lustig, A., Fedor-Chaiken, M. and Broach, J. (1987). Expression of Rous sarcoma virus transforming protein pp60v-src in Saccharomyces cerevisiae cells. Molecular and Cellular Biology *7*, 2180–2187.

[Buchner, 2010] Buchner, J. (2010). Bacterial Hsp90–desperately seeking clients. Molecular Microbiology *76*, 540–544.

[Bukau et al., 2006] Bukau, B., Weissman, J. and Horwich, A. (2006). Molecular chaperones and protein quality control. Cell *125*, 443–451.

[Carrigan et al., 2004] Carrigan, P. E., Nelson, G. M., Roberts, P. J., Stoffer, J., Riggs, D. L. and Smith, D. F. (2004). Multiple domains of the co-chaperone Hop are important for Hsp70 binding. Journal of Biological Chemistry *279*, 16185–16193.

[Chang and Lindquist, 1994] Chang, H. and Lindquist, S. (1994). Conservation of Hsp90 macromolecular complexes in Saccharomyces cerevisiae. Journal of Biological Chemistry *269*, 24983–24988.

[Chang et al., 1997] Chang, H., Nathan, D. F. and Lindquist, S. (1997). In vivo analysis of the Hsp90 cochaperone Sti1 (p60). Molecular and Cellular Biology *17*, 318–325.

[Chen and Smith, 1998] Chen, S. and Smith, D. F. (1998). Hop as an adaptor in the heat shock protein 70 (Hsp70) and hsp90 chaperone machinery. Journal of Biological Chemistry *273*, 35194–35200.

[Cherry et al., 2012] Cherry, J. M., Hong, E. L., Amundsen, C., Balakrishnan, R., Binkley, G., Chan, E. T., Christie, K. R., Costanzo, M. C., Dwight, S. S., Engel, S. R. et al. (2012). Saccharomyces Genome Database: the genomics resource of budding yeast. Nucleic Acids Research *40*, D700–D705.

[Cong et al., 2011] Cong, Y., Schröder, G. F., Meyer, A. S., Jakana, J., Ma, B., Dougherty, M. T., Schmid, M. F., Reissmann, S., Levitt, M., Ludtke, S. L. et al. (2011). Symmetry-free cryo-EM structures of the chaperonin TRiC along its ATPase-driven conformational cycle. The EMBO Journal *31*, 720–730.

[Daniel et al., 2008] Daniel, S., Bradley, G., Longshaw, V. M., Söti, C., Csermely, P. and Blatch, G. L. (2008). Nuclear translocation of the phosphoprotein Hop (Hsp70/Hsp90 organizing protein) occurs under heat shock, and its proposed nuclear localization signal is involved in Hsp90 binding. Biochimica et Biophysica Acta *1783*, 1003–1014.

[Dill, 1999] Dill, K. A. (1999). Polymer principles and protein folding. Protein Science *8*, 1166–1180.

[Dill and Chan, 1997] Dill, K. A. and Chan, H. S. (1997). From Levinthal to pathways to funnels. Nature Structural Biology *4*, 10–19.

[Doyle and Wickner, 2009] Doyle, S. M. and Wickner, S. (2009). Hsp104 and ClpB: protein disaggregating machines. Trends in Biochemical Sciences *34*, 40–48.

[Ebong et al., 2011] Ebong, I.-o., Morgner, N., Zhou, M., Saraiva, M. A., Daturpalli, S., Jackson, S. E. and Robinson, C. V. (2011). Heterogeneity and dynamics in the assembly of the Heat Shock Protein 90 chaperone complexes. Proceedings of the National Academy of Sciences *108*, 17939–17944.

[Ellis, 2001] Ellis, R. J. (2001). Macromolecular crowding: obvious but underappreciated. Trends in Biochemical Sciences *26*, 597–604.

[Ellman, 1959] Ellman, G. L. (1959). Tissue sulfhydryl groups. Archives of Biochemistry and Biophysics *82*, 70–77.

[Fersht and Daggett, 2002] Fersht, A. R. and Daggett, V. (2002). Protein folding and unfolding at atomic resolution. Cell *108*, 573–582.

[Flom et al., 2007] Flom, G., Behal, R., Rosen, L., Cole, D. and Johnson, J. (2007). Definition of the minimal fragments of Sti1 required for dimerization, interaction with Hsp70 and Hsp90 and in vivo functions. Biochemical Journal *404*, 159–167.

[Flom et al., 2006] Flom, G., Weekes, J., Williams, J. J. and Johnson, J. L. (2006). Effect of mutation of the tetratricopeptide repeat and asparatate-proline 2 domains of Sti1 on Hsp90 signaling and interaction in Saccharomyces cerevisiae. Genetics *172*, 41–51.

[Freeman et al., 1996] Freeman, B. C., Toft, D. O. and Morimoto, R. I. (1996). Molecular chaperone machines: chaperone activities of the cyclophilin Cyp-40 and the steroid aporeceptor-associated protein p23. Science *274*, 1718–1720.

[Gaiser et al., 2009] Gaiser, A. M., Brandt, F. and Richter, K. (2009). The non-canonical Hop protein from Caenorhabditis elegans exerts essential functions and forms binary complexes with either Hsc70 or Hsp90. Journal of Molecular Biology *391*, 621–634.

[Gaiser et al., 2010] Gaiser, A. M., Kretzschmar, A. and Richter, K. (2010). Cdc37-Hsp90 complexes are responsive to nucleotide-induced conformational changes and binding of further cofactors. Journal of Biological Chemistry *285*, 40921–40932.

[Gasteiger et al., 2005] Gasteiger, E., Hoogland, C., Gattiker, A., Wilkins, M. R., Appel, R. D., Bairoch, A. et al. (2005). Protein identification and analysis tools on the ExPASy server. In The Proteomics Protocols Handbook pp. 571–607. Springer.

[Genest et al., 2012] Genest, O., Reidy, M., Street, T. O., Hoskins, J. R., Camberg, J. L., Agard, D. A., Masison, D. C. and Wickner, S. (2012). Uncovering a region of Heat Shock Protein 90 important for client binding in E. coli and chaperone function in yeast. Molecular Cell *49*, 464–473.

[George and Heringa, 2002] George, R. A. and Heringa, J. (2002). An analysis of protein domain linkers: their classification and role in protein folding. Protein Engineering *15*, 871–879.

[Ghaemmaghami et al., 2003] Ghaemmaghami, S., Huh, W.-K., Bower, K., Howson, R. W., Belle, A., Dephoure, N., O'Shea, E. K. and Weissman, J. S. (2003). Global analysis of protein expression in yeast. Nature *425*, 737–741.

[Gietz and Schiestl, 2007] Gietz, R. D. and Schiestl, R. H. (2007). High-efficiency yeast transformation using the LiAc/SS carrier DNA/PEG method. Nature Protocols *2*, 31–34.

[Gong et al., 2009] Gong, Y., Kakihara, Y., Krogan, N., Greenblatt, J., Emili, A., Zhang, Z. and Houry, W. A. (2009). An atlas of chaperone–protein interactions in Saccharomyces cerevisiae: implications to protein folding pathways in the cell. Molecular Systems Biology *5*, 275.

[Greenfield, 2007] Greenfield, N. J. (2007). Using circular dichroism spectra to estimate protein secondary structure. Nature Protocols *1*, 2876–2890.

[Hagn et al., 2011] Hagn, F., Lagleder, S., Retzlaff, M., Rohrberg, J., Demmer, O., Richter, K., Buchner, J. and Kessler, H. (2011). Structural analysis of the interaction between Hsp90 and the tumor suppressor protein p53. Nature Structural & Molecular Biology *18*, 1086–1093.

[Hartl et al., 2011] Hartl, F. U., Bracher, A. and Hayer-Hartl, M. (2011). Molecular chaperones in protein folding and proteostasis. Nature *475*, 324–332.

[Hartl and Hayer-Hartl, 2002] Hartl, F. U. and Hayer-Hartl, M. (2002). Molecular chaperones in the cytosol: from nascent chain to folded protein. Science *295*, 1852–1858.

[Hartl and Hayer-Hartl, 2009] Hartl, F. U. and Hayer-Hartl, M. (2009). Converging concepts of protein folding in vitro and in vivo. Nature structural & Molecular Biology *16*, 574–581.

[Haslbeck et al., 2005] Haslbeck, M., Franzmann, T., Weinfurtner, D. and Buchner, J. (2005). Some like it hot: the structure and function of small heat-shock proteins. Nature Structural & Molecular Biology *12*, 842–846.

[Haslbeck et al., 2013] Haslbeck, V., Eckl, J. M., Kaiser, C. J., Papsdorf, K., Hessling, M. and Richter, K. (2013). Chaperone interacting TPR proteins in Caenorhabditis elegans. Journal of Molecular Biology *425*, 2922–2939.

[Hayes and Stafford, 2010] Hayes, D. B. and Stafford, W. F. (2010). SEDVIEW, real-time sedimentation analysis. Macromolecular Bioscience *10*, 731–735.

[Hernández et al., 2002] Hernández, M. P., Sullivan, W. P. and Toft, D. O. (2002). The assembly and intermolecular properties of the Hsp70-Hop-Hsp90 molecular chaperone complex. Journal of Biological Chemistry *277*, 38294–38304.

[Hessling et al., 2009] Hessling, M., Richter, K. and Buchner, J. (2009). Dissection of the ATP-induced conformational cycle of the molecular chaperone Hsp90. Nature Structural & Molecular Biology *16*, 287–293.

[Hildenbrand et al., 2011] Hildenbrand, Z. L., Molugu, S. K., Herrera, N., Ramirez, C., Xiao, C. and Bernal, R. A. (2011). Hsp90 can accommodate the simultaneous binding of the FKBP52 and Hop proteins. Oncotarget *2*, 43–58.

[Höfeld et al., 1995] Höfeld, J., Minami, Y. and Hartl, F.-U. (1995). Hip, a novel cochaperone involved in the eukaryotic Hsc70/Hsp40 reaction cycle. Cell *83*, 589–598.

[Hoffmann et al., 2012] Hoffmann, A., Becker, A. H., Zachmann-Brand, B., Deuerling, E., Bukau, B. and Kramer, G. (2012). Concerted action of the ribosome and the associated chaperone trigger factor confines nascent polypeptide folding. Molecular Cell *48*, 63–74.

[Horibe et al., 2012] Horibe, T., Torisawa, A., Kohno, M., Kawakami, K. et al. (2012). Molecular mechanism of cytotoxicity induced by Hsp90-targeted Antp-TPR hybrid peptide in glioblastoma cells. Molecular Cancer *11*, 1–11.

[Horwich et al., 2006] Horwich, A. L., Farr, G. W. and Fenton, W. A. (2006). GroEL-GroES-mediated protein folding. Chemical Reviews *106*, 1917–1930.

[Jarosz and Lindquist, 2010] Jarosz, D. F. and Lindquist, S. (2010). Hsp90 and environmental stress transform the adaptive value of natural genetic variation. Science *330*, 1820–1824.

[Johnson and Brown, 2009] Johnson, J. L. and Brown, C. (2009). Plasticity of the Hsp90 chaperone machine in divergent eukaryotic organisms. Cell Stress and Chaperones *14*, 83–94.

[Johnson and Craig, 2000] Johnson, J. L. and Craig, E. A. (2000). A role for the Hsp40 Ydj1 in repression of basal steroid receptor activity in yeast. Molecular and Cellular Biology *20*, 3027–3036.

[Kampinga and Craig, 2010] Kampinga, H. H. and Craig, E. A. (2010). The Hsp70 chaperone machinery: J proteins as drivers of functional specificity. Nature Reviews Molecular Cell Biology *11*, 579–592.

[Kastner et al., 2007] Kastner, B., Fischer, N., Golas, M. M., Sander, B., Dube, P., Boehringer, D., Hartmuth, K., Deckert, J., Hauer, F., Wolf, E. et al. (2007). GraFix: sample preparation for single-particle electron cryomicroscopy. Nature Methods *5*, 53–55.

[Kityk et al., 2012] Kityk, R., Kopp, J., Sinning, I. and Mayer, M. P. (2012). Structure and dynamics of the ATP-bound open conformation of Hsp70 chaperones. Molecular Cell *48*, 863–874.

[Knarr et al., 1999] Knarr, G., Modrow, S., Todd, A., Gething, M.-J. and Buchner, J. (1999). BiP-binding Sequences in HIV gp160. Implications for the binding specificity of BiP. Journal of Biological Chemistry *274*, 29850–29857.

[Kohn et al., 2004] Kohn, J. E., Millett, I. S., Jacob, J., Zagrovic, B., Dillon, T. M., Cingel, N., Dothager, R. S., Seifert, S., Thiyagarajan, P., Sosnick, T. R. et al. (2004). Random-coil behavior and the dimensions of chemically unfolded proteins. Proceedings of the National Academy of Sciences of the United States of America *101*, 12491–12496.

[Kundrat and Regan, 2010] Kundrat, L. and Regan, L. (2010). Balance between folding and degradation for Hsp90-dependent client proteins: a key role for CHIP. Biochemistry *49*, 7428–7438.

[Laemmli et al., 1970] Laemmli, U. K. et al. (1970). Cleavage of structural proteins during the assembly of the head of bacteriophage T4. Nature *227*, 680–685.

[Lakowicz, 2009] Lakowicz, J. R. (2009). Principles of fluorescence spectroscopy. Springer.

[Lässle et al., 1997] Lässle, M., Blatch, G. L., Kundra, V., Takatori, T. and Zetter, B. R. (1997). Stress-inducible, murine protein mSTI1 characterization of binding domains for heat shock proteins and in vitro phosphorylation by different kinases. Journal of Biological Chemistry *272*, 1876–1884.

[Laue and Stafford III, 1999] Laue, T. and Stafford III, W. (1999). Modern applications of analytical ultracentrifugation. Annual Review of Biophysics and Biomolecular Structure *28*, 75–100.

[Lee et al., 2012] Lee, C.-T., Graf, C., Mayer, F. J., Richter, S. M. and Mayer, M. P. (2012). Dynamics of the regulation of Hsp90 by the co-chaperone Sti1. The EMBO Journal *31*, 1518–1528.

[Lee et al., 2002] Lee, P., Rao, J., Fliss, A., Yang, E., Garrett, S. and Caplan, A. J. (2002). The Cdc37 protein kinase–binding domain is sufficient for protein kinase activity and cell viability. The Journal of Cell Biology *159*, 1051–1059.

[Levinthal, 1968] Levinthal, C. (1968). Are there pathways for protein folding. Journal de Chimie Physique et de Physico-Chimie Biologique *65*, 44–45.

[Li et al., 2002] Li, J., Ning, Y., Hedley, W., Saunders, B., Chen, Y., Tindill, N., Hannay, T. and Subramaniam, S. (2002). The molecule pages database. Nature *420*, 716–717.

[Li et al., 2010] Li, J., Richter, K. and Buchner, J. (2010). Mixed Hsp90-cochaperone complexes are important for the progression of the reaction cycle. Nature Structural & Molecular Biology *18*, 61–66.

[Li et al., 2013a] Li, J., Richter, K., Reinstein, J. and Buchner, J. (2013a). Integration of the accelerator Aha1 in the Hsp90 co-chaperone cycle. Nature Structural & Molecular Biology *20*, 326–331.

[Li et al., 2013b] Li, Z., Hartl, F. U. and Bracher, A. (2013b). Structure and function of Hip, an attenuator of the Hsp70 chaperone cycle. Nature Structural & Molecular Biology *20*, 929–935.

[Lindquist and Craig, 1988] Lindquist, S. and Craig, E. (1988). The heat-shock proteins. Annual Review of Genetics *22*, 631–677.

[Longshaw et al., 2004] Longshaw, V. M., Chapple, J. P., Balda, M. S., Cheetham, M. E. and Blatch, G. L. (2004). Nuclear translocation of the Hsp70/Hsp90 organizing protein mSTI1 is regulated by cell cycle kinases. Journal of Cell Science *117*, 701–710.

[Louvion et al., 1996] Louvion, J.-F., Warth, R. and Picard, D. (1996). Two eukaryote-specific regions of Hsp82 are dispensable for its viability and signal transduction functions in yeast. Proceedings of the National Academy of Sciences *93*, 13937–13942.

[Makhnevych and Houry, 2012] Makhnevych, T. and Houry, W. A. (2012). The role of Hsp90 in protein complex assembly. Biochimica et Biophysica Acta *1823*, 674–682.

[Marcinowski et al., 2011] Marcinowski, M., Höller, M., Feige, M. J., Baerend, D., Lamb, D. C. and Buchner, J. (2011). Substrate discrimination of the chaperone BiP by autonomous and cochaperone-regulated conformational transitions. Nature Structural & Molecular Biology *18*, 150–158.

[Mayer and Bukau, 2005] Mayer, M. and Bukau, B. (2005). Hsp70 chaperones: cellular functions and molecular mechanism. Cellular and Molecular Life Sciences *62*, 670–684.

[McLaughlin et al., 2002] McLaughlin, S. H., Smith, H. W., Jackson, S. E. et al. (2002). Stimulation of the weak ATPase activity of human Hsp90 by a client protein. Journal of Molecular Biology *315*, 787–798.

[Mollapour and Neckers, 2012] Mollapour, M. and Neckers, L. (2012). Post-translational modifications of Hsp90 and their contributions to chaperone regulation. Biochimica et Biophysica Acta *1823*, 648–655.

[Nelson et al., 1992] Nelson, R. J., Ziegelhoffer, T., Nicolet, C., Werner-Washburne, M. and Craig, E. A. (1992). The translation machinery and 70 kd heat shock protein cooperate in protein synthesis. Cell *71*, 97–105.

[Nicolet and Craig, 1989] Nicolet, C. M. and Craig, E. A. (1989). Isolation and characterization of STI1, a stress-inducible gene from Saccharomyces cerevisiae. Molecular and Cellular Biology *9*, 3638–3646.

[Odunuga et al., 2003] Odunuga, O. O., Hornby, J. A., Bies, C., Zimmermann, R., Pugh, D. J. and Blatch, G. L. (2003). Tetratricopeptide repeat motif-mediated Hsc70-mSTI1 interaction molecular characterization of the critical contacts for successful binding and specificity. Journal of Biological Chemistry *278*, 6896–6904.

[Ohashi et al., 2002] Ohashi, T., Hale, C. A., de Boer, P. A. and Erickson, H. P. (2002). Structural evidence that the P/Q domain of ZipA is an unstructured, flexible tether between the membrane and the C-terminal FtsZ-binding domain. Journal of bacteriology *184*, 4313–4315.

[Onuoha et al., 2008] Onuoha, S., Coulstock, E., Grossmann, J. and Jackson, S. (2008). Structural studies on the co-chaperone Hop and its complexes with Hsp90. Journal of Molecular Biology *379*, 732–744.

[Pace, 1990] Pace, C. N. (1990). Conformational stability of globular proteins. Trends in Biochemical Sciences *15*, 14–17.

[Pace et al., 1996] Pace, C. N., Shirley, B. A., McNutt, M. and Gajiwala, K. (1996). Forces contributing to the conformational stability of proteins. The FASEB Journal *10*, 75–83.

[Peña et al., 2012] Peña, Á., Gewartowski, K., Mroczek, S., Cuéllar, J., Szykowska, A., Prokop, A., Czarnocki-Cieciura, M., Piwowarski, J., Tous, C., Aguilera, A. et al. (2012). Architecture and nucleic acids recognition mechanism of the THO complex, an mRNP assembly factor. The EMBO Journal *31*, 1605–1616.

[Petoukhov et al., 2012] Petoukhov, M. V., Franke, D., Shkumatov, A. V., Tria, G., Kikhney, A. G., Gajda, M., Gorba, C., Mertens, H. D., Konarev, P. V. and Svergun, D. I. (2012). New developments in the ATSAS program package for small-angle scattering data analysis. Journal of Applied Crystallography *45*, 342–350.

[Petoukhov and Svergun, 2005] Petoukhov, M. V. and Svergun, D. I. (2005). Global rigid body modeling of macromolecular complexes against small-angle scattering data. Biophysical Journal *89*, 1237–1250.

[Pimienta et al., 2011] Pimienta, G., Herbert, K. M. and Regan, L. (2011). A Compound That Inhibits the Hop–Hsp90 Complex Formation and Has Unique Killing Effects in Breast Cancer Cell Lines. Molecular Pharmaceutics *8*, 2252–2261.

[Pratt and Toft, 1997] Pratt, W. B. and Toft, D. O. (1997). Steroid receptor interactions with heat shock protein and immunophilin chaperones. Endocrine Reviews *18*, 306–360.

[Pratt and Toft, 2003] Pratt, W. B. and Toft, D. O. (2003). Regulation of signaling protein function and trafficking by the Hsp90/Hsp70-based chaperone machinery. Experimental Biology and Medicine *228*, 111–133.

[Prodromou et al., 1997] Prodromou, C., Roe, S. M., O'Brien, R., Ladbury, J. E., Piper, P. W. and Pearl, L. H. (1997). Identification and structural characterization of the ATP/ADP-binding site in the Hsp90 molecular chaperone. Cell *90*, 65–75.

[Prodromou et al., 1999] Prodromou, C., Siligardi, G., O'Brien, R., Woolfson, D. N., Regan, L., Panaretou, B., Ladbury, J. E., Piper, P. W. and Pearl, L. H. (1999). Regulation of Hsp90 ATPase activity by tetratricopeptide repeat (TPR)-domain co-chaperones. The EMBO Journal *18*, 754–762.

[Ptitsyn et al., 1995] Ptitsyn, O., Bychkova, V. and Uversky, V. (1995). Kinetic and equilibrium folding intermediates. Philosophical Transactions of the Royal Society of London. Series B: Biological Sciences *348*, 35–41.

[Ptitsyn, 1995] Ptitsyn, O. B. (1995). Structures of folding intermediates. Current Opinion in Structural Biology *5*, 74–78.

[Raviol et al., 2006] Raviol, H., Sadlish, H., Rodriguez, F., Mayer, M. P. and Bukau, B. (2006). Chaperone network in the yeast cytosol: Hsp110 is revealed as an Hsp70 nucleotide exchange factor. The EMBO Journal *25*, 2510–2518.

[Retzlaff et al., 2010] Retzlaff, M., Hagn, F., Mitschke, L., Hessling, M., Gugel, F., Kessler, H., Richter, K. and Buchner, J. (2010). Asymmetric activation of the Hsp90 dimer by its cochaperone Aha1. Molecular Cell *37*, 344–354.

[Richter et al., 2010] Richter, K., Haslbeck, M. and Buchner, J. (2010). The heat shock response: life on the verge of death. Molecular Cell *40*, 253–266.

[Richter et al., 2003] Richter, K., Muschler, P., Hainzl, O., Reinstein, J. and Buchner, J. (2003). Sti1 Is a Non-competitive Inhibitor of the Hsp90 ATPase binding prevents the N-terminal dimerization reaction during the ATPase cycle. Journal of Biological Chemistry *278*, 10328–10333.

[Richter et al., 2008] Richter, K., Soroka, J., Skalniak, L., Leskovar, A., Hessling, M., Reinstein, J. and Buchner, J. (2008). Conserved conformational changes in the ATPase cycle of human Hsp90. Journal of Biological Chemistry *283*, 17757–17765.

[Röhl et al., 2013] Röhl, A., Rohrberg, J. and Buchner, J. (2013). The chaperone Hsp90: changing partners for demanding clients. Trends in Biochemical Sciences *38*, 253–262.

[Romano et al., 2009] Romano, S. A., Cordeiro, Y., Lima, L. M. T., Lopes, M. H., Silva, J. L., Foguel, D. and Linden, R. (2009). Reciprocal remodeling upon binding of the prion protein to its signaling partner Hop/Sti1. The FASEB Journal *23*, 4308–4316.

[Ruckova et al., 2012] Ruckova, E., Muller, P., Nenutil, R. and Vojtesek, B. (2012). Alterations of the Hsp70/Hsp90 chaperone and the HOP/CHIP co-chaperone system in cancer. Cellular & Molecular Biology Letters *17*, 446–458.

[Sambrook et al., 1989] Sambrook, J., Fritsch, E. F., Maniatis, T. et al. (1989). Molecular cloning, vol. 2,. Cold Spring Harbor Laboratory.

[Saunders and Deane, 2010] Saunders, R. and Deane, C. M. (2010). Synonymous codon usage influences the local protein structure observed. Nucleic Acids Research *38*, 6719–6728.

[Scheibel and Buchner, 2006] Scheibel, T. and Buchner, J. (2006). Protein aggregation as a cause for disease. In Molecular Chaperones in Health and Disease pp. 199–219. Springer.

[Scheufler et al., 2000] Scheufler, C., Brinker, A., Bourenkov, G., Pegoraro, S., Moroder, L., Bartunik, H., Hartl, F. U. and Moarefi, I. (2000). Structure of TPR domain-peptide complexes: critical elements in the assembly of the Hsp70-Hsp90 multichaperone machine. Cell *101*, 199–210.

[Schmid et al., 2012] Schmid, A. B., Lagleder, S., Gräwert, M. A., Röhl, A., Hagn, F., Wandinger, S. K., Cox, M. B., Demmer, O., Richter, K., Groll, M. et al. (2012). The architecture of functional modules in the Hsp90 co-chaperone Sti1/Hop. The EMBO Journal *31*, 1506–1517.

[Schreiber et al., 2012] Schreiber, T. B., Ma usbacher, N., Soroka, J., Wandinger, S. K., Buchner, J. and Daub, H. (2012). Global analysis of phosphoproteome regulation by the Ser/Thr phosphatase Ppt1 in Saccharomyces cerevisiae. Journal of Proteome Research *11*, 2397–2408.

[Seckler and Jaenicke, 1992] Seckler, R. and Jaenicke, R. (1992). Protein folding and protein refolding. The FASEB journal *6*, 2545–2552.

[Selkoe, 2003] Selkoe, D. J. (2003). Folding proteins in fatal ways. Nature *426*, 900–904.

[Sharma et al., 1998] Sharma, S. V., Agatsuma, T. and Nakano, H. (1998). Targeting of the protein chaperone, Hsp90, by the transformation suppressing agent, radicicol. Oncogene *16*, 2639–2645.

[Shiau et al., 2006] Shiau, A. K., Harris, S. F., Southworth, D. R. and Agard, D. A. (2006). Structural analysis of E. coli Hsp90 reveals dramatic nucleotide-dependent conformational rearrangements. Cell *127*, 329–340.

[Siegelin, 2013] Siegelin, M. D. (2013). Inhibition of the mitochondrial Hsp90 chaperone network: A novel, efficient treatment strategy for cancer? Cancer Letters *333*, 133–146.

[Sikor et al., 2013] Sikor, M., Mapa, K., von Voithenberg, L. V., Mokranjac, D. and Lamb, D. C. (2013). Real-time observation of the conformational dynamics of mitochondrial Hsp70 by spFRET. The EMBO journal *32*, 1639–1649.

[Siligardi et al., 2004] Siligardi, G., Hu, B., Panaretou, B., Piper, P. W., Pearl, L. H. and Prodromou, C. (2004). Co-chaperone regulation of conformational switching in the Hsp90 ATPase cycle. Journal of Biological Chemistry *279*, 51989–51998.

[Smith, 2004] Smith, D. F. (2004). Tetratricopeptide repeat cochaperones in steroid receptor complexes. Cell Stress and Chaperones *9*, 109–121.

[Soroka et al., 2012] Soroka, J., Wandinger, S. K., Mäusbacher, N., Schreiber, T., Richter, K., Daub, H. and Buchner, J. (2012). Conformational switching of the molecular chaperone Hsp90 via regulated phosphorylation. Molecular Cell *45*, 517–528.

[Southworth and Agard, 2011] Southworth, D. R. and Agard, D. A. (2011). Client-loading conformation of the Hsp90 molecular chaperone revealed in the cryo-EM structure of the human Hsp90: Hop complex. Molecular Cell *42*, 771–781.

[Spiess et al., 2004] Spiess, C., Meyer, A. S., Reissmann, S. and Frydman, J. (2004). Mechanism of the eukaryotic chaperonin: protein folding in the chamber of secrets. Trends in Cell Biology *14*, 598–604.

[Stryer, 1978] Stryer, L. (1978). Fluorescence energy transfer as a spectroscopic ruler. Annual Review of Biochemistry *47*, 819–846.

[Taipale et al., 2010] Taipale, M., Jarosz, D. F. and Lindquist, S. (2010). Hsp90 at the hub of protein homeostasis: emerging mechanistic insights. Nature Reviews Molecular Cell Biology *11*, 515–528.

[Taipale et al., 2012] Taipale, M., Krykbaeva, I., Koeva, M., Kayatekin, C., Westover, K. D., Karras, G. I. and Lindquist, S. (2012). Quantitative analysis of Hsp90-client interactions reveals principles of substrate recognition. Cell *150*, 987–1001.

[Thompson et al., 1994] Thompson, J. D., Higgins, D. G. and Gibson, T. J. (1994). CLUSTAL W: improving the sensitivity of progressive multiple sequence alignment through sequence weighting, position-specific gap penalties and weight matrix choice. Nucleic Acids Research *22*, 4673–4680.

[Thulasiraman et al., 1999] Thulasiraman, V., Yang, C.-F. and Frydman, J. (1999). In vivo newly translated polypeptides are sequestered in a protected folding environment. The EMBO Journal *18*, 85–95.

[Torres et al., 2009] Torres, J. H., Papandreou, N. and Chomilier, J. (2009). Sequence analyses reveal that a TPR–DP module, surrounded by recombinable flanking introns, could be at the origin of eukaryotic Hop and Hip TPR–DP domains and prokaryotic GerD proteins. Cell Stress and Chaperones *14*, 281–289.

[Tyagi et al., 2009] Tyagi, N. K., Fenton, W. A. and Horwich, A. L. (2009). GroEL/GroES cycling: ATP binds to an open ring before substrate protein favoring protein binding and production of the native state. Proceedings of the National Academy of Sciences *106*, 20264–20269.

[Tyedmers et al., 2010] Tyedmers, J., Mogk, A. and Bukau, B. (2010). Cellular strategies for controlling protein aggregation. Nature Reviews Molecular Cell Biology *11*, 777–788.

[Vaughan et al., 2006] Vaughan, C. K., Gohlke, U., Sobott, F., Good, V. M., Ali, M. M., Prodromou, C., Robinson, C. V., Saibil, H. R. and Pearl, L. H. (2006). Structure of an Hsp90-Cdc37-Cdk4 complex. Molecular Cell *23*, 697–707.

[Vaughan et al., 2008] Vaughan, C. K., Mollapour, M., Smith, J. R., Truman, A., Hu, B., Good, V. M., Panaretou, B., Neckers, L., Clarke, P. A., Workman, P. et al. (2008). Hsp90-dependent activation of protein kinases is regulated by chaperone-targeted dephosphorylation of Cdc37. Molecular Cell *31*, 886–895.

[Walsh et al., 2011] Walsh, N., Larkin, A., Swan, N., Conlon, K., Dowling, P., McDermott, R. and Clynes, M. (2011). RNAi knockdown of Hop (Hsp70/Hsp90 organising protein) decreases invasion via MMP-2 down regulation. Cancer Letters *306*, 180–189.

[Wandinger et al., 2006] Wandinger, S. K., Suhre, M. H., Wegele, H. and Buchner, J. (2006). The phosphatase Ppt1 is a dedicated regulator of the molecular chaperone Hsp90. The EMBO Journal *25*, 367–376.

[Wang et al., 2009] Wang, X., Song, X., Zhuo, W., Fu, Y., Shi, H., Liang, Y., Tong, M., Chang, G. and Luo, Y. (2009). The regulatory mechanism of Hsp90α secretion and its function in tumor malignancy. Proceedings of the National Academy of Sciences *106*, 21288–21293.

[Wang et al., 2012] Wang, Y., Gibney, P. A., West, J. D. and Morano, K. A. (2012). The yeast Hsp70 Ssa1 is a sensor for activation of the heat shock response by thiol-reactive compounds. Molecular Biology of the Cell *23*, 3290–3298.

[Wegele et al., 2003] Wegele, H., Haslbeck, M., Reinstein, J. and Buchner, J. (2003). Sti1 is a novel activator of the Ssa proteins. Journal of Biological Chemistry *278*, 25970–25976.

[Wilkinson and Gilbert, 2004] Wilkinson, B. and Gilbert, H. F. (2004). Protein disulfide isomerase. Biochimica et Biophysica Acta *1699*, 35–44.

[Willander and Al-Hilli, 2009] Willander, M. and Al-Hilli, S. (2009). Analysis of biomolecules using surface plasmons. In Micro and Nano Technologies in Bioanalysis pp. 201–229. Springer.

[Willmund et al., 2013] Willmund, F., del Alamo, M., Pechmann, S., Chen, T., Albanèse, V., Dammer, E. B., Peng, J. and Frydman, J. (2013). The cotranslational function of ribosome-associated Hsp70 in eukaryotic protein homeostasis. Cell *152*, 196–209.

[Xu et al., 2012] Xu, W., Mollapour, M., Prodromou, C., Wang, S., Scroggins, B. T., Palchick, Z., Beebe, K., Siderius, M., Lee, M.-J., Couvillon, A. et al. (2012). Dynamic Tyrosine Phosphorylation Modulates Cycling of the HSP90-P50¡ sup¿ CDC37¡/sup¿-AHA1 Chaperone Machine. Molecular Cell *47*, 434–443.

[Yam et al., 2005] Yam, A. Y.-W., Albanèse, V., Lin, H.-T. J. and Frydman, J. (2005). Hsp110 cooperates with different cytosolic Hsp70 systems in a pathway for de novo folding. Journal of Biological Chemistry *280*, 41252–41261.

[Yi et al., 2010] Yi, F., Doudevski, I. and Regan, L. (2010). Hop is a monomer: Investigation of the oligomeric state of the co-chaperone Hop. Protein Science *19*, 19–25.

[Young et al., 2004] Young, J. C., Agashe, V. R., Siegers, K. and Hartl, F. U. (2004). Pathways of chaperone-mediated protein folding in the cytosol. Nature Reviews Molecular Cell Biology *5*, 781–791.

[Zhang et al., 2010] Zhang, M., Kadota, Y., Prodromou, C., Shirasu, K. and Pearl, L. H. (2010). Structural basis for assembly of Hsp90-Sgt1-CHORD protein complexes: implications for chaperoning of NLR innate immunity receptors. Molecular Cell *39*, 269–281.

[Zhu et al., 1996] Zhu, X., Zhao, X., Burkholder, W. F., Gragerov, A., Ogata, C. M., Gottesman, M. E. and Hendrickson, W. A. (1996). Structural analysis of substrate binding by the molecular chaperone DnaK. Science *272*, 1606–1614.

[Zhuravleva et al., 2012] Zhuravleva, A., Clerico, E. M. and Gierasch, L. M. (2012). An interdomain energetic tug-of-war creates the allosterically active state in Hsp70 molecular chaperones. Cell *151*, 1296–1307.

[Zuehlke and Johnson, 2012] Zuehlke, A. D. and Johnson, J. L. (2012). Chaperoning the chaperone: a role for the co-chaperone Cpr7 in modulating Hsp90 function in Saccharomyces cerevisiae. Genetics *191*, 805–814.

Publications

Schmid*, A. B., Lagleder*, S., Gräwert*, M. A., Röhl*, A., Hagn, F., Wandinger, S. K., Cox, M. B., Demmer, O., Richter, K., Groll, M. et al. (2012). The architecture of functional modules in the Hsp90 co-chaperone Sti1/Hop. The EMBO Journal *31*, 1506-1517.

Röhl*, A., Rohrberg*, J. and Buchner, J. (2013). The chaperone Hsp90: changing partners for demanding clients. Trends in Biochemical Sciences *38*, 253-262.

*These authors contributed equally to this publication.

Dank

An erster Stelle möchte ich mich bei meinem Doktorvater **Johannes Buchner** für die Unterstützung bei dieser Arbeit bedanken, für die ständige Erreichbarkeit und prompte Antworten, für das Vertrauen und den großen wissenschaftlichen Freiraum.

Ganz herzlich möchte ich meinen Kooperationspartner danken: **Sara Alvira** und **José Valpuesta** für die tolle und aufregende Zeit in Madrid und natürlich für die exzellente Zusammenarbeit, die wirklich Spaß gemacht hat. **Tobias Madl** für die gute und zuverlässige Kollaboration in Sachen SAXS. Ich möchte auch **Jelle Hendrix**, **Daniela Wengler** und **Don Lamb** für die Zusammenarbeit bei den smFRET Experimenten danken.

Besten Dank auch an den vielzähligen Studenten, die mich im Laufe der Arbeit immer für einige Wochen oder Monate unterstützt haben. Besonders hervorzuheben sind hier "meine" beiden Masterstudentinnen **Monika Herrmann** und **Evelyn Bender**, die das Projekt ein gutes Stück weitergebracht haben.

CompInt und die **TUM GS** haben mich vor allem finanziell und durch das breite Angebot an interessanten Kursen und Veranstaltungen gefördert.

Bei den vielen Lehrstuhlmitgliedern möchte ich mich bedanken für die tolle Atmosphäre und die vielen interessanten fachlichen Diskussionen. Hervorzuheben sind die "Alten", die mir einen guten Start ermöglicht haben; **Andi** für die unkomplizierte Projektübergabe, **Moritz** für Hilfe in Sachen Proteinlabeling und FRET, **Julia** für die Tipps bei der Hefe-Biologie und **Christoph** für das ausführliche Beantworten von Fragen aller Art.
Meine Kollegen aus Büro 4, Labor 2 und 12: **Maike**, **Lars**, **Danae**, **Tilly**, (**Vroni**), **Daniel**, **Hannah** und **Flo**, haben eine spaßige Zeit im Partybüro ermöglicht und mich wissenschaftlich unterstützt. Mit euch ließ es sich sogar zu sechst im Büro bei 30 Grad aushalten ;-) Zusätzlich möchte ich hier auch das Klaus-Büro erwähnen: **Vroni**, **Julia**, **Katha**, ihr wart die zweite Heimat für mich! Vielen Dank für experimentelle Tipps und Tricks sowie Gefälligkeiten wie das Platten rausstellen. Vroni, danke für's ständige Beratschlagen und Ermutigen! Ein großes Dankeschön geht an **Klaus** selbst für die zahlreichen UZ-Läufe und Diskussionen.

Lieber **Flo**, ohne dein jahrelanges Bekräftigen, Unterstützen, das Einrichten meiner PC Programme, Korrekturlesen und Umsorgen wäre diese Arbeit gar nicht möglich gewesen!